Cand. Scient. Thesis in Geosciences

Magmatic differentiation and mixing processes among mafic to evolved lavas and syenites in the Diego Hernández Formation, Tenerife, Canary Islands: Evidence from the geochemistry of clinopyroxenes and amphiboles

Thomas Denstad

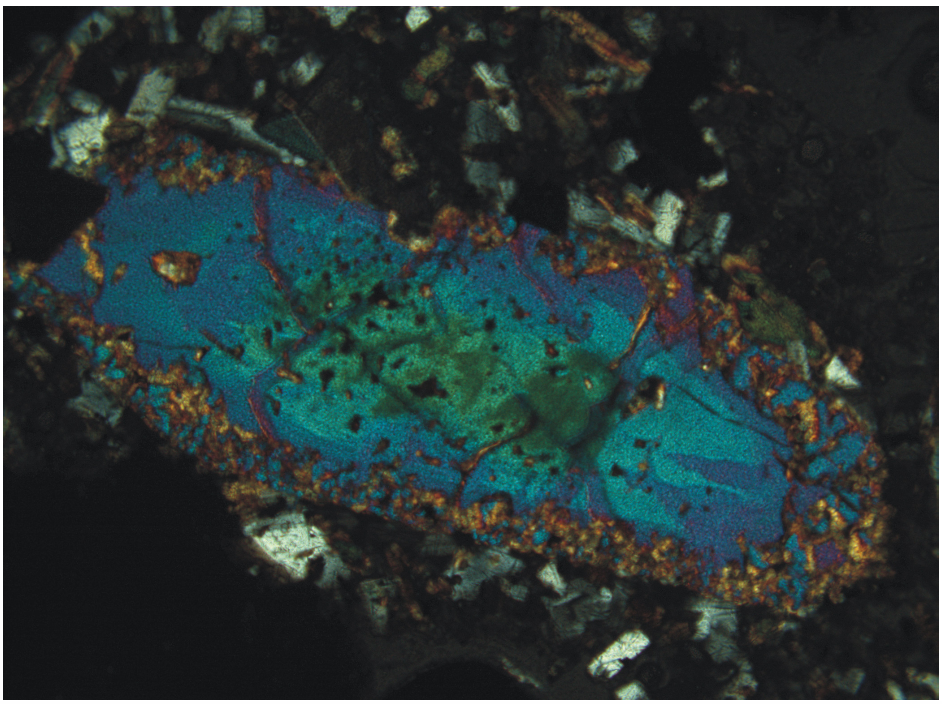

UNIVERSITY OF OSLO

FACULTY OF MATHEMATICS AND NATURAL SCIENCES

Magmatic differentiation and mixing among mafic to evolved lavas and syenites in the Diego Hernández Formation, Tenerife, Canary Islands: Evidence from the geochemistry of clinopyroxenes and amphiboles

Thomas Denstad

Cand. Scient. Thesis in Geosciences

Discipline: Petrology and Geochemistry

Department of Geosciences

Faculty of Mathematics and Natural Sciences

UNIVERSITY OF OSLO

May 2007

Tutor: Else-Ragnhild Neumann (PGP)

This work is published digitally through DUO – Digitale Utgivelser ved UiO

http://www.duo.uio.no

It is also catalogued in BIBSYS (http://www.bibsys.no/english)

Table of Contents

1 Introduction

Petrology involves the description, identification, classification, the interpretation of data and the generation of theories on the origin of rocks (Philpotts, 1990). When applied on igneous systems this means the interpretation of rocks formed from a molten material, found either as extrusive bodies on the earths surface, or as intrusive bodies found within the earth. One of the primary goals of igneous petrology is the development of geochemical models of the differentiation processes that produce the observed variety of igneous rocks. In this context it is fundamental to understand the chemistry and distribution of elements between different phases found in the rocks (i.e. different minerals, trapped liquids, mineral-melt partitioning).

This thesis will, in addition to whole rock data, centre around the geochemistry of two important rock forming minerals, commonly associated with the products of primary and differentiated alkaline ocean island basalts: *Clinopyroxenes* and *Amphiboles*. While whole rock data give only the average result of the processes to which magmas have been subjected, individual minerals faithfully record information about the changing physical and chemical compositions in the magmas from which they grow (Neumann et al., 1999).

Pyroxenes and amphiboles are both termed inosilicates and crystallise as single or double chained silicates, respectively. Pyroxenes are the most important group of rock-forming ferromagnesian silicates, and occur as stable phases in almost every type of igneous rock. Clinopyroxenes can be considered broadly in terms of two major subgroups based on their cation occupancy in the general formula $[(M2)(M1)(T)_2O_6]$: Calcic pyroxenes in which Ca occupies more than two-thirds of the M2 position, and sodium pyroxenes where the M2 site is largely occupied by Na. Since there exists no miscibility gap between clinopyroxenes, coupled substitutions within the crystallographic lattice create a haven for a number of differently charged cations. Amphiboles occur in a wide range of P-T environments and are common constituents of both metamorphic and igneous rocks. Among igneous rocks they are found in all the major groups ranging from ultrabasic to acid and alkaline types, but

are particularly common constituents of the intermediate members of the calc-alkali series, where they can put important constrains on the crystallisation process. Amphiboles occur characteristically in the plutonic rocks and, in general, are relatively unimportant minerals of the volcanic rocks.

A rising number of recent papers have shown that ocean island magmas may undergo complex processes such as fractional crystallisation at different depths, crystal accumulation, magma mixing, and contamination by oceanic sediments, melts generated in the mantle lithosphere, or through assimilation of hydrothermally altered basement (Neumann et al., 1999).

Substantial literature on the mineralogy and petrology of nepheline syenites and related rocks has accumulated, with particular emphasis on compositional trends and relations among mafic phases such as aegirine-augite and alkali amphiboles. To a great extent all these studies deal with intrusive rock bodies presently exposed at the surface, such as the plutons of the Precambrian (Gardar) and Tertiary Provinces in Greenland and elswere. However, the levels of erosion in these areas are usually such that undisputable co-magmatic volcanics are absent. In contrast, the occurrence of nepheline syenite blocks in the late Quarternary phonolitics of the Diego Hernández Formation (0,37 – 0,175 Ma), a product of the latest caldera forming event in the Las Cañadas caldera, Tenerife, provides an excellent opportunity to compare syenite mineralogy with that of the co-magmatic eruptive products.

In this thesis, through petrographical observations and geochemical modelling, I will try to shed light on the evolution of primitive to highly evolved magmatic products, both intrusive and extrusive, produced during the magmatic cycle of the Diego Hernández Formation, and study the effects of shallow level processes working on open system magma chambers beneath oceanic islands.

2 Geological Setting

2.1 Canary Islands

The Canary Islands consist of an archipelago of seven large and several small islands in the eastern Atlantic ocean located off the passive continental margin of Morocco, Northwest Africa (Figure 2.1). The Islands were generated as the African continent moved slowly over a deep mantle hotspot that is now believed to be centred beneath El Hierro (Morgan, 1972; Holik & Rabinowitz, 1992), the westernmost island in the chain. Canary Islands active volcanism has occurred over the past 20 million years, and has involved mainly the eruption of poorly differentiated alkali basaltic to tholeiitic lavas from fissures oriented in parallel with the main tectonic trends, NE-SW and NW-SE, of the Canarian archipelago (Martí et al., 1994). Only the two central islands, Gran Canaria and Tenerife, have undergone the construction of central volcanic edifices characterized by the eruption of differentiated phonolitic magmas (Fúster et al., 1968).

2.2 Tenerife

The largest island of the Canarian archipelago, Tenerife (Figure 2.1), was originally built up by eruptions of ankaramites, basanites and alkali basalts which form the Old Basaltic Series ranging from 12 to 3.3 Ma (Fúster et al., 1968; Ancochea et al., 1990). These deeply eroded series represent the oldest exposed massifs on Tenerife and can be divided into three separate localities where K-Ar analyses suggest age ranges of 8.3-3.8 Ma for Roque del Conde in the SW, 6.7-4.5 Ma for Teno in the NW and 6.5-3.3 Ma for the Anaga massif in the NE (Ancochea et al., 1990). Although the massifs are called the Old Basaltic Series, their upper parts include more evolved lavas such as phonolites and tephrites.

More recent volcanism on Tenerife crops out mainly in the central part of the island which consists of a large volcanic complex; the Las Cañadas edifice. K-Ar dating of the Las Cañadas edifice suggest an age range of >3.3 – 0.17 Ma (Martí et al., 1990, 1994; Fúster et al., 1994). The edifice is divided into a dominantly mafic to intermediate Lower Group (3.3-2.2 Ma), and an Upper Group compromising of the

products of three felsic volcanic cycles, which on the basis of age, stratigraphy and petrology, can be divided into the Unca (1.59-1.18 Ma), Guajara (0.85-0.65 Ma), and Diego Hernández (0.37-0.175 Ma) formations (Martí et al., 1994). Each Upper Group cycle was terminated by a caldera collapse episode associated with felsic pyroclastic eruptions and followed by a migration in the focus of eruptive activity (Martí et al., 1994, 1997).

Figure 2.1. Geological map of Tenerife.

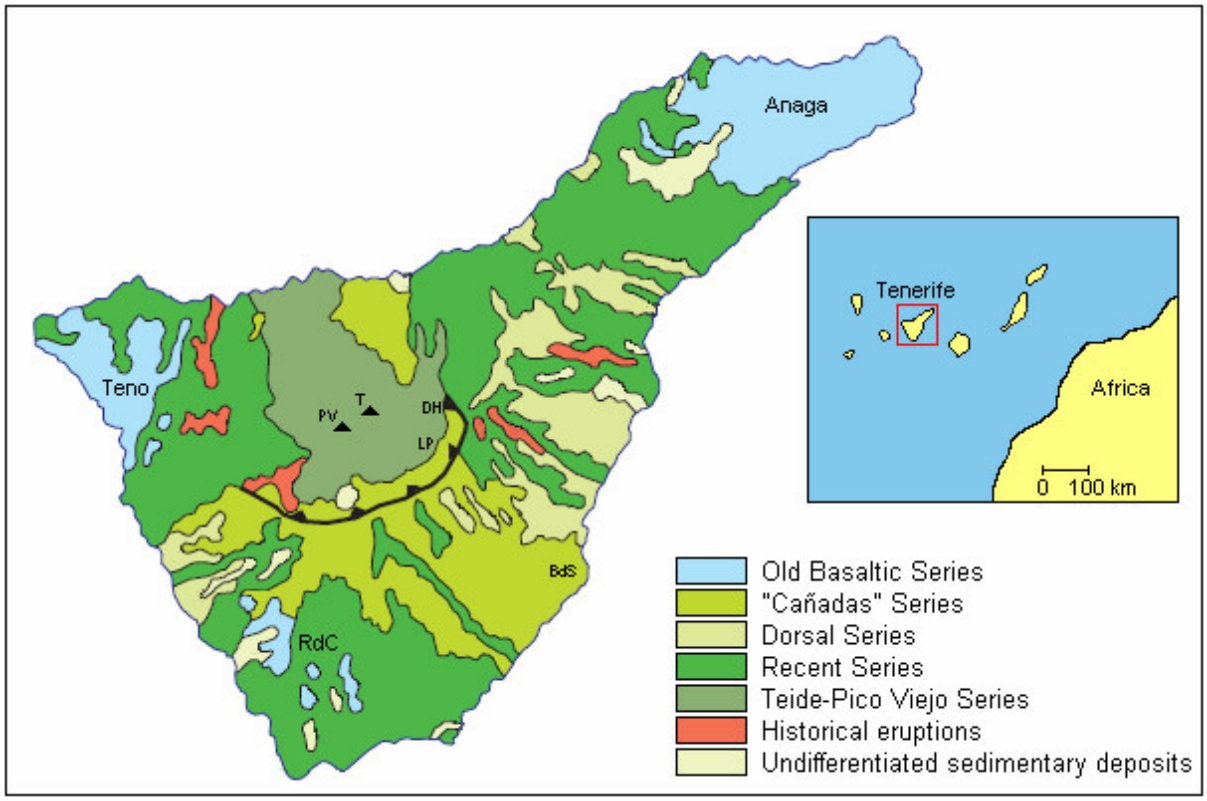

Simplified geological overview of the different magmatic units found at Tenerife. T, Teide; PV, Pico Viejo; DH, Diego Hernández; LP, Las Pilas; RdC, Roque del Conde; BdS, Bandas del Sur. See table 2.1 for the relative timing of deposits.

Map is based on cartography from IGME (Spanish Geological Survey).

These destructive events formed the las Cañadas caldera, within which renewed volcanic activity since the most recent collapse at 175 ka (Mitjavila & Villa, 1993) has constructed the Teide-Pico Viejo volcanic complex and numerous satellite vent systems (Ablay et al., 1998). The two stratovolcanes within the caldera show geochemical evolution ranging from basanites to phonolites. A series of lava flows with mostly basaltic composition erupted simultaneously (dated 0.87-0.56 Ma) with the Upper Group of the las Cañadas volcano and formed the Dorsal ridge between

the Las Cañadas edifice and the Anaga massif (Fúster et al., 1968; Ancochea et al., 1990).

2.3 Diego Hernández Formation

The Diego Hernández Formation (DHF) is exposed in the eastern and northeastern sides of the caldera wall (Figure 2.1) and shows a more restricted distribution than the older formations. The DHF has a maximum thickness of 250 meters in the Diego Hernández wall and represents the youngest pre-caldera deposits (Martí et al., 1994).

The DHF was deposited in a palaeovalley that was excavated on the eastern side of the Las Cañadas edifice and was bounded to the south by the rocks of the Las Pilas sector (Figure 2.1) and towards the north by several strombolian cones of basaltic composition formed contemporaneously with the phonolitic deposits (Martí et al., 1994). The DHF was built up in two stages separated by a period of erosion and non-deposition. A basaltic lava from the first stage was dated by Ancochea et al. (1990) as 0.542±0.06 Ma. However, Mitjavila (unpub. Ph.D. thesis, University of Barcelona, 1990) and Mitjavila & Villa (1993) have proved the existence of excess Ar in the basalt, suggesting a younger age. The main part of the DHF is represented by the second stage of deposition that occurred between 0.266 and 0.179 Ma. The DHF includes several non-welded peralkaline phonolitic pyroclastics deposits and interbedded lapilli deposits and basaltic lavas derived from the strombolian cones located at the northern margin of the Diego Hernández wall. Poorly developed palaeosols and erosion surfaces indicate several minor periods of dormancy (Martí et al., 1994).

Non-welded ignimbrites with variable contents of lithic and pumice fragments, occasionally associated with intraformational breccias, are the most abundant deposits in the upper parts of the DHF. Hydrothermally altered lithics and nephelinithic syenite clasts are common in some units and may constitute up to 50 wt% of the deposits. Another distinctive feature, described in detail by Wolff (1985) from the Tajao ignimbrite, is the presence of streaky black-and-white pumices in many deposits.

Table 2.1. Simplifiede overwiev of the stratigraphy of Tenerife, showing the relative timing of central and flank volcanism.

<table>
<tr><td rowspan="11">POST-SHIELD VOLCANISM</td><td colspan="2">FLANKS</td><td colspan="3">CENTRAL VOLCANIC COMPLEX</td></tr>
<tr><td rowspan="10">DORSAL SERIES (>1,0 Ma – present)</td><td>RECENT SERIES BASALTS</td><td colspan="3">TEIDE-PICO VIEJO COMPLEX
(0,18 Ma – present)</td></tr>
<tr><td rowspan="9"></td><td rowspan="9">LAS CAÑADAS EDIFICE</td><td rowspan="8">UPPER GROUP</td><td>CALDERA COLLAPSE</td></tr>
<tr><td rowspan="2">SERIES III BASALTS</td><td>Diego Hernández Formation
(0,37 – 0,18 Ma)</td></tr>
<tr><td>(repose period)
CALDERA COLLAPSE</td></tr>
<tr><td>Guajara Formation
(0,85 – 0,57 Ma)</td></tr>
<tr><td>(repose period)
CALDERA COLLAPSE</td></tr>
<tr><td>Ucanca Formation
(1,57 – 1,07 Ma)</td></tr>
<tr><td colspan="2">(repose period)</td></tr>
<tr><td>LOWER GR.</td><td>Undifferentiated
(3,3 – 2 Ma)</td></tr>
<tr><td>SHIELD</td><td colspan="5">OLD BASALTIC SERIES
Anaga, Teno & Roque del Conde Massifs
(12 – 3,3 Ma)</td></tr>
</table>

Table from Edgar et al. (2002).

2.4 Stratigraphy of The Diego Hernández Formation

The stratigraphy of the Diego Hernández Formation has been interpretated and divided in different ways by different authors (e.g. Martí et al., 1990; Wolff et al., 2000). A common criterion for the stratigraphic division is the presence of basaltic layers interbedded with phonolitic deposits. The occurrence of basaltic rocks suggests an interruption of the explosive activity of phonolitic magma. This thesis uses a modified and more simplified stratigraphy than that of Martí et al. (1990) and Wolff et al. (2000). Disregarding erosion surfaces and sediments, indicating periods of dormacy of the volcanic activity, the following stratigraphy (Table 2.2) is solely based on lithological features. As will be presented below, the stratigraphic units display both similar and different chemical signatures, adding speculation to the already complex nature of the magmatic products of Tenerife.

Three xenoliths from separate localities corresponding to DHF eruptions and one xenolith from the Pico Viejo volcanic series, a product of the post Diego Hernández volcanic cycle, have been analysed to shed light on processes working in subvolcanic magma chambers. The xenoliths have been sampled in both proximal and distal facies from the Diego Hernández wall. Correlations have stratigraphically positioned these samples to within the El Abrigo ignimbrite, which is supposed to represent the youngest sequence in the DHF, corresponding to caldera forming eruption.

The DH37 series represents the proximal facies and are sampled from a gabbro boulder in the lithic breccia at the uppermost level of the Diego Hernández wall (El Abrigo ignimbrite). The DH39, TF12 and TF16 series consist of gabbro-syenitic samples collected in the Bandas del Sur (BdS) pyroclastics, south-south west of the Diego Hernández wall. The final group of xenoliths (TDKS series) is collected from the volcanic products of the Pico Viejo cycle.

Table 2.2. Stratigraphy and unit classification of the Diego Hernández wall.

Sample	Rock type	Sequence	Data
Bandas del Sur	Syenitic / Gabbro		Major&Trace(Cpx,Amph,WR)
CALDERA WALL – TOP			
El Abrigo ignimbrite	Lithic breccia (Gabbro)		Major&Trace(Cpx,Amph,WR)
DH97-17	Lava	DHF 3	Major(Cpx,WR)/Trace(WR)
DH97-13B	Basalt		Major(Cpx,WR)/Trace(WR)
DH97-13A	Basalt		Major(Cpx,WR)/Trace(WR)
DH97-12	Basalt		Major(Cpx,WR)/Trace(WR)
DH97-4	Mixed porphyritic fallout	DHF 2	Major/Trace(Cpx,WR)
DH97-30B	Basalt		Major(Cpx,WR)/Trace(WR)
DH97-30A	Basalt		Major(Cpx,WR)/Trace(WR)
DH97-29B	Basalt		Major(Cpx,WR)/Trace(WR)
DH97-29A	Basalt		Major(Cpx,WR)/Trace(WR)
DH97-28B	Basalt		Major(Cpx,WR)/Trace(WR)
DH97-28A	Scoria		Major/Trace(WR)
DH97-27B	Ignimbrite	DHF 1	Major/Trace(Cpx)
DH97-27A	Ignimbrite		Major/Trace(Cpx)
DH97-26C	Less welded ignimbrite		Major/Trace(Cpx)
DH97-26B	Welded ignimbrite		Major
DH97-26A	Pumice		Major/Trace(Cpx)
DH97-24	Ignimbrite		Major/Trace(Cpx)
DH97-22D	Phonolitic pumice		Major(Cpx,Amph,WR)/Trace(Cpx,WR)
DH97-22C	Black pumice block		Major/Trace(Cpx)
DH97-22B	Black glass		Major(Cpx,Amph)/Trace(Cpx)
DH97-22A	Ignimbrite		Major/Trace(Cpx)
DH97-20	Phonolite lava		Major(Cpx,WR)/Trace(WR)
DH97-19B	Lava		Major(Cpx,WR)/Trace(WR)
DH97-19A	Lava		Major(Cpx,WR)/Trace(WR)
DH97-18C	Basalt		Major/Trace(WR)
DH97-18B	Basalt		Major(Cpx,WR)/Trace(WR)
DH97-18A	Basalt		Major(Cpx,WR)/Trace(WR)
BASE OF CALDERA WALL			

Schematic overview of the stratigraphic successions in the Diego Hernández wall. Each stratigraphic unit; DHF 1, DHF 2 and DHF 3 begins with a basaltic series followed by more evolved products. Dotted line shows the transition from dominantly mafic to dominantly felsic deposits. The lithic breccia on top of the wall (El Abrigo ignimbrite) and the Bandas del Sur rocks represents the stratigraphical successiopn correlated with xenoliths.

Based on the stratigraphy of Wolff et al. (2000) and Neumann (pers. comm., 2001).

3 Analytical Methods

Clinopyroxenes from the lavas have been analysed for major elements on an automatic wavelength Cameca Camebax electron microprobe fitted with a LINK energy dispersive system for quantitative analysis at the Mineralogical-Geological Museum, University of Oslo. Before analyses were conducted, thin sections were coated with C-film. An acceleration voltage of 15 kV, sample current of 20 nA, and counting time of 10 seconds were used. For quantitative analysis the intensity of elements in the unknown sample is compared to standards. Both natural and synthetic minerals were used as standards. Matrix corrections were preformed by the PAP-procedure in the CAMECA software. Analytical precision (2σ) evaluated by repeated analysis of individual grains is better than ±1% for elements with concentration ≥20 wt% oxide, better than ±2% in the range 10-20 wt% oxide, better than 5% for elements in the range 2-10 wt% oxide, and better than 10% for elements in the range 0,5-2 wt% oxide.

Amphibole phenocrysts and trace scan of clinopyroxene from the lavas have been analysed at the Department of Geology, Univ. of Oslo, using a Cameca SX100 microprobe fitted with five crystal spectrometers at an accelerating voltage of 15 kV and a sample current of 20 nA.

Analyses of major elements of minerals from the syenites were carried out at the Geochemical Analysis Unit (GAU), GEMOC, Macquarie Univ., Sydney. Values were obtained using a Cameca SX50 electron microprobe (EMP), fitted with five crystal spectrometers, at an accelerating voltage of 15 kV and a sample current of 20 nA. The width of the focused beam was 15 µm. Standards were natural minerals and matrix corrections were done by the PAP method (Pouchou & Pichoir, 1984). Counting times were 10 s for peaks and 5 s for background on either side of the peak.

Trace element concentrations in clinopyroxenes and amphiboles were determinated using a Laser Ablation Microprobe (LAM) ICP-MS (Inductively Coupled Plasma Mass Spectrometer) on polished thick sections (110 µm) at the GAU, GEMOC, Maquarie

Univ., Sydney. A detailed description of the LAM and ICP-MS instrumentation and operating procedures has been given by Norman et al. (1996). The laser is a Q-switched Nd-YAG laser, operating at 266 nm (UV) and is focused through a petrographic microscope onto the sample. Operating conditions were preformed with repetition rate of 2-4 Hz and an energy of ~0,5-2 mJ/pulse, producing a sampling area of 30-50 µm in diameter and a maximum drill rate of ~0,5 µm/s. The ablated material is transported in a stream of high purity Ar directly into the ICP-MS system. Plasma operating conditions for the Perkin Elmer ELAN 5100 ICP-MS system included a forward power of 1040 W and nebulizer gas flow of 0,96 l/min, which gave a $^{248Th}/^{232}Th$ ratio of 0,5-1 %. Dwell times of 50-100 ms were used and counts were collected in peak hopping mode with one sweep per reading and one reading per replicate. Data collection, reduction procedures, precision and accuracy have been described by Norman et al. (1996). They demonstrate an instrumental precision of <5% at ppm levels.

Whole rock analyses were carried out in the Geoanalythical Laboratory at Washington State University. Major elements and Ni, Cr, V, Rb, Sr, Zr, Y, Nb, Ga, Cu and Zn were analysed by XRF using a Rh tube on low dilution Li-tetraborate fusion beads. REE, Ba, Th, U, Y, Hf, Nb, Ta, Rb, Cs, Sr, Pb and Sc were determined by quadropole ICP-MS after dissolution. Full details are given by Johnson et al. (1999) and Knaack et al. (1994), also available on WSU Department of Geology website at http://www.wsu.edu/~geolab/note.html.

4 Petrography

The phenocryst assemblages observed in this study from the Diego Hernández Formation cover the entire range of lithologies located at Tenerife, and correlates well with the data presented by Wolff (1985), Ablay et al. (1998) and Neumann et al. (1999). The compositional ranges of the Diego Hernández rocks are classified using the total alkalis-silica scheme of Le Bas et al. (1986), with nomenclature after Le Maitre (1989) on whole rock data. Basaltic, intermediate and phonolitic assemblages refer to basanite/plagioclase basanite, phono-tephrite/tephri-phonolite and phonolite, respectively (Figure 4.1). From basanites to phonolites the corresponding phenocryst assemblages are presented in table 4.1. Detailed petrographic descriptions of thin sections are given in Appendix I.

Figure 4.1. TAS diagram of whole rock data.

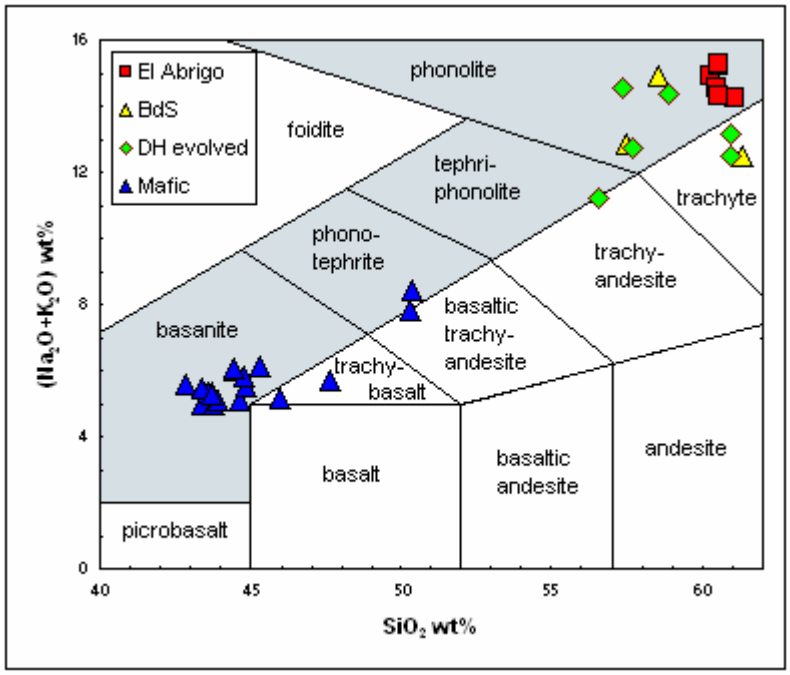

Total alkalis-silica classification diagram (Le Bas et al., 1986), nomenclature after Le Maitre (1998). Basanite compositions are termed primitive/mafic, intermediate rocks refers to phono-tephrite and tephri-phonolite compositions, and evolved rocks refers to phonolitic compositions.

The mafic lavas and scoria from the Diego Hernández Formation contain olivine, pyroxene and plagioclase as phenocryst phases. Phenocryst assemblages associated with different magma compositions in mingled units can be unravelled on

the basis of enclosing relations and intergrowths in aggregate grains. The phonolitic, intermediate and basaltic phenocryst assemblages are shown in Table 4.1. The Diego Hernández Formation mingled-magma pumices may contain up to 18 phenocryst phases (Wollf, 1985)

Nepheline syenites consist of a framework of alkali feldspar, feldspathoids and of mafic and accessory phases. On textural grounds, feldspar, nepheline, clinopyroxene and titanite are primocrysts.

Table 4.1. Schematic overview of phenocryst variations.

Rock type	**Accosiated phenocryst assemblages**
Basanite	ol+cpx(Al-salite)+mt
Plagioclase basanite	ol+cpx(Al-salite)+mt+plag±ap±ilm
Phono-tephrite	(ol)+cpx+mt+plag±ap±krs±ilm
Tephri-phonolite	cpx(Na-salite)+mt+plag+alk+ap+krs±ilm
Phonolite	cpx(Na-salite/Aegirine)+mt+alk+ap+krs±ne±ilm±sp

Variation in phenocryst assemblage corresponding to host rock composition. Ol, olivine; cpx, clinopyroxene; plag, plagioclase; mt, magnetite; ap, apatite; ilm, ilmenite; krs, kaersutite; alk, alkali feldspar; sp, sphene.

The relative onset of crystallisation of the different phases is graphically presented in Figure 4.3, where the mg# are used for the mafic phases and [Ca/(Ca+Alkalies)] for felsic phases.

Olivine (0,2-4 mm grains) is encountered as a phenocryst phase of mainly euhedral to subhedral texture among the mafic lavas and gabbroic xenoliths. The mineral is also found scattered as fragmented, anhedral and highly corroded crystals with visible reaction rims in more evolved compositions, associated with clinopyroxene and oxides. Mg-number[1] ranges from 84-39, with high mg# among the mafic compositions.

[1] mg# = atomic proportion: $\frac{Mg \times 100}{(Mg + Fe_{total})}$

Figure 4.2. Photomicrographs of samples.

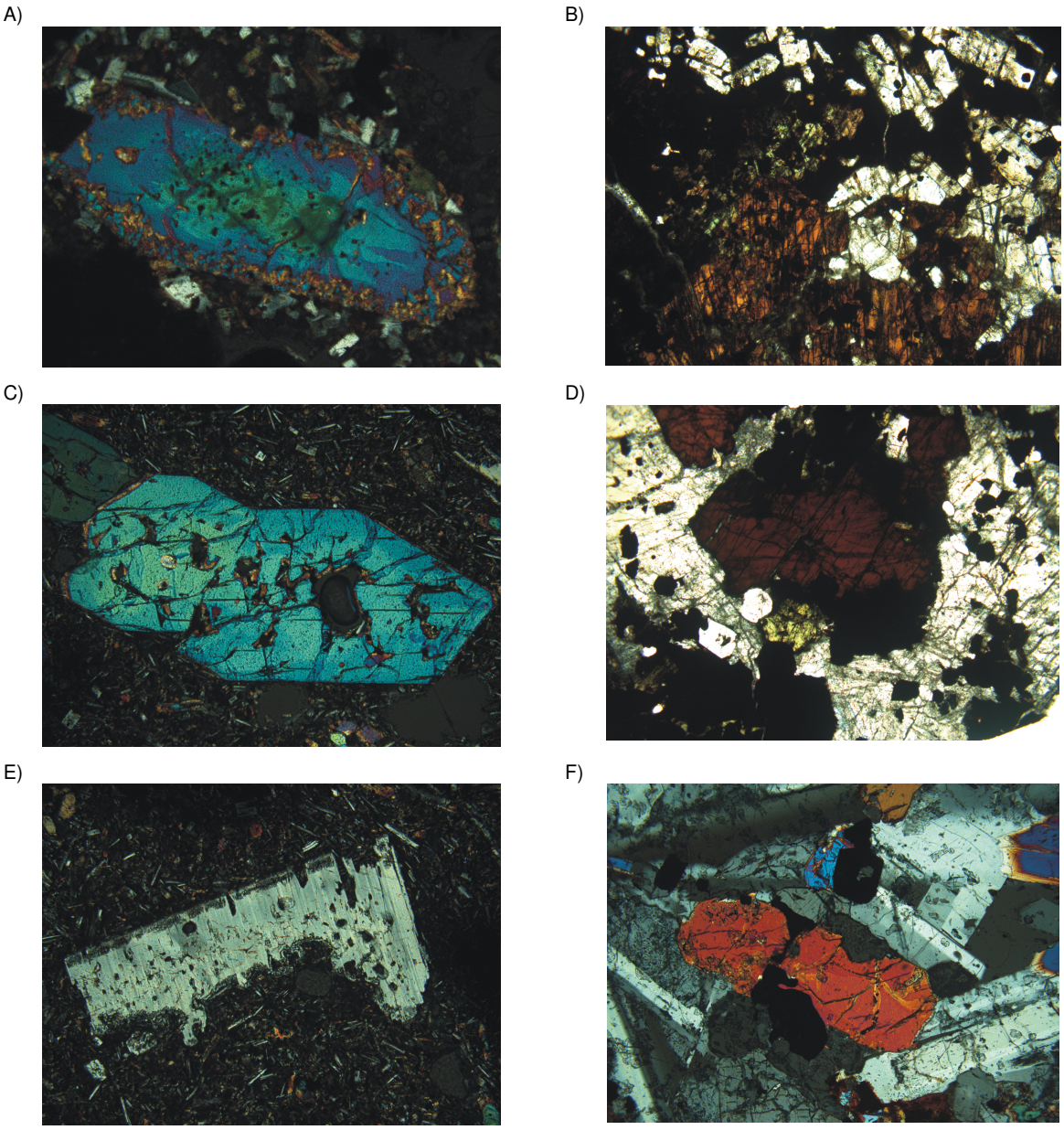

A) Zoned clinopyroxene (DH97-22; x10;scan analysis Figure 5.2). Green core showing signs of incipient melting mantled by two zones of different composition. Reaction rim towards matrix. B) Overview (x2,5) of sample TF12.2 showing large, corroded, anhedral laths of amphibole (brown), partially consumed clinopyroxene (green), oxides and anhedral plagioclase (white). All phases are clearly out of equilibrium to each other. C) Zoned euhedral clinopyroxene with inclusions of apatite in lava DH97-19B. Fine grained matrix of plagioclase needles and other minerals. D) Large corroded amphibole grains in a plagioclase matrix (TF12.3; x2,5). Reactions between oxides, amphibole and clinopyroxene(green). E) Corroded anhedral plagioclase grain with clear signs of melt disequilibrium (DH97-19B; x10). F) Crystalline syenite (TDKS17.11;x20) showing groundmass crystals of plagioclase surrounding corroded clinopyroxene with reaction rims towards oxides.

Clinopyroxene (<4 mm) occurs as euhedral to anhedral phenocryst and groundmass phase in all the rock types. Colours vary from olive- and pale-green through light-grey to pinkish-brown (Figure 4.2). Grey to pink clinopyroxenes show more euhedral textures in mafic domains and lesser signs of disequilibrium than green

clinopyroxenes, whereas in more evolved host rock compositions, observed green clinopyroxenes seems to be more in equilibrium (sub- to euhedral crystals) than grey to pink phenocrysts (corroded). Crystals are commonly observed with alternating green – pink zones (complex zoning), often fragmented, and frequently show signs of incipient dissolution (depending on host rock composition).

Plagioclase (<2 cm) occurs as the dominantly groundmass phase and as a phenocrystal (An_{90-21}) in mafic to intermediate rocks. Textures vary from euhedral to anhedral, often observed as broken fragments, and frequently have reaction rims (Figure 4.2). Signs of incipient dissolution ('sieve-texture') are present in some rocks. Phenocrysts are generally zoned.

Alkali feldspar and feltspathoids are restricted to the most evolved compositions where they occur as groundmass phases, creating a framework of (~1 mm) laths, or as large oikiocrysts growing interstitially. Crystals are subhedral to anhedral, have reaction rims, and are often zoned. Alkali feldspar varies from anorthoclase (Or_{22}) in the least evolved phonolites to sodic sanidine (Or_{75}) in the most evolved. Feltspathoids are rare in the the lavas but ubiquitous in the syenites.

Oxides are present in all the rocks as (Ti-) magnetite or ilmenite. In the most mafic compositions they are usually found as small grains (<0,2 mm) in the groundmass, or as inclusions in clinopyroxene. In more evolved compositions grains are scattered in the samples, but usually associated with mafic silicates (clinopyroxene and amphibole), where they form large (<3 mm) clusters replacing the silicates.

Amphibole (0,01-1 cm) occurs as an accessory phase in the intermediate lavas, but forms a major phenocryst phase in the syenites. Phenocrysts vary from euhedral to subhedral. Large anhedral grains which often show signs of corrosion and fragmentation are interpreted as xenocrysts. Most amphiboles observed are zoned.

Apatite is frequently present as small inclusions in clinopyroxene, plagioclase and amphibole, and forms an accessory phenocrystphase in the most evolved compositions. Apatite is observed in all compositions of syenitic origin, but restricted to intermediate to evolved compositions among lavas.

Figure 4.3. Generalised overview of changes in phenocryst assemblages.

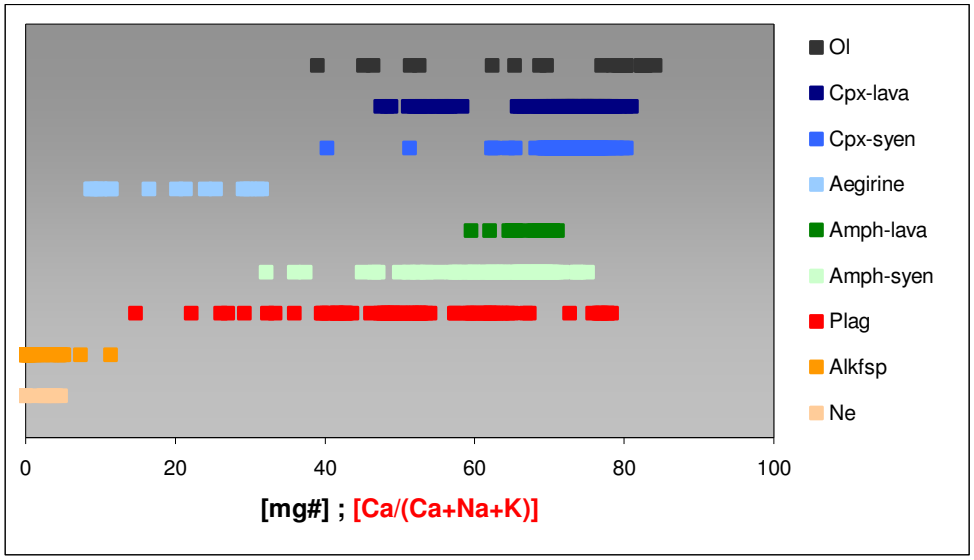

Schematic presentation of selected minerals from the Diego Hernández formation. Horisontal lines indicate the compositiional range for each spieces. X-axis is [Ca/(Ca+Na+K)] for feldspar an feltspathoids, and [Mg/(Mg+Fe)] for other minerals. Oxides, biotite and sphene are omitted.

5 Mineral Geochemistry

5.1 Clinopyroxenes

Clinopyroxenes from the analysed samples of lavas and syenites cover a wide range in compositions (e.g. mg# varying between 40,3 and 80,9). Within this range three compositional groups, similar to those of Wolff (1985), may be identified based on their major element relationships in oxide content plotted vs. mg#, and their trace element behaviour in spider diagrams plotted against primitive mantle (McDonough & Sun, 1995) composition.

5.1.1 Major Elements

The analyses were separated into the three groups based on their behaviour in two component diagrams. Since the Mg/Fe ratio of the analysed samples varies considerably, and the Mg content in clinopyroxenes is a function of temperature, where decreasing Mg content reflects crystallisation under decreasing temperature (Philpotts, 1990), plots of oxide vs. mg# where used to separate the groups. In Figure 5.1 the major elements of the clinopyroxenes are plotted in two-component diagrams.

In the TiO_2-mg# and Al_2O_3-mg# diagrams (Figure 5.1), the analysed clinopyroxenes fall in three separate groups. Groups 2 and 3 have similar, high mg#, 65,7 - 77,6 and 69,0 - 80,9, respectively, but differ in their TiO_2 and Al_2O_3 contents which are significantly higher for a given mg# in Group 3 (1,88-5,29 wt% TiO_2 and 4,41-10,33 wt% Al_2O_3) than in Group 2 (0,77-2,45 wt% TiO_2 and 1,81-8,90 wt% Al_2O_3). Group 1 has low mg#, 47,4 - 58,3, and low TiO_2 and Al_2O_3 contents (0,41-1,19 wt% TiO_2 and 1,16-2,76 wt% Al_2O_3).

Groups One and Two, referred to as Na-salite, display trends of increasing Na and Mn with falling Mg content, varying from 0,63 - 2,79 wt% Na_2O and 0,28 - 1,53 wt % MnO, whereas the Al_2O_3 and TiO_2 contents are relatively constant. Group Three, referred to as Al-salite, is the most common clinopyroxene found in the rocks (58% of analysis). Al-salites display a different trend from the Na-salites; little variation in Na

(0,37 - 0,83 wt% Na_2O) and Mn (0,01 - 0,25 wt% MnO), and an increasing trend in Al and Ti content with falling mg#. Ca content decreases with falling mg# (from 23,7 to 19,5 wt% CaO),

Figure 5.1. Selected major element oxides vs. mg#.

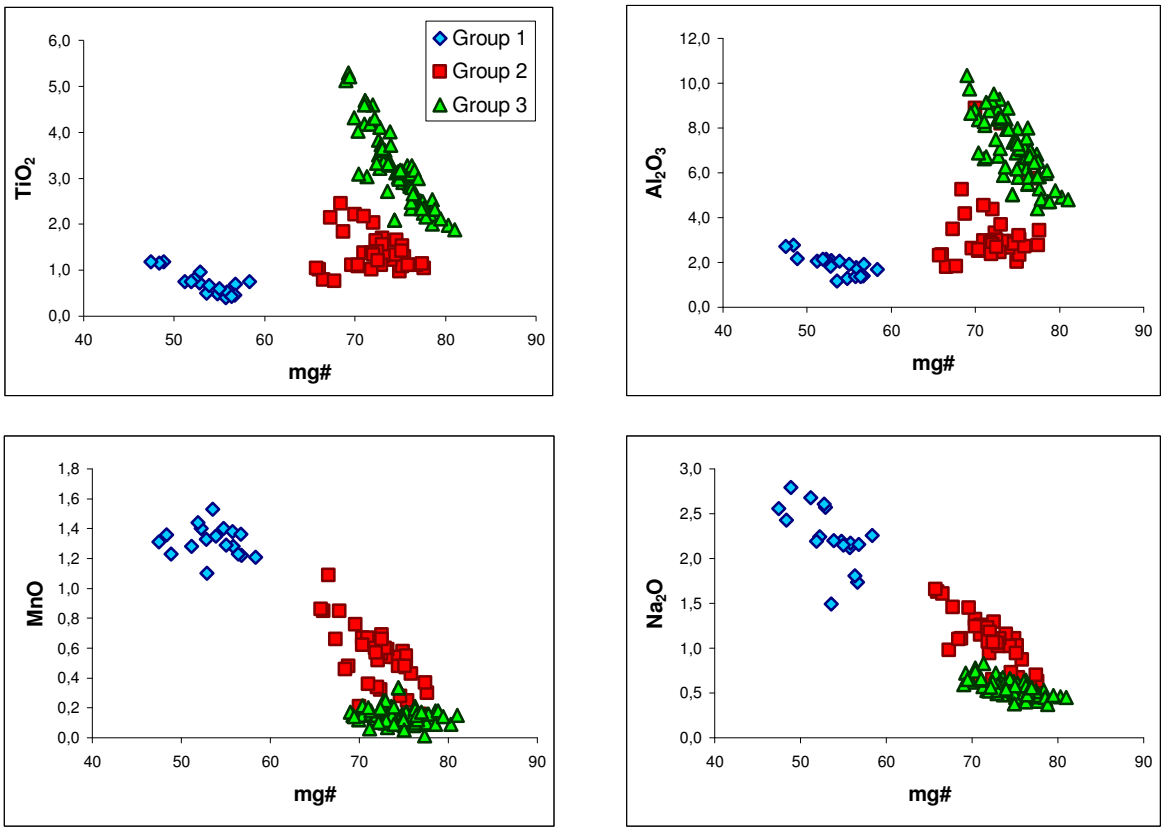

Binary plot of selected major elements vs. mg#. The clinopyroxenes define separate groupings within the plots. Although similar in mg# there is clearly no direct relationship between groups Two and Three. An evolutionary trend between Na-salites of Group One and Two may also be recogniced.

Lava analysis show, in general, good consistency in the distribution of elements between the different groups although some analysis displays deviations from the general trend. Sample DH97-18A illustrates this (Figure 5.1; Table A2.1) by having large differences in the Al/Ti ratio compared to other analysis, ascribing them to Assemblage Three when plotted against Al_2O_3, and Assemblage Two when plotted against TiO_2.

Most clinopyroxenes are zoned and display normal, inverse, alternating and sector zoning. Different types of zoning may be observed within the same sample. Complex

and inverse zoning are equally common. Within a single grain all three clinopyroxene groups may be present. Normal zoning is usually present in samples in which all clinopyroxenes belong to the same group, while inverse zoning is often associated with transition between groups. The complex zoning patterns shown in clinopyroxenes are illustrated by a point scan analysis of a representative clinopyroxene in sample DH97-22B (Figure 5.2). The inner corroded core (Z1) consists of a highly sodic salite of Group One, mantled by an intermediate sodic salite (Z2) of Group Two, which again is mantled by an outer rim of aluminous salite (Z3) of Group Three.

Figure 5.2. Zoning profile for the mantled clinopyroxene in sample DH97-22B.

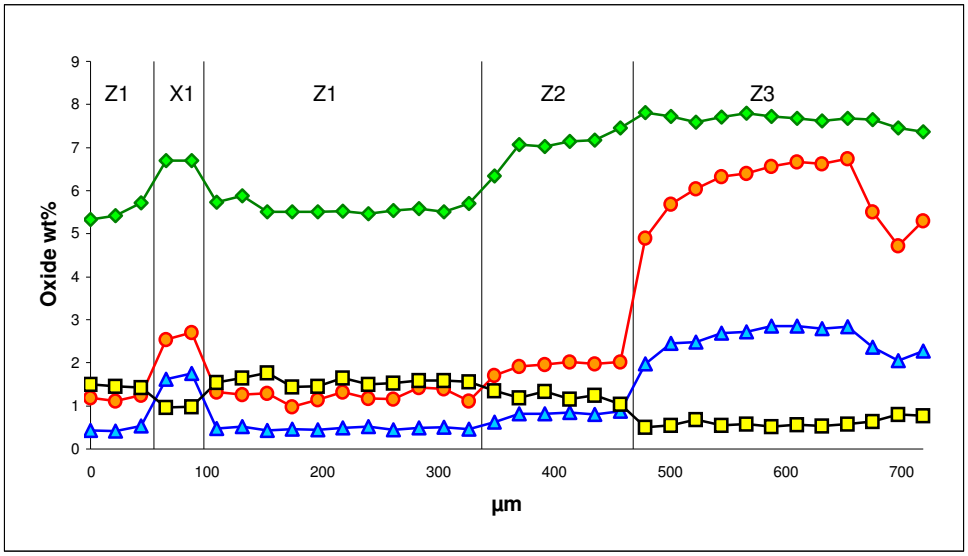

The mantled grain show incipient melting of the corroded inner core of Group One (Z1) between 50-90 microns (X1), causing a transition into Group Two. The abrupt transition in composition from the intermediate Na-salite of Group Two (Z2) to Al-salite overgrowth (Z3), and the homogeneous behaviour shown by major elements within each group should be noted. Diamonds: mg#/10; Circles: Al2O3; Squares: TiO2; Triangels: Na2O.

The clinopyroxene phenocrysts in the lavas and pyroclastic deposits from the different stratigraphical units in the Diego Hernández wall are distributed differently among the geochemical major element groups. Basaltic samples from the primary eruptive sequence (DHF 1; see Table 2.2) are slightly dominated by Al-over Na-salites when compared in TiO_2 content vs. mg# (Figure 5.3). In Contrast to DHF 1 samples, all basaltic DHF 2 samples are confined within Group Three, displaying an almost linear trend. The final basaltic eruptive sequence (DHF 3) show the same consistency as the DHF 2 samples (Figure 5.3).

Representative major element data on clinopyroxenes from evolved samples are only available from the DHF 1 sequence. Unlike those in the basaltic samples, the clinopyroxenes in the evolved samples from DHF 1 exhibit a more random distribution among the groups (Figure 5.3). Core to rim analysis are dominated by inverse zoning while mixing between groups are rare, only displayed in three samples. A sample (DH97-4) from the evolved DHF 2 pyroclastic deposits has also been analysed. Although too few major element data exist to give a general trend, these clinopyroxsenes, which are dominated by Al-salites, would seem to have a more mafic character than in the evolved DHF 1 samples (Figure 5.3). All samples show normal zoning and very consistent evolution within a single grain.

Figure 5.3. Stratigraphical separation of The Diego Hernández Formation.

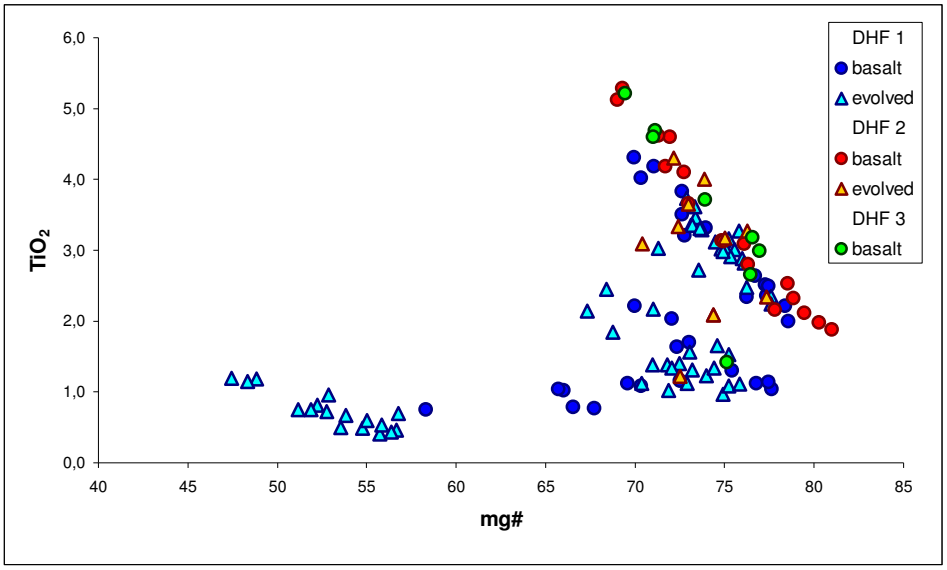

Major element variations according to stratigraphy of the DH cycle. With each new cycle of basaltic lava in the stratigraphical succession (Table 2.2), the analysed clinopyroxene phenocrysts start to evolve along the Al-salite trend.

Xenoliths of plutonic origin are a locally common feature of the entire Tenerife succession, and mostly range from ultramafic types through alkali gabbros to mafic syenites (Wolff, 1987). Nepheline syenite xenoliths occur as lithics in some of the pyroclastic deposits in the Diego Hernándes Formation or from its more distal facies and represents phonolitic magmas which crystallised in the subvolcanic magma system. Analyses of syenitic xenoliths, interbedded in the eruptive sequences of the Diego Hernándes Formation, display many of the same characteristics seen among

the extrusives and provide an unusual opportunity to compare syenite mineralogy with that of equivalent material quenched at the magmatic stage.

The three groups recognised from the lava analysis are all present in the syenite analysis (Figure 5.4). However, there are clear differences in the distribution between groups. Contrary to the extrusives, syenites are dominated by Na-salites (75%) over Al-salites (25%). Group One samples are absent from the corresponding Diego Hernándes lavas, only recognised from the post DH-cycle (TDKS samples corresponding to the Pico Viejo cycle).

Figure 5.4. Selected syenite major elements vs. mg#.

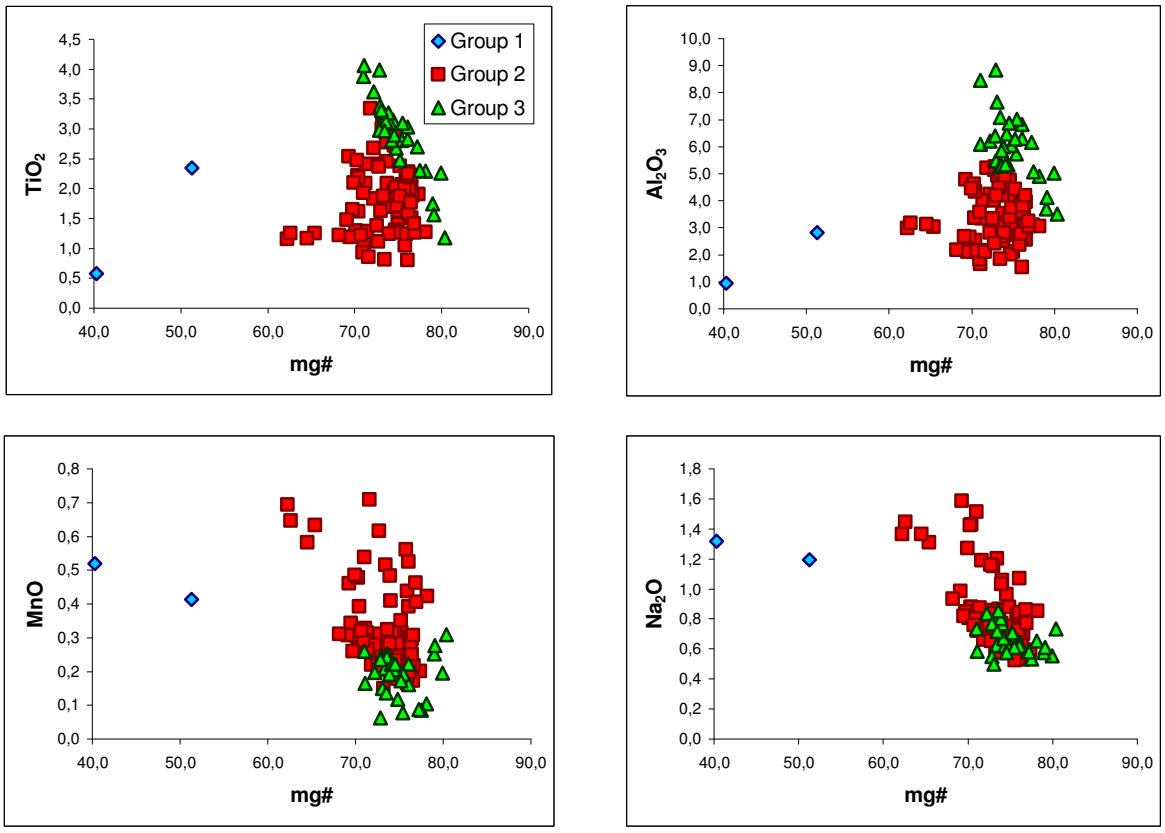

Binary plot of selected syenite major elements vs. mg#. The same three compositional groups presented among lavas (Figure 5.1) are recogniced. However, lower Mn and Na content in syenites does not support the Na-salite trend found in the lava samples. Also, Group Two and Three samples are more scattered and overlap each other to a great extent, especially in Mn and Na plots.

The general trends among the syenitic Na- and Al-salites are the same as for the lavas. Na-salites [Group One (mg# 40,3 - 51,3) and Two (mg# 62,2 - 78,2)] display the same flat patterns for Al and Ti (Al_2O_3 and TiO_2 varying between 0,94 - 6,21 wt%

and 1,07 - 4,06 wt%, respectively) as seen in the lavas. Na and Mn contents (0,80 - 1,59 wt% Na_2O and 0,18 - 0,71 wt% MnO) of syenites mirrors those of the lavas with increasing oxide contents with falling mg#. However, the syenites exhibit the highest Na and Mn contents among the Group Two analysis. The Al-salites (mg# 71,1 - 80,4) contain 1,07 – 4,06 wt% TiO_2, 1,66 – 8,85 wt% Al_2O_3, 0,06 – 0,31 wt% MnO and between 0,50 – 0,85 wt% Na_2O, and define a trend of increasing TiO_2 and Al_2O_3, and a relatively constant MnO and Na_2O with decreasing mg# (Figure 5.4).

Although not enough data exists to give a general trend, the two Group One analyses seemingly display different characteristics than the lavas. Their mg# range from 40,3 to 51,3 and show large differences in their oxide contents with decreasing Mg content (Figure 5.4).

Most syenitic clinopyroxenes are either normal, invers, complex or sector zoned. Normal zoning (decreasing mg#) dominates when Na-salites are converted to Al-salites, and inverse zoning dominates where assemblage trasitions from Al-salites to Na-salites occur.

5.1.2 Trace Elements

Magmatic processes and multicomponent phase relations are still too poorly understood for petrologists to explain precisely the major element variations in suites of differentiated igneous rocks. However, trace element variations are often simpler to understand. Unlike major elements, trace elements are not essential to the stability of the phases involved, and thus play a relatively passive role. Nonetheless, their concentrations are affected by magmatic processes. Distribution coefficients for many trace elements do not vary significantly over the temperature intervals through which most magmatic differentiation takes place. They can therefore be used to determinate the equilibrium distribution of trace elements between crystals and magma during differentiation.

The trace element concentrations were normalised to the composition of the primordial mantle (PM) of McDonough & Sun (1995), and plotted in spider diagrams in order of increasing compatibility from left to right. Particular minerals will have a

characteristic effect upon the shape and curves in such diagrams during melting and crystallisation. Effects produced by a given mineral depend on its relative abundance and on the magnitude of its D value (partition coefficient) for a particular element (Cox et al., 1979).

Ten thin sections from evolved units in the Diego Hernández formation were selected for trace element analysis (Table 2.2). The differences in major element compositions exhibited by Al- and Na-salites are reflected in their trace element concentrations. Since corresponding major and trace element data exists, the same three assemblages defined from major element data are recognised in trace element concentrations.

Compared to Na-salites, the Al-salites in general show lower concentrations in rare-earth elements (REE[2]) and Y, and are higher in compatible elements such as Cr, Ni and Co, typical for their more 'mafic' character (e.g. Al-salites: 4,4-10,8 ppm La, 3-184 ppm Ni, and 57-127 ppm Sc; Na-salites: 14,3-74,2 ppm La, 0,3-2,5 ppm Ni, and 18-38 ppm Sc; Appendix II, Figure 5.5). However, striking differences between Groups One and Two of the Na-salites are revealed in the spider diagrams. The unison and orderly behaviour of the two groups displayed among the major elements may not readily be transferred to the trace elements. Thus, comparing groups rather than the supposedly defined geochemical trend seen among major elements vs. mg# seems more appropriate for the trace elements.

Group One trace element concentrations display a uniform distribution in spider diagrams (Figure 5.5), with only small deviations from the mean trend. PM-normalised values show pronounced negative anomalies for Sr, high concentrations of La (light-REE; LREE), Yb and Lu (heavy-REE; HREE), separated by a concave pattern with low concentrations for middle-REEs (MREE), high values for Zr and Hf (994-2777 ppm, and 26-85 ppm, respectively). The low concentration of Ti, the negative anomaly of Eu, and the negative correlations (>1) between (Sc, V)/REE should also be noted.

[2] Rare-earth elements (REE) refers to the lanthanides, Lanthanium(57)-Lutetium(71), of the transitional group of the perodic table. Light-REE: La-Sm; Heavy-REE: Eu-Lu. Promethium(61) does not occur in nature.

Figure 5.5. PM normalised lava trace element patterns.

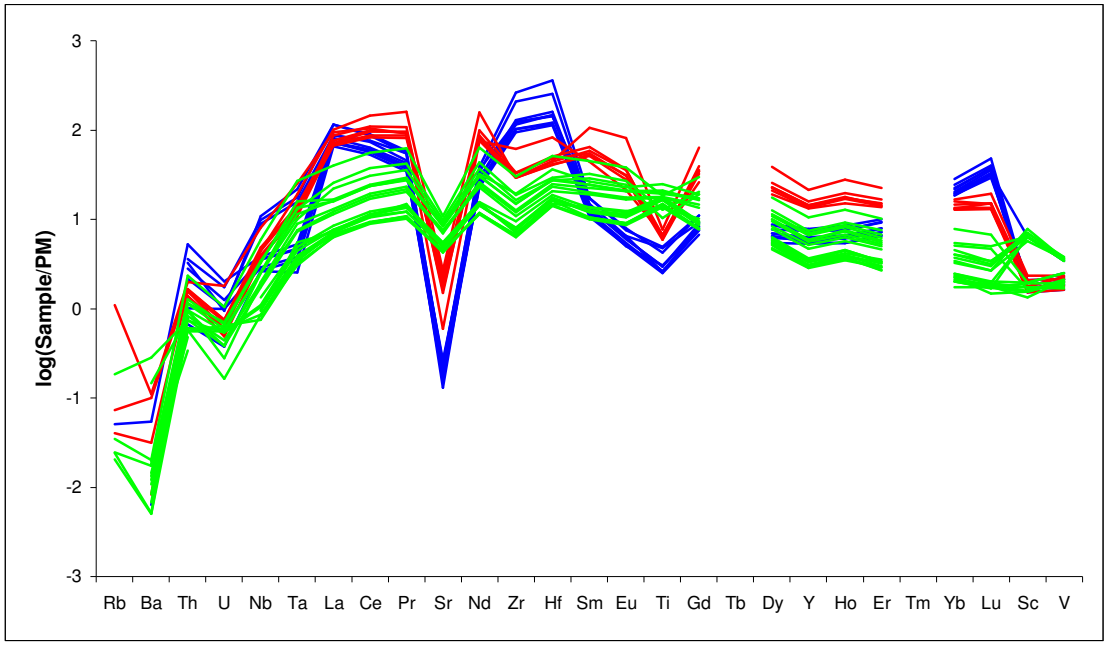

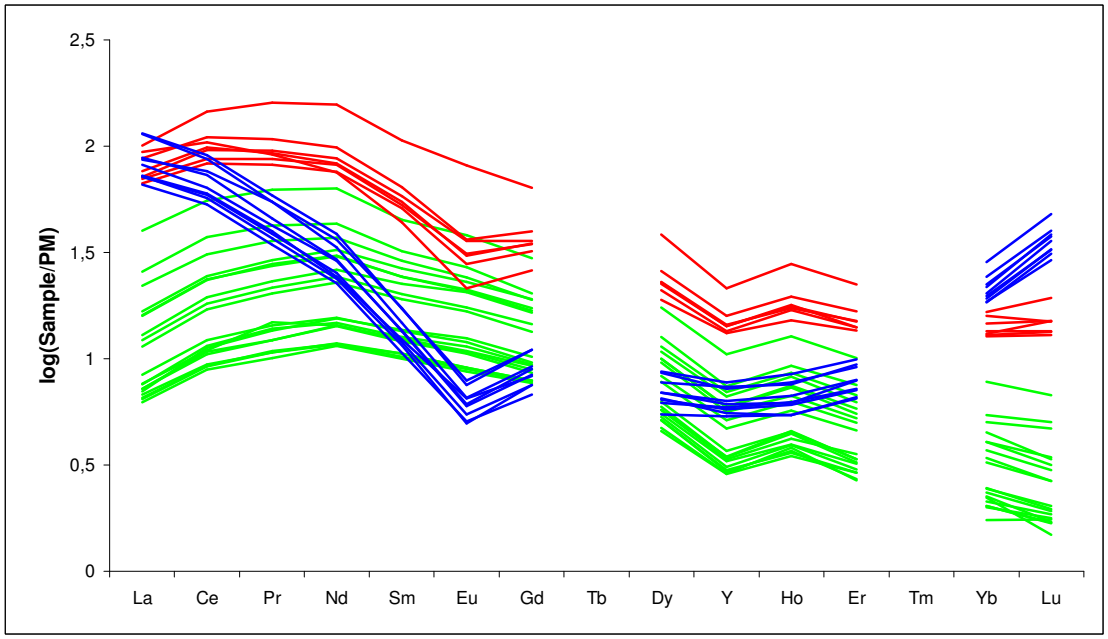

Trace element concentrations in lavas normalised to the primitive mantel of McDonough & Sun (1995). The three compositional groups recognise from major elements are also found among trace elements. Blue, red and green lines are Group One, Two and Three, respectively. The downward concave pattern of Group Three samples should be noted.

Group Two clinopyroxenes shows (Figure 5.5) an upwards convex REE pattern with elevated values from La to Eu, and a gradually decreasing trend towards the most incompatible elements (e.g. 14,3-65,1 ppm La, 11,7-43,1 ppm Sm, 2,2-7,0 ppm Yb), yielding positive ratios for LREE/HREE, weakly negative anomalies for Zr and Hf, and

low Sr* and Ti* values[3] . The data also display positive ratios for REE/(Sc, V). Note that there is a slight difference in trace element concentration between DHF1 and DHF 2 samples (Figure 5.6).

Primitive-mantle normalised values of Group Three display two different patterns, distinguished by variations in Ti*, Sr*, Sc anomaly, and in their overall trace element concentrations. (Figure 5.5). Group Three samples of DHF 2 have smaller positive Ti anomalies, larger negative Sr anomalies, and have overall higher trace element concentrations than DHF 1 samples. Spider diagrams show a positive slightly streched convex pattern for REEs and, unlike Na-salites, no negative Eu anomaly.

Similar to the major elements, within a single thin section all three assemblages may be present. Differences between the stratigraphical sequences are also evident from trace element data. The Al-salites of DHF 1 and DHF 2 are easily recognised based on their Ti concentrations, where DHF 1 samples have a much larger positive Ti anomaly than DHF 2 samples. In general all DHF 2 analyses show higher trace element concentrations than DHF 1 samples (Figure 5.6).

Nine syenite samples were selected for trace element analysis, yielding a total of 83 analyses distributed among DH, TF and TDKS series.

Syenitic Group One analysis was divided into two groups; High and Low, based on their trace element concentrations (Figure 5.7). Their general trace element pattern mirrors each other, but the High Group One display overall higher trace element concentrations compared to the Low Group One (High Group One: 2,28-2,33 ppm Ta, 114-123 ppm La, 79,9-81,1 ppm Sr, 6423-7123 ppm Ti and 14,8-17,8 ppm Er; Low Group One: 0,36-1,77 ppm Ta, 33,4-46,9 ppm La, 94,1-142 ppm Sr, 8771-10574 ppm Ti and 2,57-3,78 ppm Er). Both Group One samples are enriched in LREE, Zr and Hf with respect to MREE, show pronounced negative Sr and Ti anomalies, and show a weak tendency of enrichment in HREE/MREE, forming a

[3] Negative Sr and Ti anomalies are measured as the ratio between PM-normalised Sr and Ti (Sr_N and Ti_N), and hypothetical values falling on the straight lines Pr_N-Nd_N and Eu_N-Gd_N, respectively. [$Sr_N/Sr_N^* = Sr^N \times 2/(Pr_N+Nd_N)$, $Ti_N/Ti_N^* = Ti_N \times 2/(Eu_N+Gd_N)$]. Neumann et al. (1999).

slightly downward concave pattern for REEs. Of the two groups it is the Low group that resembles the Group One clinopyroxenes in the lavas (Figure 5.5 & 5,7).

Figure 5.6. PM normalised trace pattern for DHF 1and DHF2 samples.

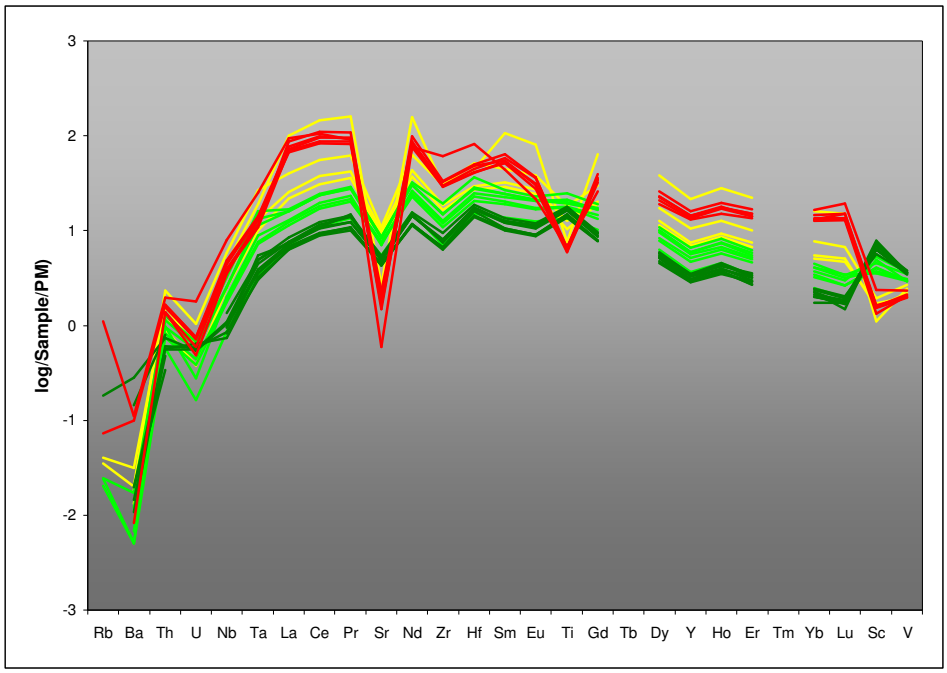

Spider diagram showing the compositional differences in trace element concentrations between DHF 1 and DHF 2 samples. DHF 2 samples occupy an intermediate position between Group Two and Three samples of the DHF 1 sequence, with higher trace element concentrations when comparing Group Three samples, and generally lower trace element concentrations when comparing Group Two samples. Dark green and red lines, DHF1; light green and yellow lines, DHF 2.

The syenitic Group two, although the sample set of analyses cover a wider range of trace element concentrations (e.g. 22,5-247 ppm Sr, 14,1-47,8 ppm Sm), are almost identical to those in the lavas when averages are compared. Only Sr and Ti anomalies are slightly less negative for the syenites (Figure 5.5 & 5.7). The absence of a negative Eu anomaly should be noted.

Group three also mirrors that in the lavas when averages are compared (Figure 5.5 & 5.7), the only deviation being the slightly negative Ti anomaly in syenites.

Figure 5.7. PM normalised syenite trace patterns.

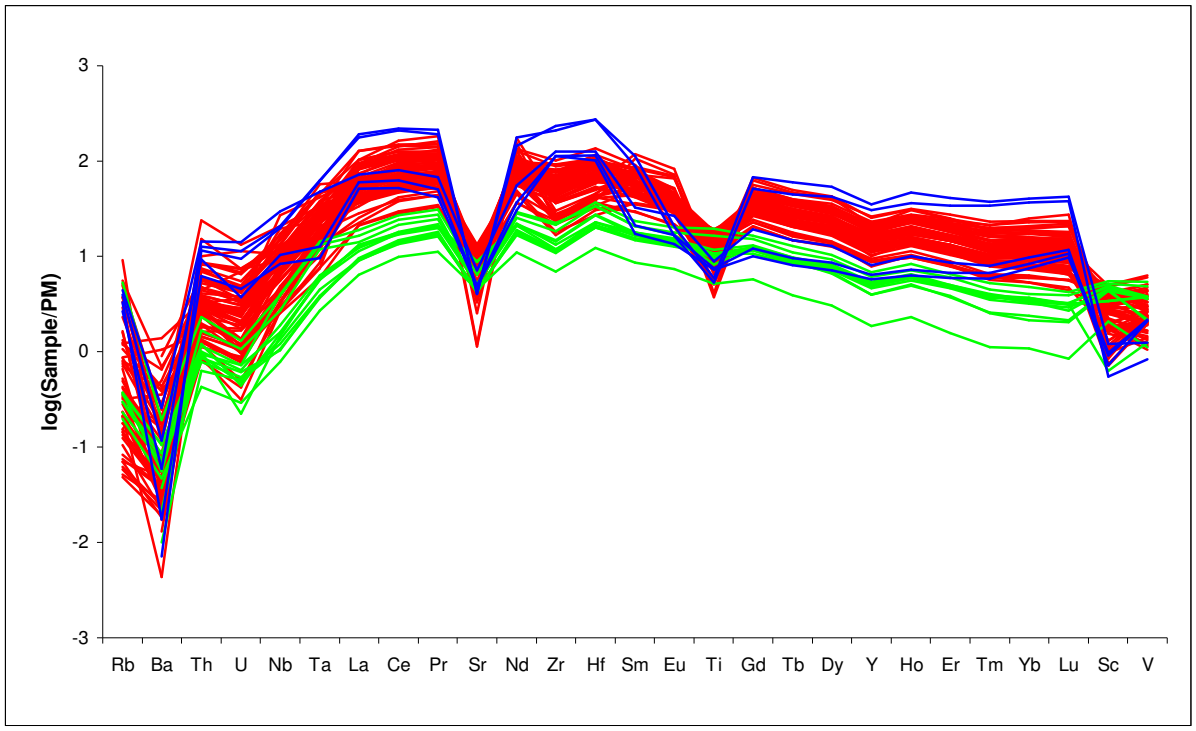

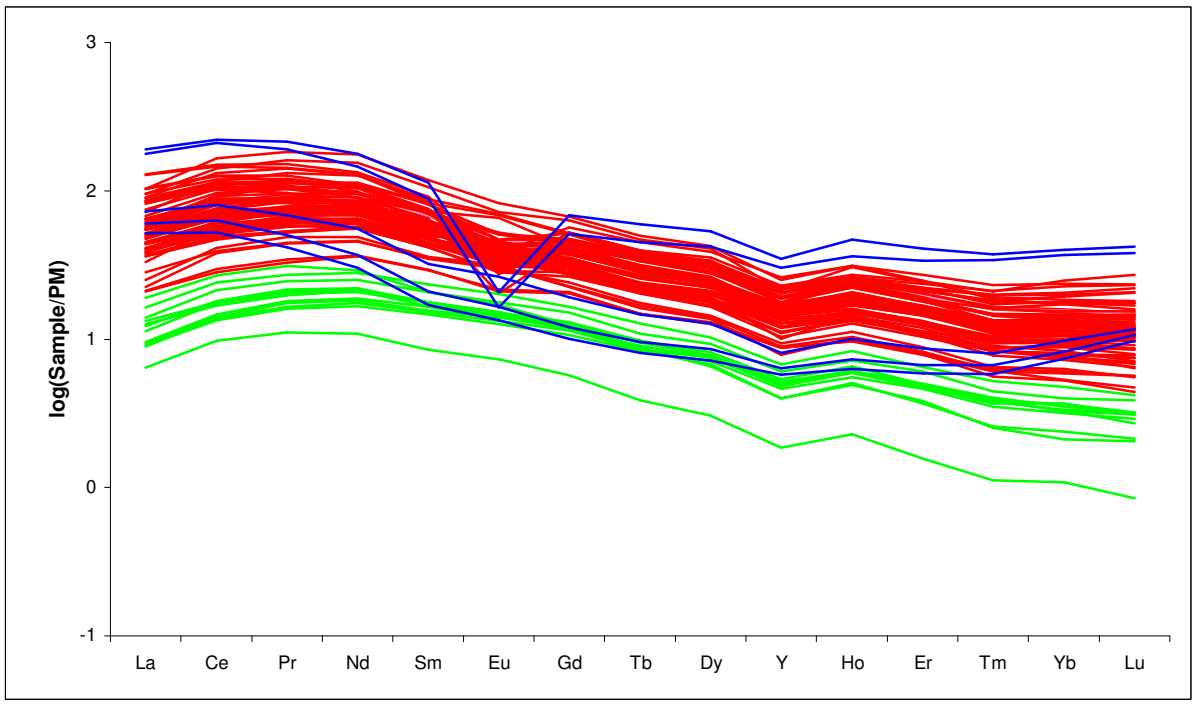

PM normalised syenitic trace element concentrations. Blue, red and green lines corresponds to Group One, Two and Three, respectively. Note that Group One lines define two separate trends, evident from the Eu anomaly and the overall concentrations in REE and very incompatible elements.

5.2 Amphiboles

The most commonly found amphibole in the Tenerife rocks is the high-Ti bearing kaersutite, a typical constituent of alkaline volcanism. Although kaersutite only present itself as an accessory phase in the intermediate rocks, several authors (e.g. Kesson & Price, 1972; Ablay et al., 1998) have pointed out the importance of an amphibole on the liquidus during fractination as a mineral that can impose significant constraints on other phases and element distribution. Since few analyses from lavas are presented, these data will be presented among syenite analysis.

5.2.1 Major Elements

As for clinopyroxenes, the mg# of amphiboles cover a wide range in compositions (32,1 - 75,1), is a function of temperature, and thus serves as a way to determine crystallisation trends. Amphiboles appear on the liquidus during the intermediate stage of crystallisation (Ablay et al., 1998), and are therefore not suspected to show the basaltic component (high-mg#) displayed by the clinopyroxenes.

Two-component diagrams of mg# vs oxides are presented in figure 5.8 and show a grouping of two different crystallisation trends. Although not present in all plots there is a clear distinction between the two trends, especially when comparing Al, K and F content with mg#. The Ti content varies between 2,52 - 6,71 wt% TiO_2, with highest content in the mafic part of Trend 1, displaying decreasing concentrations towards lower mg#. Trend 2 displays an almost flat, linear trend with a slight decrease in Ti content in the lower mg# range in the TiO_2-mg# diagram. Al_2O_3 wt% varies between 7,45 - 13,53 and show a linear slightly decreasing and slight increasing trend for Trend 1 and Trend 2, respectively, merging at low Mg content, with Trend 1 always being the most Al-rich. Mn content lie in the range 0,07 - 0,78 wt% MnO. Trend 1 analysis cover the lowest values at highest mg# and steadily increase with falling Mg content until mg#=50, where Mn content decreases. Trend 2 analysis show two lineages; one with a flat pattern between 0,2 - 0,4 wt% MnO, and one increasing trend with falling mg# (DH97-39.9 series). The distribution of alkalis shows somewhat different characteristics. Sodium (2,45 – 3,54 wt% Na_2O) display a flat pattern with no

clear difference between the trends, while potassium (0,73 – 1,82 wt% K_2O) show an increasing tendency while mg# is dropping for both trends, with Trend 2 being the most K-rich. Another feature clearly dividing the trends is the F content (0,13 – 1,92 wt%). Trend 1 shows similar concentrations unrelated to mg#, situated below 0,40 wt% F, and Trend 2 displays a somewhat scattered decreasing pattern with falling mg#, but never occurs below 0,56 wt% F.

Figure 5.8. Selected amphibole major element oxides vs. mg#

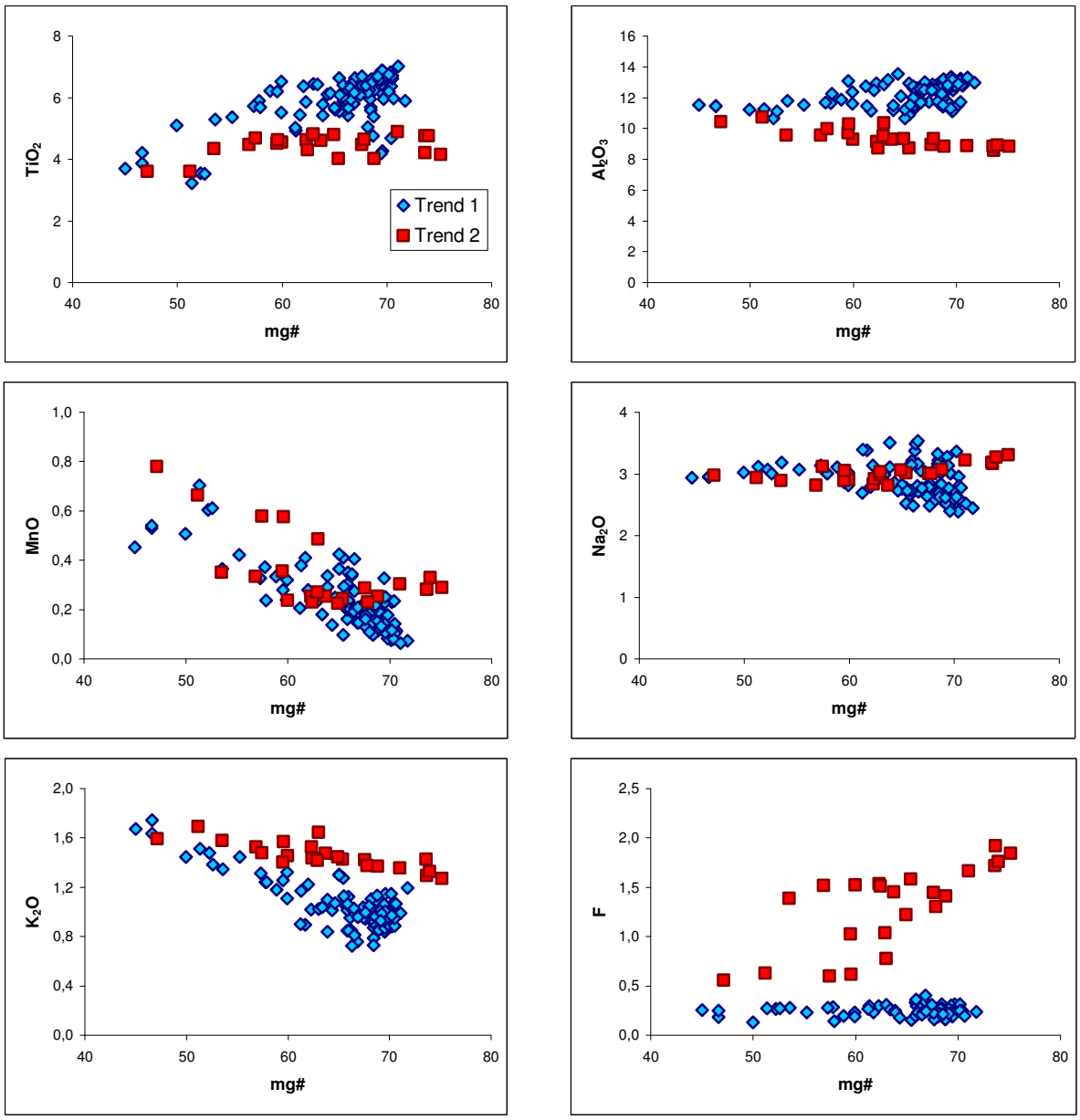

Large variations in F content reveal two crystallisation trends for amphiboles. These crystallisation trends are also recognised in K, Al, and to a lesser degree in Ti plots, but absent in other major element plots.

5.2.2 Trace Elements

Six syenitic samples have been selected for trace elements analysis. Individual analyses within each sample overlap each other to the extent that only averages need to be presented (Figure 5.9). The two trends among major elements are also recognised in trace element concentrations.

Trend 1 and Trend 2 analysis comprise both the TF and DH series (Figure 5.9). The pattern exhibited by DH97-39.9 deviates somewhat from the mean Trend 2 analysis. Trend 2 amphiboles (excluding DH97-39.9) are overall higher in REE and HFSE[4] concentrations (e.g. Trend 1: 17-43 ppm La, 61-124 ppm Nd, 3,4-8,1 ppm Er, 4,1-8,4 ppm Ta and 114-250 ppm Zr; Trend 2: 183-288 ppm La, 177-341 ppm Nd, 11,4-21,1 ppm Er, 20-79 ppm Ta and 870-2852 ppm Zr).

Characteristics of Trend 1 analysis are positive correlations of HREE/LREE, with a convex pattern for HREE and a gradually linear decreasing pattern for LREE, no negative Eu anomaly ($Eu^{*}>1$), positive anomalies for Nb and Ta, and negative anomalies for Zr and Hf (Figure 5.9). Sr anomalies shift from slight positive to slight negative for TF12.1 and TF12.2, respectively, and Ti anomalies are more negative for TF12.2 than TF12.1 samples ($Ti^{*}_{TF12.1}<Ti^{*}_{TF12.2}$). Trend 2 trace element concentrations display the same pattern as Trend 1 analysis for REEs except a marked negative Eu anomaly, they have positive HFSE anomalies, and marked negative anomalies for Sr and Ti (Figure 5.9).

The DH97-39.9 series have elevated PM-normalised values for HREE/LREE, where HREE display a gradual decrease and LREE show a concave pattern, a slight positive Ti anomaly, negative Sr anomaly, and elevated values for HFSE with peaks for Zr and Hf and large differences in Nb and Ta (Figure 5.9).

[4] High Field Strength Elements. Cations with relatively small size and high charge (e.g. U^{4+}, Th^{4+}, Nb^{5+}, Ta^{5+}, Zr^{4+}, Hf^{4+})

Figure 5.9. PM normalised trace element patterns for amphiboles.

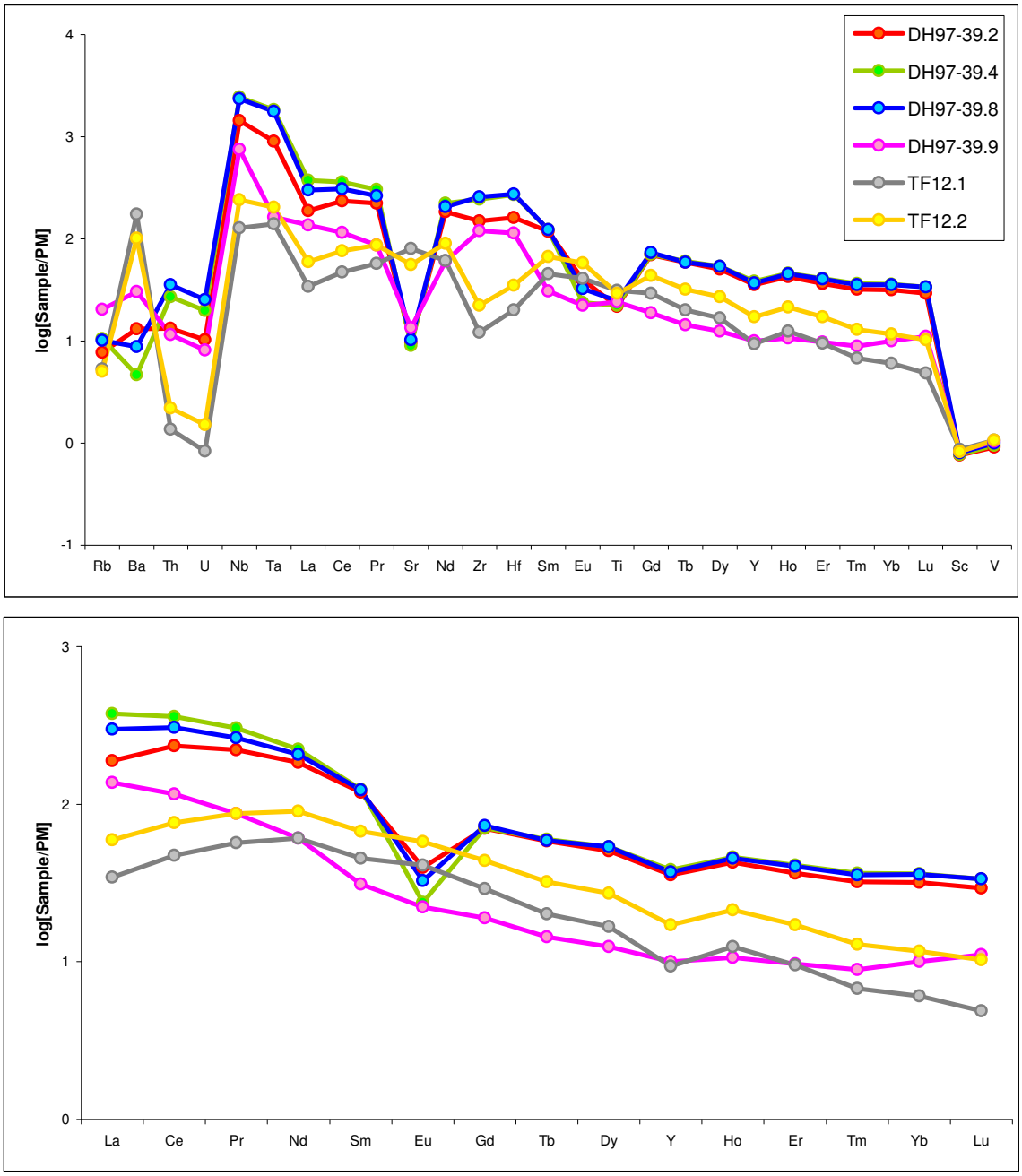

Amphibole trace elements concentrations normalised to the primitive mantle of McDonough & Sun (1995). *Patterns reveal three different crystallisation trends, manifested in the overall trace element concentrations, Nb/Ta ratios, and Sr and Eu anomalies.

6 Whole Rock Analysis

In order to directly measure and quantify the igneous differentiation process, bulk rock compositions of representative samples are presented to track changes and evolution of the Diego Hernándes magmatic cycle.

Whole rock samples are divided into mafic (DH lavas and gabbroic xenoliths; 8,8-4,5 wt% MgO) and evolved (DH phonolitic pumices, El Abrigo and Bandas del Sur syenites; 1,6-0,2 wt% MgO) compositions. Major element variations of Ti (0,33 - 4,18wt% TiO_2), Fe (2,61 - 12,3 wt% Fe_2O_3), Ca (0,56 - 11,8 wt% CaO) and P (0,03 - 1,67 wt% P_2O_5) all display the same crystallisation trend (Figure 6.1). The highest content of oxides is found in the mafic samples, showing a relatively flat trend, followed by a decreasing trend among evolved samples with decreasing MgO content. The Al (14,7 - 22,0 wt% Al_2O_3) content show a steadily increase from the mafic to the evolved compositions with decreasing MgO content. The agpaitic index[5] of the mafic composition show a relative constant ratio of ~0,5, but increases towards peralkalinity (>1) in the evolved compositions (Figure 6.1).

Whole rock mafic compositions show (Figure 6.2) decreasing trace element concentrations in Ni (88 - ~0 ppm) and Cr (350 - 4,5 ppm), relatively constant low concentrations in La(60 - 90 ppm) and Nb (83 - 190 ppm), constant high concentrations in Sm (9,5 - 16,5 ppm), and a general trend of slightly increasing concentrations in Sr (647 - 1378 ppm) with decreasind MgO content. Evolved compositions show an entirely different trend than the mafic samples. Trace element concentrations in Cr and Ni are low (9,0 – 0,0 ppm; 10 – 4,0 ppm, respectively), they display a decreasing trend in Sr (581 - 22,3 ppm) and Sm (13,9 - 2,7 ppm), and an increasing trend in La (84 -207 ppm) and Nb (153 - 653 ppm).

Primitive mantle normalised whole rock trace element concentrations are presented in Figure 6.3. The mafic trend recognised from major elements are also defined in the spider diagram, defined by a slightly decreasing trend from left to right, without any

[5] $\frac{Na + K}{Al}$, total alkalies over aluminium.

significant deviating anomalies. Evolved compositions define two trends in the spider diagram. One trend show elevated concentrations in HFSE, negative Sr and Ti anomalies, and a trend of decreasing LREE-MREE and flat MREE-HREE pattern.

Figure 6.1. Whole rock major element variations

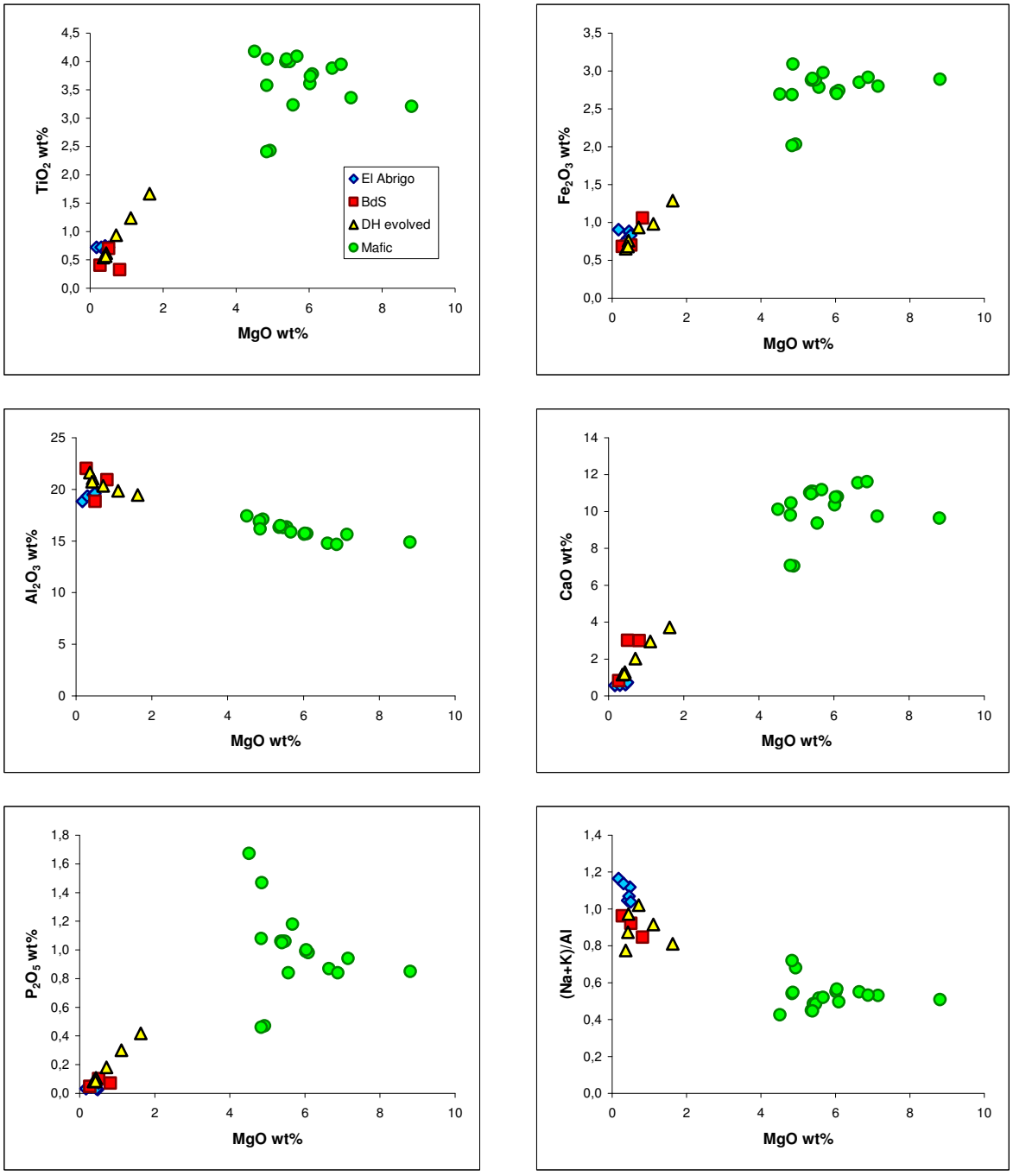

Variations in selected WR major elements vs. MgO. See text for discussion.

Figure 6.2. Whole rock trace element variations.

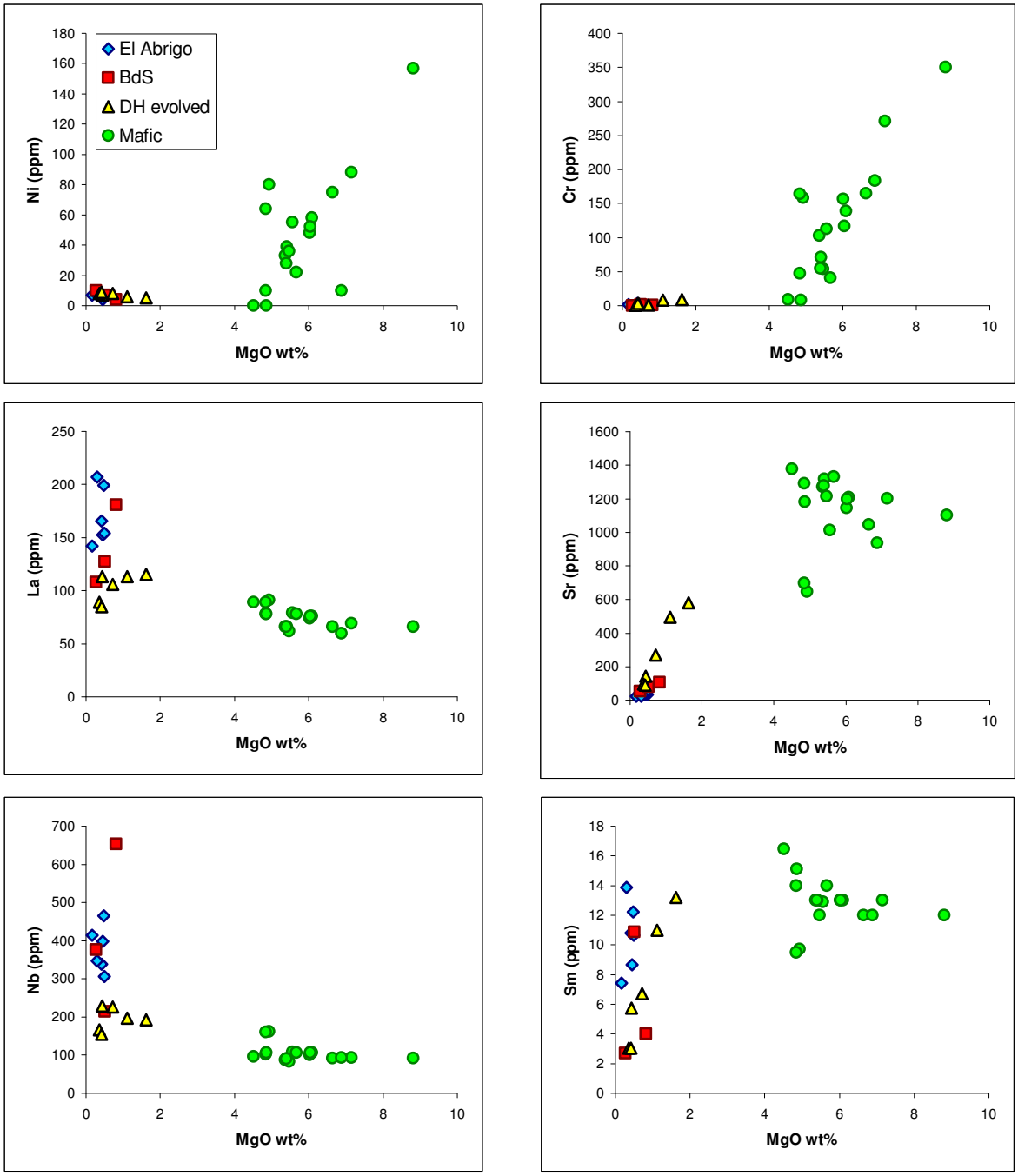

Variations in selected trace elements vs. MgO. Mafic and evolved compositions display different crystallisation trends. See text for further discussion.

The majority of these samples are from the El Abrigo samples. The other trend found among the evolved compositions mirrors the trend described above, but show more depletion in REEs, displaying a downward concave pattern with positive (LREE,HREE)/MREE ratios, smaller Sr anomaly, and is enricher in Zr and Hf, with respect to LREE. Various degrees of enrichment in Zr, Hf and HREE concentrations,

where BdS syenites define the most enriched trend, and DH samples define the least enriched trend, should be noted.

Figure 6.3. Primitive mantle normalised values of whole rock trace elements.

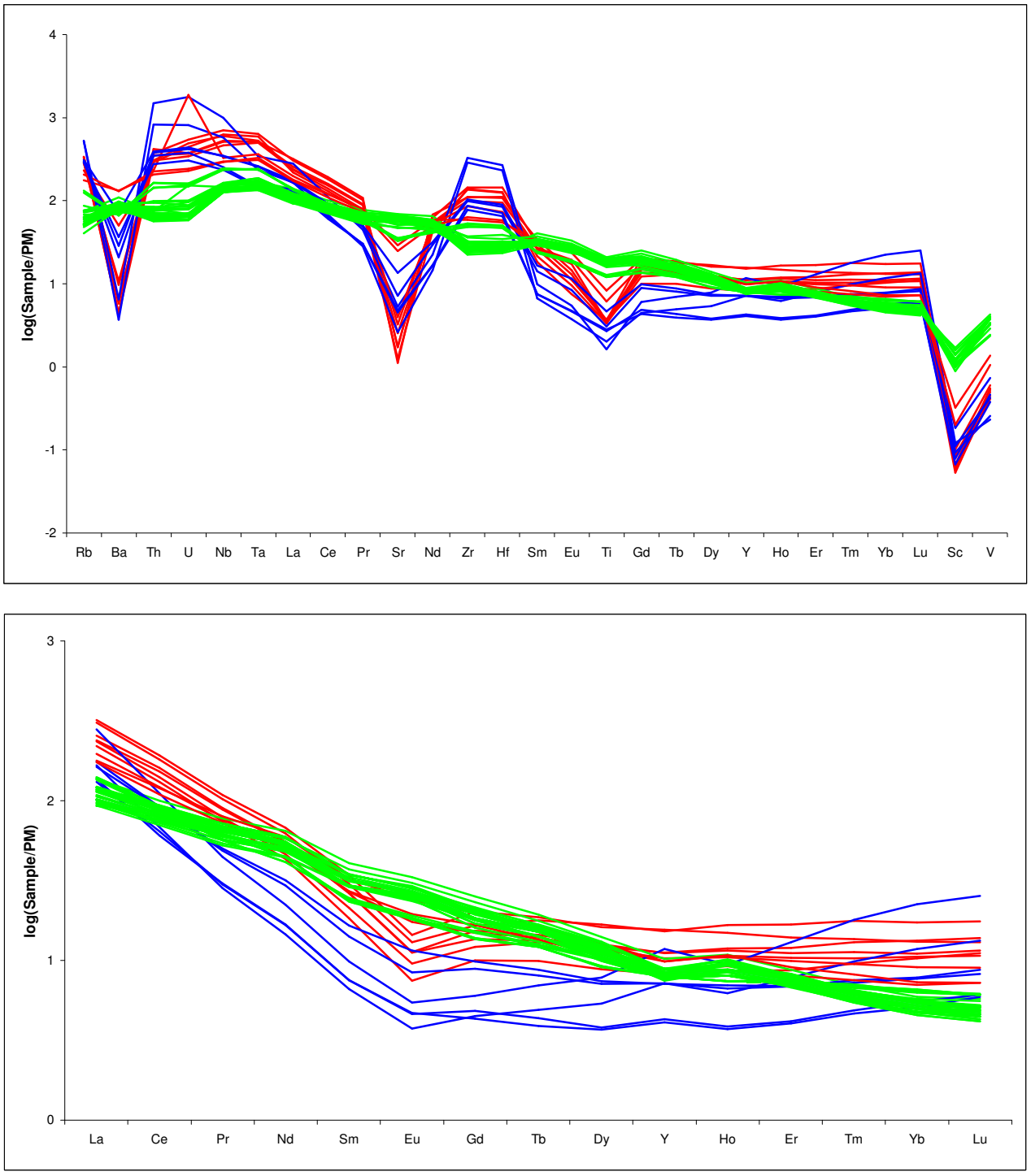

Spider diagram of trace elements in whole rock normalised to the primitive mantel of McDonough & Sun (1995). Trace elements are plotted with increasing compatibility according to a peridotitic melt from left to right. The diagram shows three distinct trends, manifested by variations in Zr, Hf and REE concentrations, and by the anomalies displayed by Sr and Ti. See text for further explanations.

7 Temperature and Pressure Estimates

Geothermobaromethry refers to methods used to estimate the temperature and pressure at which a crystal phase within a rock is formed. Geothermometry is built on reactions that are sensitive to temperature changes, where both the changes in entalpy (ΔH) and entropy (ΔS) are large. Geobarometry is based on reactions that are sensitive to pressure changes, where a change such as volume (ΔV) is involved. A basic assumption for thermobarometry is that that a mineral assemblage is formed under equilibrium conditions.

Since the chemical composition of clinopyroxenes reflects the nature of their host rocks, as well as the depth and temperature of crystallisation, they may be used as a basis for temperature and pressure estimates. Temperature and pressure estimates in this study are based on the multivariate statistical analysis of clinopyroxene compositions developed by Soesoo (1997). The method uses a principal component analysis (PCA), a mathematical technique for reducing a number of original variables by using a correlation matrix and computing a set of eigenvectors which can be presented in a two-dimentional X_{PT} and Y_{PT} space. A flaw in this technique is the modification of low pressure clinopyroxsenes, originally in equilibrium with the melt, caused by oxide mineral saturation in long-duration assemblages. The mineral assemblages from Tenerife all contain oxide phases (magnetite/ilmenite) and this may drive the clinopyroxene eigenvector scores to the right in Figure 7.1, yielding both higher temperatures and pressures than originally present in the precipitating liquid.

The two eigenvectors are calculated on the basis of the formulae given by Soesoo (1997) as:

$$X_{PT}=0,446SiO_2+0,187TiO_2-0,404Al_2O_3+0,346FeO_{(tot)}-0,052MnO+0,309MgO+0,431CaO-0,446Na_2O$$

$$Y_{PT}=-0,369SiO_2+0,535TiO_2-0,317Al_2O_3+0,323FeO_{(tot)}+0,235MnO-0,516MgO-0,167CaO-0,153Na_2O$$

The results are presented in Figure 7.1 and show that the estimated temperatures for clinopyroxenes lie in the range 1040 – 1275°C, and the geobarometer gave a pressure range of <12 kb. The Al-salites generally give higher pressure and temperature ranges than Na-salites. These estimates are in agreement with previous ones. Neumann et al. (1999) have estimatimated temperatures and pressures in Tenerife rocks, covering the entire range of exposed rocks on the island, by using several methods. Temperatures based on clinopyroxene - liquid equilibria (Putirka, 1997) and olivine - liquid equilibria (Leeman, 1978; Putirka, 1997) yield temperatures in the range 1040 - 1260°C. Pressures based on olivine - clinopyroxene - liquid equilibria (Grove et al., 1989) and clinopyroxene – liquid equilibria (Putirka, 1997) gave pressures in the range 3 - 11 kb, with a mean of 8 kb.

Figure 7.1. Temperature and pressure estimates.

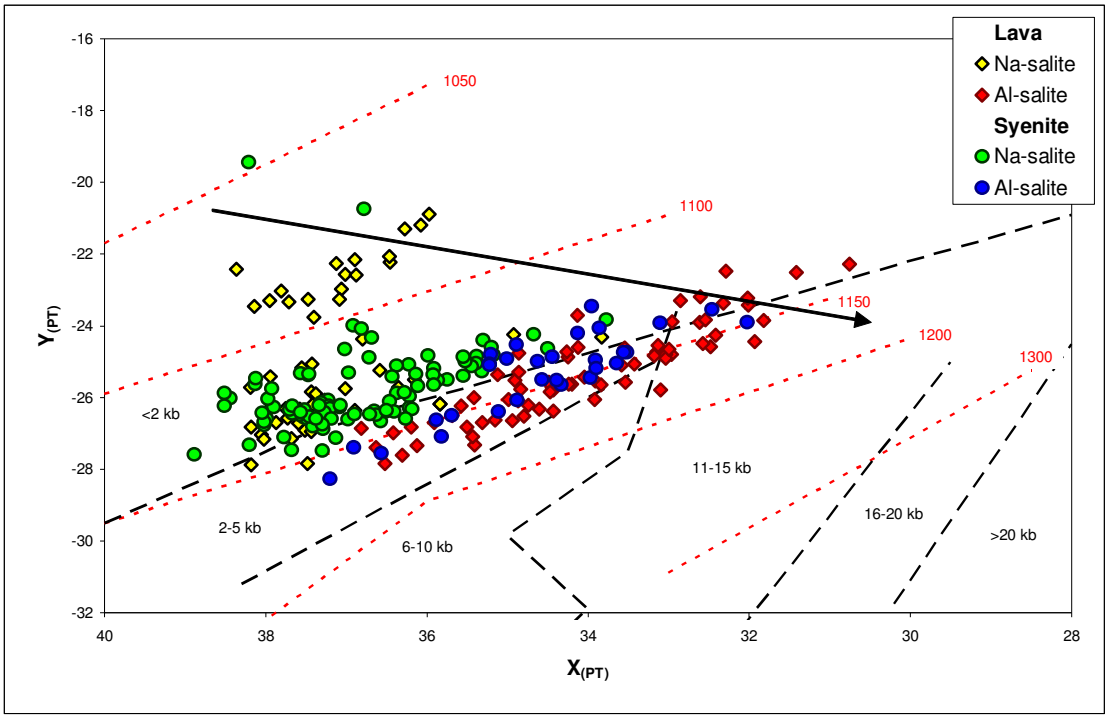

Graphical presentation of clinopyroxenes in the two-dimensional PT-space defined by the eigenvectors of Soesoo (1997). Red dotted lines show the temperature intervals in °C; Black semi-dotted lines indicate pressure intervals in kb. Arrow shows the effect of long duration assemblages, see text for further explanation.

8 Discussion

Lavas erupted from a single volcano at different times, like the formation of the Diego Hernández Formation, can reasonably be assumed to be genetically related. The same is true of different igneous rocks within a single pluton or even in separate, but closely spaced bodies, especially when the different rocks share some striking geochemical signature. Igneous rocks that are related to a common source are said to be comagmatic, implying a clear genetic lineage. However, the relationship between lavas erupted from a single volcano, or different rocks within a single pluton may be quite complex. This is the case for the rocks in the Diego Hernández Formation.

The textural and geochemical data of clinopyroxenes and amphiboles presented above clearly imply that the magmas which gave rise to the Tenerife lavas were subjected to a complex combination of processes, including fractional crystallisation and magma mixing.

8.1 Fractional Crystallisation

The data presented supports the derivation of the Diego Hernándes Formation by fractional crystallisation from an evolved basanite/plagioclase basanite parent magma. Geochemical contrasts can largely be accounted for by variations in the compositions and proportions of the fractionating mineral assemblage, resulting in the diversity of mineral compositions and rocks formed.

The concentrations of elements in the different phases in a magmatic system may be considered in terms of their partitioning between crystalline and liquid phases, expressed as the partition coefficient, **D**[6] ($^{\alpha / \beta}D = C_\alpha / C_\beta$). Elements with D values <1 are termed *incompatible elements*, and are concentrated in the liquid during melting and crystallisation. In contrast, elements with D values >1 are termed *compatible elements* and are retained in the residual solids during melting and extracted into the crystallising solids during crystallisation. This distinction refers normally to basaltic

[6] This is the ”Teilungskoefficient” of Nernst (1891)

melts and their early-crystallising minerals or the mantle minerals from which basalt is extracted, but can be extended to more siliceous magmas if it is recognised that that crystallisation of different minerals may change element compatibilities in the residual magma. The ability of a crystalline or melt phase to incorporate a given element into its structure is controlled by the size of the available crystallographic sites and the ability of the phase to charge balance the incorporated cation. These controls are well illustrated by peaks corresponding to specific crystallographic sites found on plots of Ln D vs. Ionic radius (Onuma diagrams) for cations of a given valence state in a given mineral (Onuma et al., 1968; Jensen, 1973).

8.1.1 Whole Rock Chemical Variations

From whole rock data the petrology of the Diego Hernández Formation are classified into the basanite – tephrite/trachyte – phonolite suite (Figure 4.1) characteristic of many ocean islands. The data show the typical geochemical features of fractionation that are consistent with the removal of minerals belonging to each host rock presented in Table 4.1:

1) General trends of increasing concentrations of lithophile elements (e.g. HFSE and REE), and decreasing concentrations of compatible elements such as Ni, Sc and Cr, with decreasing MgO (removal of olivine [$(Fe,Mg)SiO_4$] and clinopyroxene; Figure 6.1, 6.2 & 6.3)).
2) Increasing agpaitic index ($[Na_2O+K_2O]/Al_2O_3$) with decreasing MgO (removal of plagioclase [$CaAl_2Si_2O_8$]; Figure 6.1).
3) The onset of Fe-Ti fractionation (magnetite [Fe_3O_4]; ilmenite [$FeTiO_3$]) is marked by a shift from incompatible to compatible behaviour of TiO_2 and V with decreasing MgO (FIG 6.1 & 6.3).
4) Transition from incompatible to compatible behaviour of P_2O_5, and Sr with the removal of apatite [$Ca_5(PO_4)_3(OH,F,Cl)$] and plagioclase, respectively, with decreasing MgO, and increasing concentrations of strongly incompatible elements such as HFSE (Figure 6.1 & 6.2).
5) Transition from strongly incompatible to mildly incompatible behaviour of LREE and HREE with increasing enrichment of strongly incompatible elements (e.g. HFSE). This may be caused by saturation and precipitation

of apatite with its compatible behaviour in REE (mineral-melt partition coefficients of 10-100; e.g. Wörner et al., 1983; Figure 6.2 & 6.3).

8.1.2 Clinopyroxene

Indications of fractional crystallisation as the dominant factor of melt evolution are also evident from clinopyroxene chemistry.

1) The analysed clinopyroxenes frequently show normally zoned (decreasing mg#) phenocrysts within each group (Table A2.1 & A2.2).
2) They display wide ranges in concentrations of lithophile elements (Figure 5.5, 5.7 & 8.1), with positive correlations between e.g. La and MREEs, and a trend of decreasing concentrations of compatible elements such as Sc with the progressively enrichment of MREEs (Figure 8.1).

The trace element composition of a magmatic clinopyroxene is the product of the trace element content of its host melt, and cpx-melt partitioning. The clinopyroxene-melt equilibria of the REEs are important because clinopyroxene is the only major anhydrous phase which incorporates these trivalent cations to any significant extent during mantle melting and low-pressure crystallisation. Variations in pyroxene compositions affect the incorporation of the REEs in two ways: (1) through variations in the size of the 6-8 coordinated M2 crystallographic site related to Ca^{2+} content (McKay et al., 1986; Gallahan & Nielsen, 1992), and (2) through the ability of the pyroxenes to charge balance trivalente trace elements with coupled substitutions (Colson et al., 1989; Gaetani & Groove, 1991; Gallahan & Nielsen, 1992; Hauri et al., 1994).

Gaetani & Grove (1995) concluded that increasing mole fraction of Al in the melt increase the partition coefficients ($D^{CPX\text{-}melt}$) for REEs due to the formation of the 'Ca-Tschermaks' component (CaTs). This component is formed when coupled substitution of the octahedral crystallographic M1 site, normally occupied by a divalent cation, and the tetrahedral T site, normally occupied by Si^{4+}, are both exchanged and charge balanced with the trivalent cation Al: $M^{2+}+Si^{4+} \Leftrightarrow 2Al^{3+}$.

Figure 8.1. Selected clinopyroxene trace elements plotted vs. Sm and mg#.

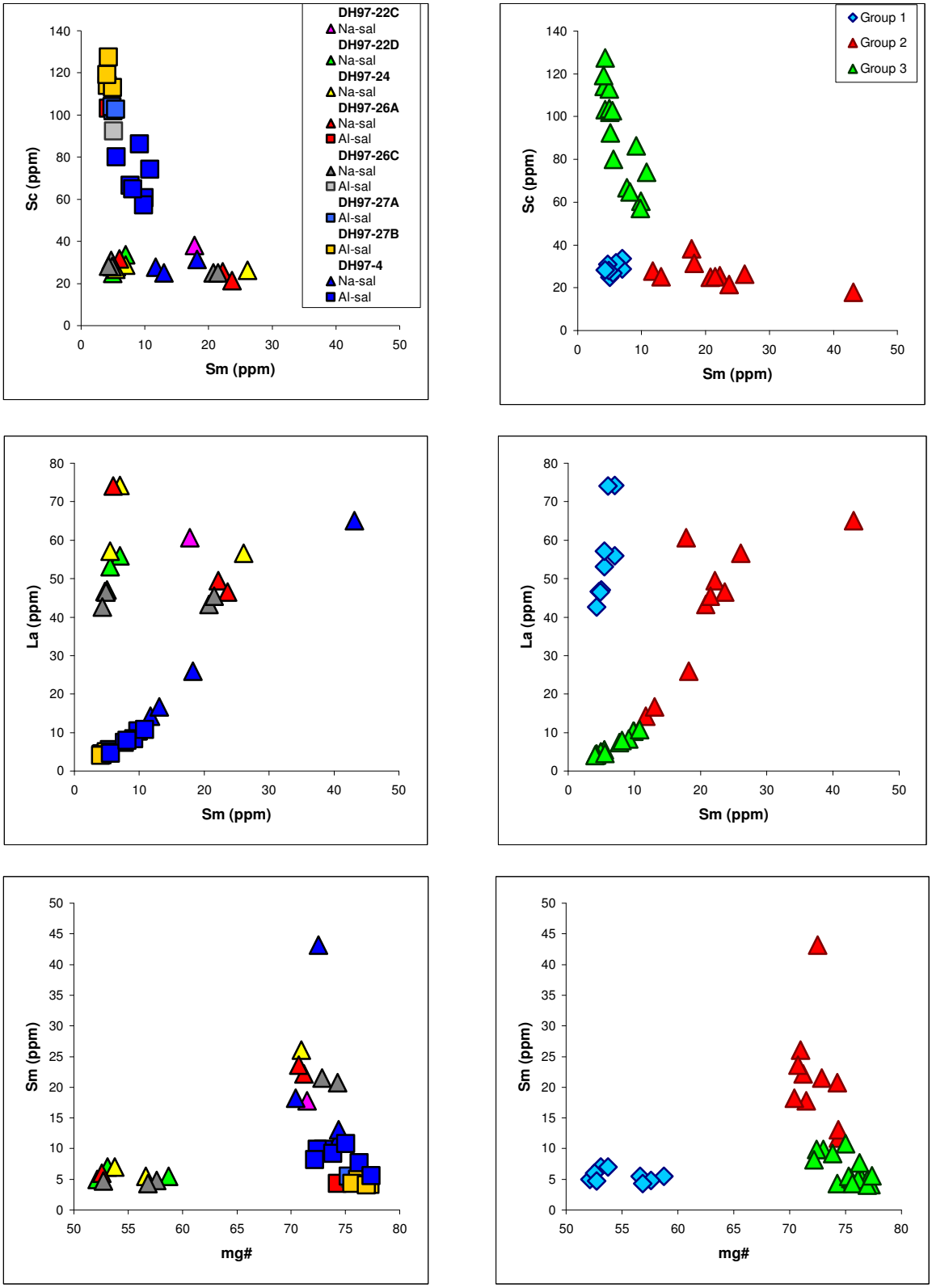

Concentrations in selected lithophile elements in DH lavas plotted against Sm and mg#. The figure shows covariations between REE and Sc for group Two and Three, but only weak covariations with mg# and group One samples. This suggests a genetic linkage in trace element concentrations between the two high-mg# groups, such as formation from the same magma chamber.

However, Al-Ti rich pyroxenes incorporates REE to a lesser extent due to the preferential incorporation of Ti ($D_{Ti}>D_{REE}$) which in turn leads to a charge balance with the coupled substitution $Ti^{4+}+2Al^{3+}\Leftrightarrow M^{2+}+2Si^{4+}$, forming the theoretical endmember $CaTiAl_2O_6$, and requiring a vacancy for each REE cation (Gallahan & Nielsen, 1992).

The clinopyroxene analyses (Table A2.1 & A2.2) show that the total amount of Al increases with decreasing Si content in Al- and Na-salites. Estimates of Al in the different available crystallographic sites; M1, M2 and T, show that Al occupancy in the tetrahedrally coordinated T site, normally occupied by Si, increases, while Al in the octahedrally coordinated M sites display a more constant occupancy (Figure 8.2). Thus, a negative charge balance in the molecule is obtained, and the possibility for the incorporation of higher valency cations, instead of the normally occupying M^{2+} cations, in the lattice is reached. However, as the Al content increases, and progressively enhances the precipitation of the Al salite component, the Ti content also increases (Figure 8.2), favouring formation of the 'Ti-Tschermaks' component (TiTs). This seems to preclude any effective enrichment of REEs in the Al-salites. This effect would not affect the Na-salites in the same way as they tend to have significantly higher $Al^{(VI)}$/Ti ratios than Al-salites. This would lead to a higher ratio of CaTs/TiTs, especially among the low-mg# Na-salites, and therefore the crystal lattice in evolved Na-salites are more able to accommodate the incorporation of REEs.

There is also evidence that increasing polymerisation of the coexisting silicate melt (e.g. Ryerson & Hess, 1978; Green & Pearson, 1985), falling temperature (Green & Pearson, 1985), and decreasing pressure within the range 0,5 – 3,0 Gpa (Adam & Green, 1994), decreases the number of sites stable for REE, Sr and Ti, leading to higher clinopyroxene/melt partition coefficients.

Estimated polymerisation (R[7]) of melts in this study are based on whole rock data displayed in Figure 8.3 and show a typical relationship between D^{Cpx} values and R^{Melt}.

[7] $R = \frac{O}{(Si + Ti + P + Al^{T})}$, Al^{T} is stabilised in the tetrahedral position by combination with Na and K.

Figure 8.2. Ca-Tschermak, Al^{VI} and Ti variations vs. Si^{T}.

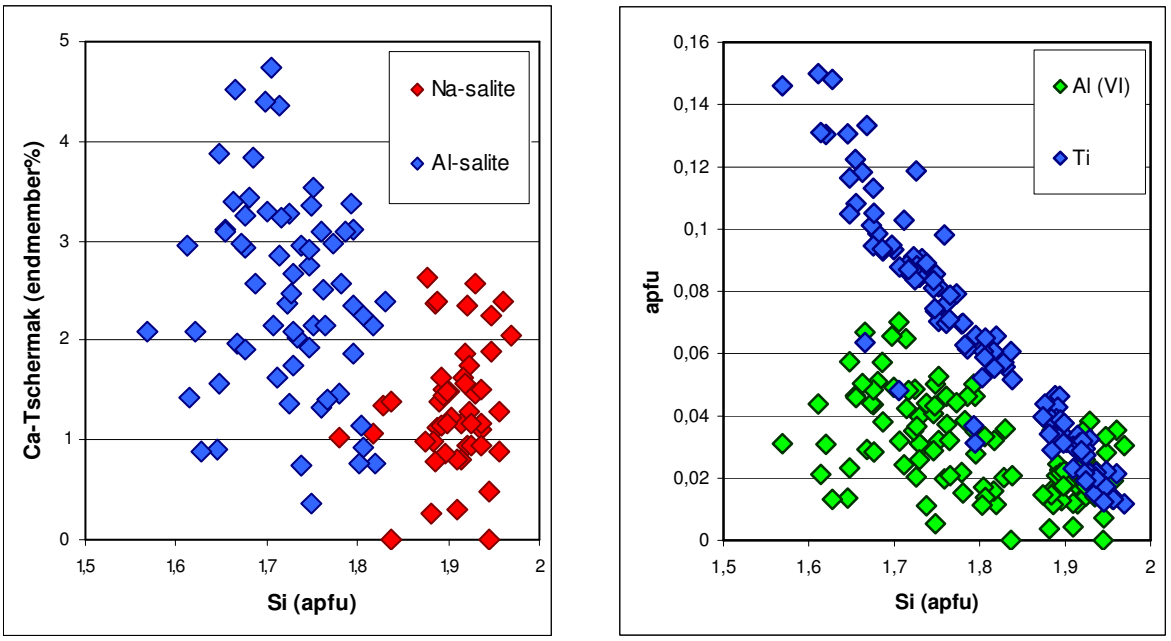

Variations in CaTs and coordinated Al and Ti plotted against Si apfu. Na salites show lower percentages in CaTs endmember and have higher Al^{VI}/Ti ratios than Al-salites. See text for discussion.

Basaltic to intermediate compositions, comprising melts generating high-mg# clinopyroxenes, are slightly depolymerised yielding R values in the range 2,4-2,8, whereas evolved melts are highly polymerised with R values in the range 2,0-2,2. Small deviations in melt structure from the estimated R values will, to a significant extent, affect the D^{Cpx} values in the evolved melts, while small deviations in melt structure among the more primitive melts will not affect Cpx-Melt partition coefficients in any significant way. In addition, temperature and pressure estimates (Figure 7.1) shows that Al-salites crystallise at both higher temperatures and pressures than Na-salites.

Summarising the aspects discussed above, the differences in crystallisation trends between evolved Na-salites and more primitive Na- and Al-salites seems to indicate precipitation from melts of different compositions.

Figure 8.3. Estimated polymerisation of melts.

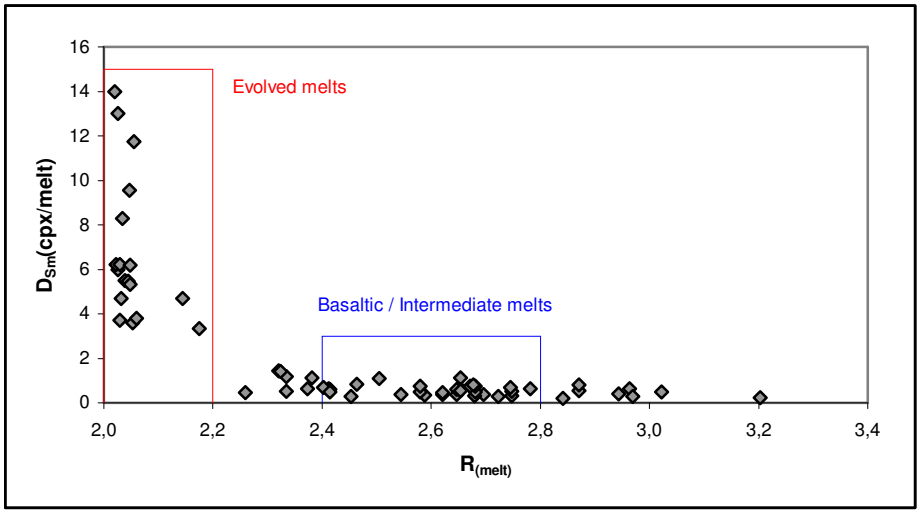

Estimated polymerisation of whole rock compositions plotted against clinopyroxene –melt partition coefficients for Sm. High mg# clinopyroxenes are expected to crystallise from the basaltic to intermediate estimates, while low mg# clinopyroxenes crystallise from evolved melts. Data on $D_{cpx\text{-}melt}$ are from Onuma et al. (1968, 1981); Grutzeck et al. (1974); Matsui et al. (1977); Nicholls & Harris (1980); Dostal et al. (1983); Mahood & Hildreth (1983); Wörner et al. (1983); Fujimaki et al. (1984); Green & Pearson (1985); Nash & Crecraft (1985); McKay et al. (1986); Francalanci (1989); Sisson (1991) and Foley et al. (1996). See text for discussion.

8.1.3 Amphibole

The amphiboles presented in this study mirrors the behaviour of clinopyroxenes to a large extent when trace elements are compared (Figure 5.5, 5.7 & 5.9). However, the presence of strongly Zr, Hf – depleted amphiboles with no significant Sr anomaly (Figure 5.9) deviates from this norm. Wulff-Pedersen et al. (1996) presented data on kaersutite in basaltic xenoliths in mantle melts from La Palma, which shows the same overall trace pattern as the TF12-1 and TF12-2 series of this study. Investigative studies by Neumann et al. (2002) on mantle xenoliths from Tenerife reveal complex mechanisms during formation of Tenerife melts. Xenoliths show a clear genetic lineage with Tenerife magmas and evidence of metasomatism and recrystallisation, overprinting the effects of extensive partial melting. Evidence includes the formation of REE-Cr-enriched, Zr, Hf, Ti-depleted clinopyroxene at the expense of orthopyroxene. Petrographical observations of these samples show anhedral amphiboles with reaction rims (Figure 4.2). In this context it is possible to draw the conclusion that the amphibole in these samples (TF12-1;2) are not the products of

evolved Tenerife melts, but rather accidentally introduced xenocrysts originally precipitated from more primitive mafic melts.

Figure 8.4. Selected amphibole trace elements vs. Nb.

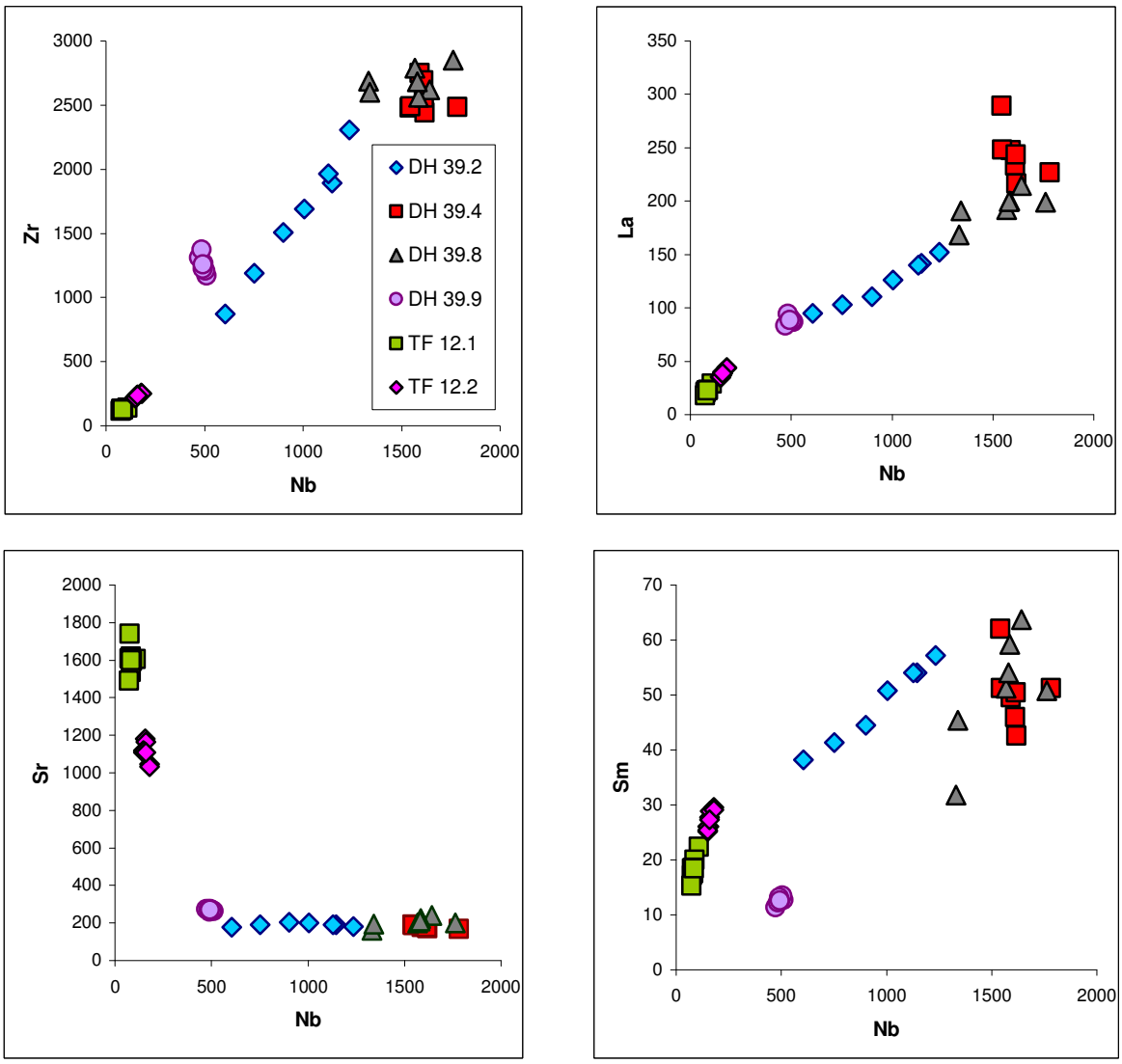

Variations in trace element concentrations of amphiboles showing the fractional crystallisation trends. Note the DH39.9 sample which deviates from the 'normal' trend in Zm and Sm plots. See text for discussion.

Figure 8.4 shows selected trace elements plotted against Nb as a way to determinate evidence for fractional crystallisation. Incompatible elements such as HFSE (Zr) and REE (La, Sm) both display progressively enrichment with increasing Nb content, while Sr shows a flat trend at around 200 ppm. Combined with trace patterns in Figure 5.9 where Sr exhibits a strong negative anomaly, this would indicate precipitation from evolved melts with a history of extensive plagioclase fractionation.

However, several of the observed features present in the DH extrusives and corresponding nepheline syenitic xenoliths cannot be explained by simple fractional crystallisation. Geochemical data presented from whole rock and clinopyroxenes show that samples with similar mg# display wide differences in concentrations of incompatible elements. Such differences can only be explained by processes that lead to decoupling between major and trace elements.

8.2 Magma Mixing

The alkaline volcanic rocks of Tenerife constitute a very Si-undersaturated compositionally continuous series, which originally was thought to have evolved by fractional crystallisation from an alkali basalt parent melt in shallow magma chambers (Ridley, 1970; Borley et al., 1971; Borley, 1974). However, evidence of magma mixing described from several parts of the island covering the entire units of rocks exposed implies that magma mixing was also important (e.g. Wolff & Storey, 1984; Ancochea et al., 1990; Martí et al., 1994; Neumann et al., 1999). Evolved melts in magma chambers located within the oceanic crust and the overlying sequence of Canary Island lavas are mixed with poorly differentiated mafic magmas, periodically injected into the magma chambers (Wolff, 1985; Neumann et al. 1999).

From stratigraphical observations of the DHF with its alternating mafic and felsic layers of basaltic and evolved compositions, respectively, and the commingling of magmas visible as streaky black and white pumice clasts, magma mixing has certainly been a common occurrence. Mixing of magmas has been described from several parts of the island covering the entire units of rocks exposed (e.g. Ancochea et al., 1990; Martí et al., 1994; 1995). Evidences of magma mixing in the rocks of this study include:

1) Corrosion and fragmentation of many phenocrysts, indicating considerable mineral-melt diseqilibria and turbulent chamber dynamics.
2) Highly corroded crystals of plagioclase associated with white glass of evolved compositions alongside euhedral alkali feldspar.
3) Corroded crystals of olivine with reaction rims found in evolved lavas.
4) Inverse zoning of clinopyroxenes (increasing mg# and compatible elements such as Cr, Ni and Sc, and decreasing REE and HFSE), an evidence of

mixing between melts depleted in lithophile elements and melts enriched in lithophile elements.

5) Abrupt changes in chemistry of zoned clinopyroxenes where transition between groups occur (Figure 5.2).

A series of different processes may lead to evidence of commingling of magmas. The magmas may be successive pulses from a common source, in which case their composition may be similar, or they may be magmas with very different compositions from completely different sources and be related only through a common thermal event. In addition, the magma in a magma chamber may cool, fractionally crystallise, or assimilate country rocks before the next pulse arrives. Successive batches of mafic intruding magma may therefore encounter residual magmas that have had their compositions and physical properties modified by processes taking place in the chamber (Philpotts, 1990).

Individual mineral analysis will always reflect the composition of its precipitating host melt. It is shown that major elements distinguish between the different compositions of the clinopyroxenes crystallising, and that this pattern is reflected in trace element concentrations. As shown above, three separate groups are recognised based on binary mg# vs. oxide plots (Figure 5.1 & 5.4). These plots clearly distinguish between separate melt compositions, but does not discriminate in any way if there are initial compositional differences within the groups yielding similar crystallisation trends. As commented in the presentation of data, the Ti/Al ratio in some samples seems to indicate a deviation between analyses within each group. Figure 8.5 show the binary plot of TiO_2 vs. Al_2O_3, and reveal two separate evolutionary trends, roughly divided by the line $TiO_2/Al_2O_3 \approx 2$.

The data show an overwhelmingly dominance of syenites among the Low-Al/Ti series, whereas the lavas are dominated by the High-Al/Ti series. When plotted in mg# vs. oxide plots (Figure 8.5) the Low- and High-Al/Ti series seems to occupy an intermediate position between groups One and Two. Wolff (2000) described similar trends, labelling them high and low Si/Al groupings, and commented on the striking resemblance between the high Si/Al samples and the geochemical character of the Guajara formation (Pre- DH cycle). However, Wolff (2000) confined the high Si/Al

samples to include only the second and third cycle of the DHF, but in the data presented here based on clinopyroxenes, such samples (Low-Al/Ti series of this study) are also found in the first sequence of the DHF.

Figure 8.5. Binary plots of Ti/Al grouping of pyroxenes.

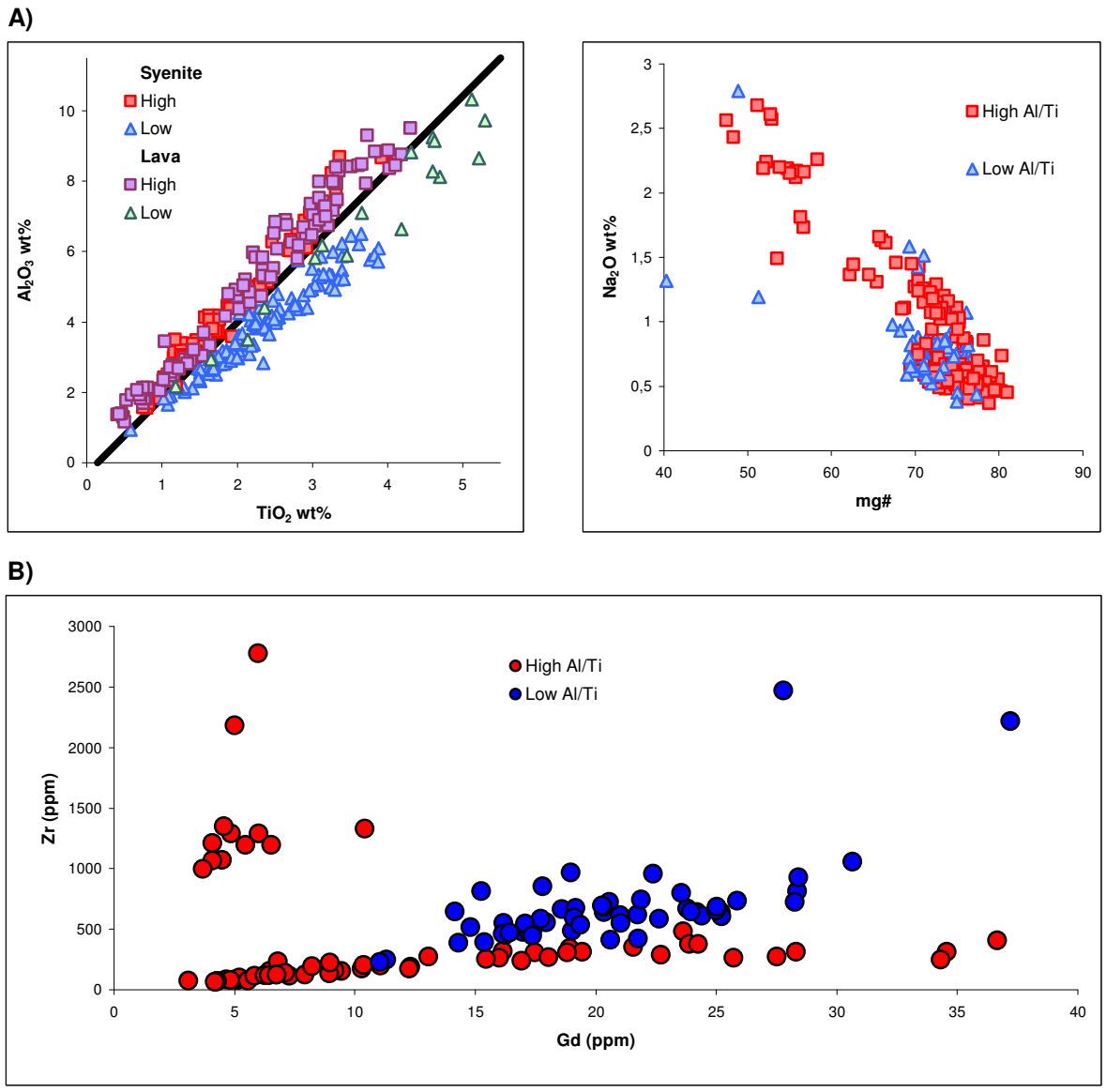

A) Schematic presentation of the two evolutionary trends among all analysed pyroxenes (lava and syenitic) based on Ti/Al variations and mg# vs. Na_2O. B) Gd vs. Zr plot of syenitic samples illustrating the co variation between high- and low-Al/Ti series and Zr concentrations. See text for further explanations.

The variations in the Ti/Al ratios are also expressed in the trace element compositions in the clinopyroxenes. The Low-Al/Ti clinopyroxenes tend to have higher ratios of (Zr,Hf)/MREE than the High-Al/Ti clinopyroxenes (Figure 8.5), independent of mg#. Such differences can not be attributed to differences in the

fractionating assemblage but must be ascribed to initial differences in the fractionating melt. Furthermore, both trends are found to be present within single syenite samples (Table 8.1, Figure 8.6).

Table 8.1. Overview of samples designated to different evolutionary trends.

High (Al/Ti) / Low Zr samples: Trend 1	**Low (Al/Ti) / High Zr samples: Trend 2**
DH39-5; 7-series	DH39-2; 4; 8-series
TF-series	TDKS-series
DH37-series	
Lava analyses with few exceptions	
In addition DH39-1 and 9 series contain both trends	

Similar observations are made in the amphibole data, where the Low-Al/Ti samples correlate with samples labelled Trend 2 (Figure 5.8). Amphibole samples are plotted in binary plots of TiO_2 vs. Al_2O_3 (Figure 8.7), and show the same variations in the Al/Ti ratios of the same samples as clinopyroxenes.

Figure 8.6. Variations in Gd vs. Zr concentrations among amphiboles and clinopyroxenes.

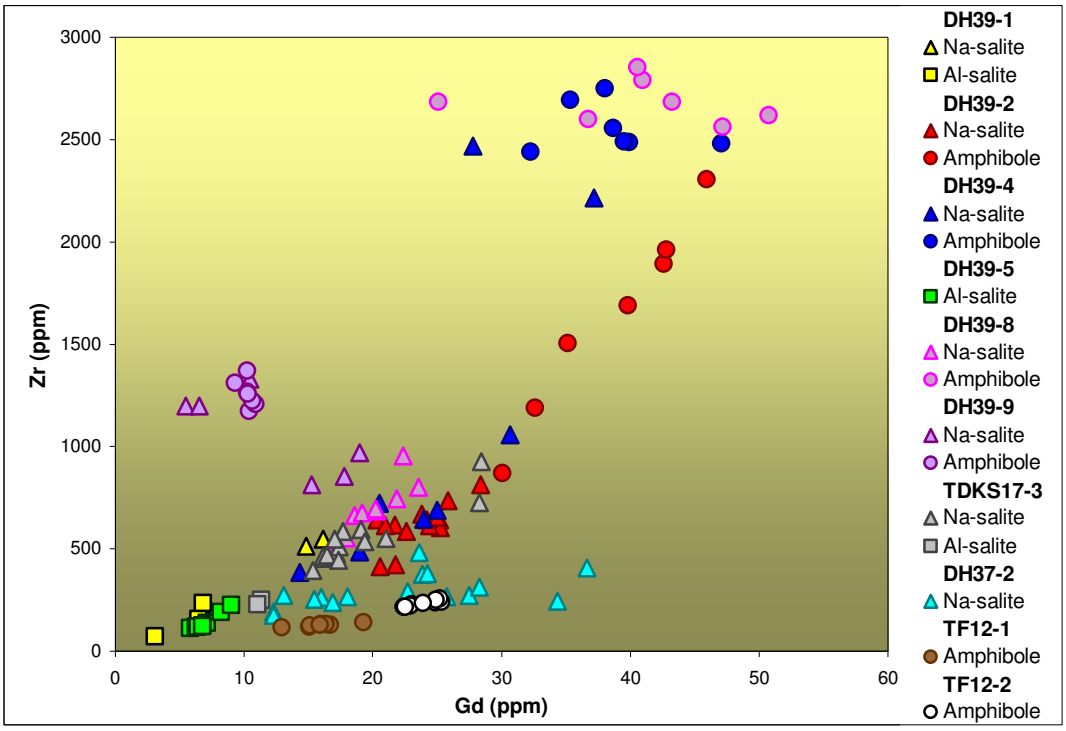

The plot designates specific samples creating the evolutionary trends of clinopyroxenes and amphiboles. See text for discussion.

The agpaitic index of amphiboles also reveals patterns which are in agreement with magma mixing. The alkalinity of fractionating melts of the Tenerife magmas are expected to increase towards late stage crystallisation (Wolff, 1984). This is mainly caused by extensive plagioclase fractionation, and this trend is evident from whole

Figure 8.7. Individual sample presentation and high/low F trends of amphiboles.

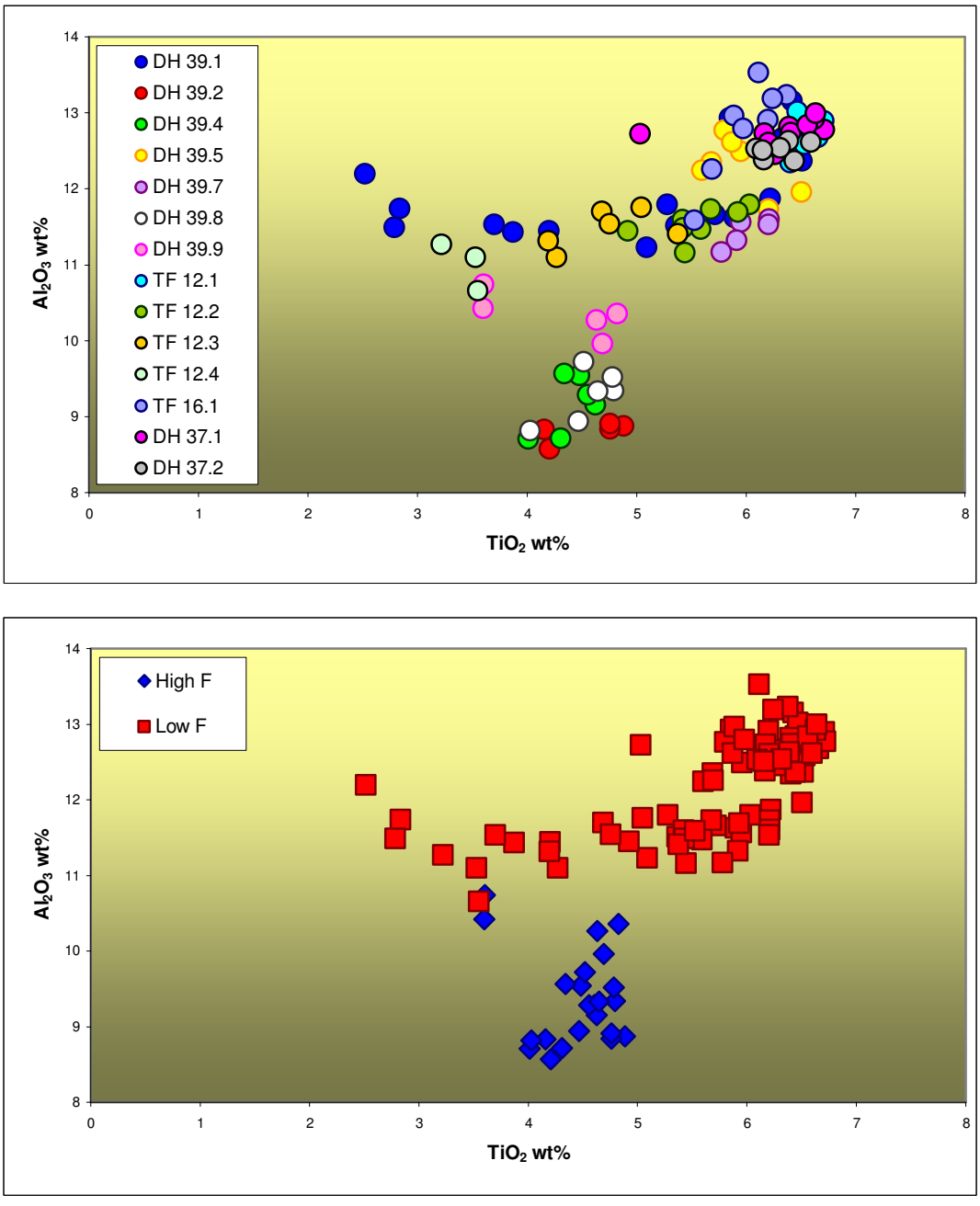

Plots of Al_2O_3 vs. TiO_2 showing that the the Trend 2 samples coincide with the High-F series among amphiboles. The same samples are recognised among clinopyroxenes.

Figure 8.8. Agpaitic index plot vs. mg# of amphiboles.

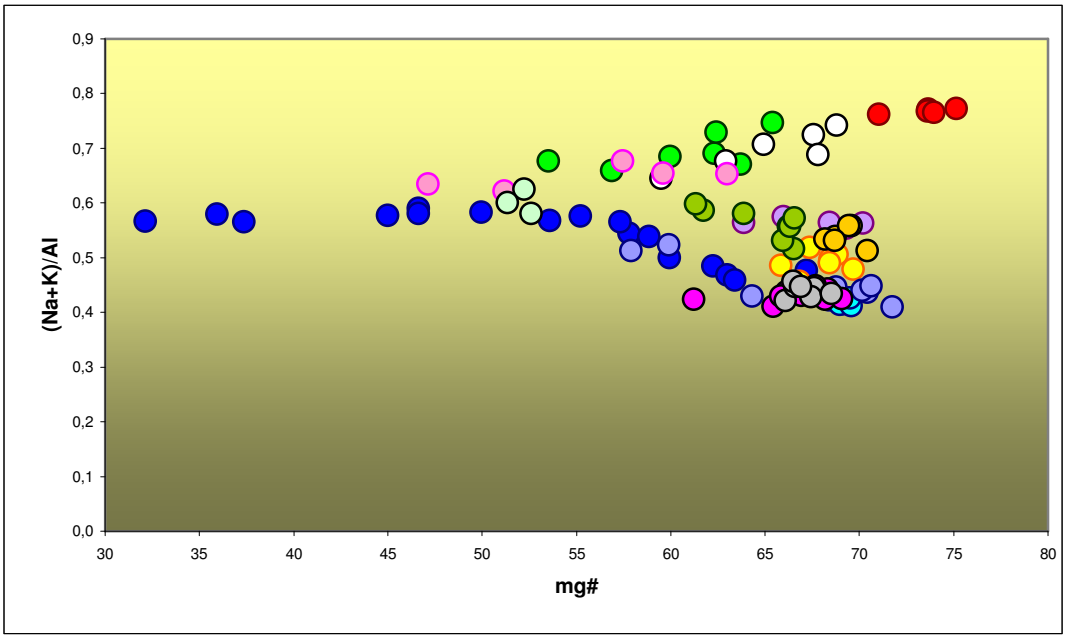

The agpitic index of amphiboles shows that they crystallise along two different evolutionary trends. See text for discussion. Figure captions as Figure 8.7.

rock data presented in Figure 6.1. However, plotting total alkalies vs. mg# for amphiboles, two separate trends are revealed (Figure 8.8). The two trends correlate with the samples defining the high/low F trend (Figure 8.7). Samples comprising the high F trend show, contrary to expected observations, the highest agpaitic index towards the highest mg#. The low F trend show a gradually increase in the agpaitic index from high towards low mg#', and merging with the high F trend around mg#=50. Amphiboles mainly crystallise during the intermediate stage of magma evolution (Ablay at al., 1998) from melts with a history of plagioclase fractionation. Thus, deviations in the agpaitic index might be expected if the amphiboles precipitate from melts where plagioclases have fractionated in different proportions. However, at mg# above 70 this effect is supposedly smaller than what is observed. The trend defined by high F samples should in any way display an increasing trend with decreasing mg#, not the decreasing trend shown, if the system was governed by processes such as fractional crystallisation. Such trend may be achieved through magma mixing between primitive magma and evolved melts of peralkaline composition.

8.3 Mixing and Fractional Crystallisation

O'Hara (1977) described open system processes in magma chambers; RTF ("Refilled", "Tapped" and "Fractionated"), mathematically, and showed several of the compositional features observed in the Tenerife lavas. Lavas extracted from steady-state magmas[8] continuously fed and mixed with batches of parental magma will show the following characteristics:

(1) Uniformity of composition, given constant physio-chemical parameters.
(2) Large differences of composition between lava and parental magma with respect to major and trace element concentrations and ratios.
(3) Strong control of liquid composition by the low pressure phase equilibria.

Steady state lavas developed from the same parental magma but in magma chambers with different physio-chemical parameters may show the further characteristics:

(4) Decoupling between incompatible trace elements and more compatible major elements.
(5) Significant variations in the ratio of two incompatible elements.

Addressing the conclusions put forward by O'Hara (1977) on the chemical changes which magmas undergoing RTF processes may be exposed, it is clear that Tenerife magmas are largely governed by such open system processes.

Summarising some of the geochemical work done on clinopyroxenes from Tenerife (Figure 8.9), it is clear from the diagram that the processes working in magma chambers located beneath the island have been consistent and produced the same geochemical evolutionary trend during the last 12 Ma. This period of time includes both the shield building phase and the construction of the Las Cañadas Edifice. The data also show that the Na-salites of this study occupy an intermediate position with respect to mg#, in the total evolutionary trend towards the most peralkaline compositions. Thus reflecting the possibilities of even larger differences between

[8] The extreme case of an RTF magma chamber; where magma resupply rate equals the rate of crystallisation and eruption, thus maintaining a constant volume of liquid. In such a magma chamber, the concentrations of all elements eventually reach steady-state after many cycles of refilling, eruption, and fractional crystallisation. Steady-state occurs when the rate of supply of the element becomes equal to the rate of loss.

Figure 8.9. Evolutionary trends among clinopyroxenes from Tenerife.

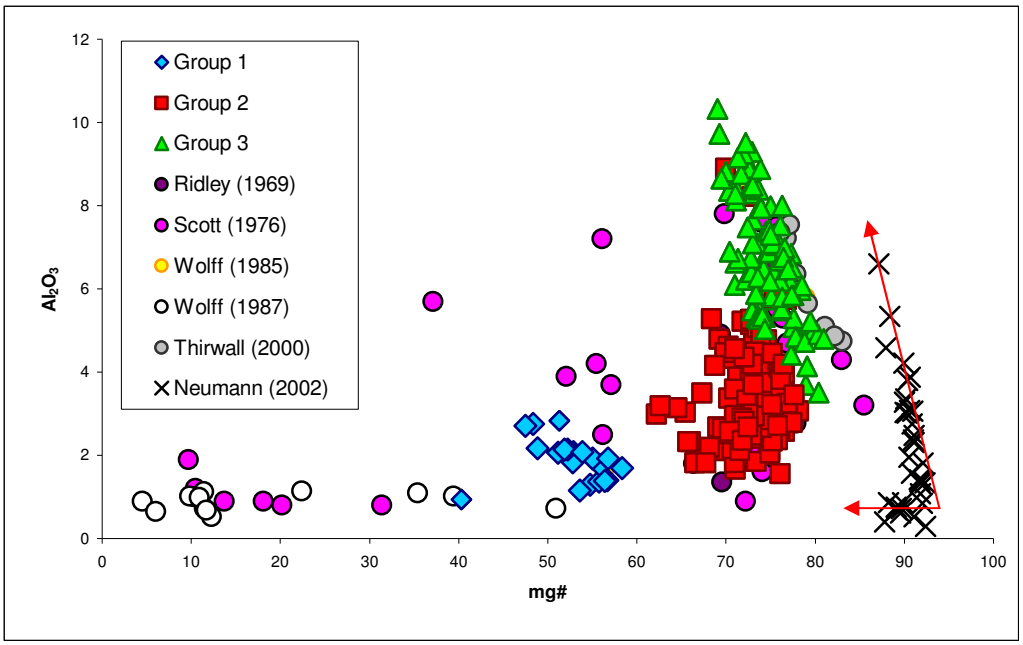

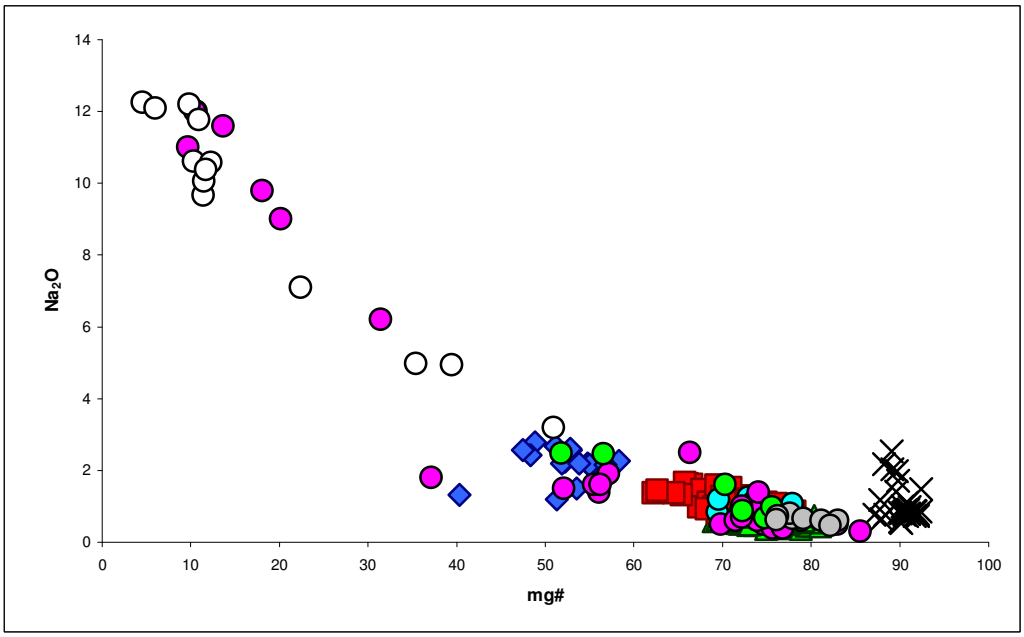

Plots of Al_2O_3 and Na_2O vs. mg#. The clinopyroxenes of this study shows the same overall patterns exhibited by previous studies and reveal that the most evolved samples occupy an intermediate position in the total evolutionary trend towards the most alkaline compositions. The data presented from Neumann (2002) show crystallisation trends of clinopyroxenes involving Canarian melts. These melts, which pre-dates melts forming clinopyroxenes of this study, show that clinopyroxenes possibly adopt their evolutionary trend from these magmas, indicated by the red arrows.

primitive melts and the most evolved products than is presented in this study. Supporting the estimations that DH lavas and syenites crystallise at low pressures (Figure 7.1), the Na content of Na-salites is balanced by Fe^{3+} in the acmite molecule,

not the high pressure molecule jadeite ($NaAlSi_2O_6$). Thus, the low pressure phase equilibria may be able to put constraints on the liquid composition.

The formation of the initial mafic melts with its major and trace element contents must be ascribed to processes pre-dating the migration and formation of shallow magma chambers producing the rocks present in this study. Such processes have been described by e.g. Wulff-Pedersen et al. (1996) and Neumann et al. (2002), and are out of the scope of this paper. However, the data on clinopyroxenes in mantle xenoliths (Neumann et al., 2002) presented in Figure 8.9, show a wide range in Al concentrations and Al/Na ratios in clinopyroxenes in the lithospheric mantle beneath Tenerife. These clinopyroxenes have crystallised from, or in the presence of, Canarian melts (Neumann et al., 2004). These clinopyroxenes show that primitive Canarian melts cover a cover a wide range in compositions, including Al/Na ratios. The major element variations in the liquids which eventually caused the clinopyroxenes of this study to crystallise either as Al-salites or high-mg# Na-salites, have therefore probably inherited their compositional characteristics from more primitive melts. This suggests that that the two trends among high-mg# clinopyroxenes relate to different melt compositions continuously feeding the shallow magma chambers.

Elements thought to be very incompatible, such as HFSE, are expected not to fractionate from the most primitive melts. However, the ratio of Th/Ba varies enormously during differentiation to felsic compositions, due to the compatibility of Ba into alkali feldspar. The same is true for Zr, which is an incompatible element in mafic magma, with similar bulk/mineral distribution coefficients as MREEs. However, Zr is compatible in the presence of titanite, and MREE in the presence of apatite. Whole rock evolved DH and syenite samples show a positive correlation between Th/Ba and Zr/Sm (Figure 8.10). This trend is also mirrored by the mafic DH samples. Neither of these element pairs should be fractionated by precipitation of olivine, clinopyroxene of plagioclase, which are phases on the basanite liquidus. The DH mafic trend can only be modelled through magma mixing by addition of phonolite or evolved syenitic compositions.

8.3.1 Melt Modelling

In order to quantify the magma chamber processes working on Tenerife magmas the mathematical calculations of O'Hara (1977) on RTF processes were used.

First step is to find suitable fractionating assemblages corresponding to the mineralogy in the rocks present. Assuming a parental basaltic melt in eutecticum crystallisation according to the phase diagram of Yoder & Tilley (1962), the fractionating assemblage would be olivine, clinopyroxene and plagioclase, in proportions 10%, 40% and 50%, respectively, which seems reasonable in view of

Figure 8.10. Zr/Sm vs. Th/Ba for DH and syenite rocks.

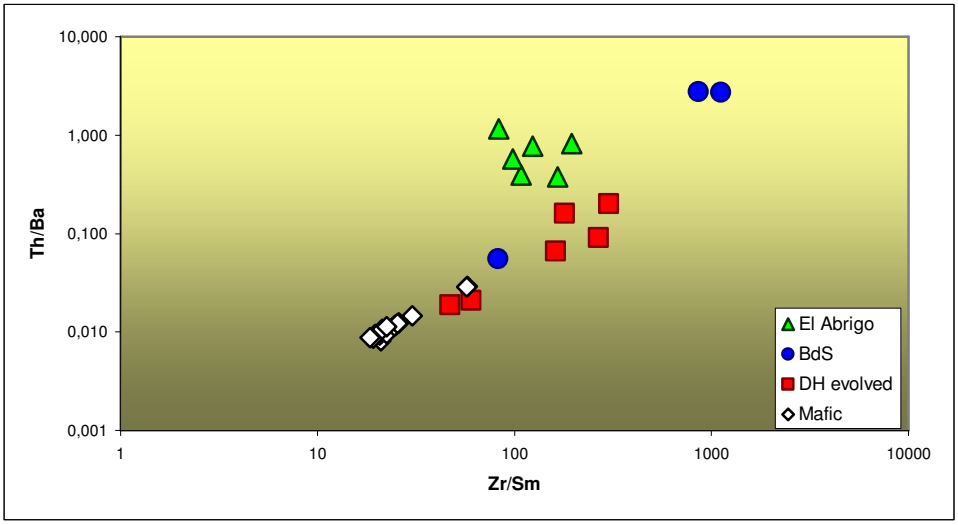

Variations among incompatible element ratios in whole rock samples. The figure shows, contrary to expected evolution of mafic liquids undergoing fractional crystallisation, an increasing trend of these highly incompatible elements (Th and Zr). Such enrichment can only be attributed to mixing of more evolved melts. See text.

petrographical and geochemical observations. From the data presented and discussed above it is shown that the fractionating liquids precipitating Na- and Al-salites differ in terms of composition and thus in the fractionating assemblage. The low-mg# Na-salites crystallise from more evolved melts, with different trace element concentrations and degree of polymerisation in the melts, than high-mg# clinopyroxenes. The evolved melts are therefore expected to contain additional accessory phases present on the liquidus. Whole rock trace patterns (Figure 6.3)

show that with progressively enrichment in VICE[9], the REE and Ti concentrations decrease. This is in accordance with the crystallisation of apatite and Ti-oxides. These phases are therefore added to the fractionating low-mg# Na-salite assemblage as accessory phases in proportions 1% (Apatite) and 2% (Oxides).

Secondly, appropriate mineral/melt partition coefficients (PC) must be found for the crystallising phases. This in order to determinate bulk distribution coefficients (D) to be applied in mixing models, and be able to estimate the evolution of melt compositions. In this model three sets of D's are used (Table 8.2) for the three crystallising trends seen among clinopyroxenes; low and intermediate D's for high-mg# basaltic melts and high D's for the most evolved melts. Bulk distribution coefficients are calculated using the equation $D_i = \Sigma W_A \times PCi_A$[10].

Table 8.2. Estimated distribution coefficients.

	Low PCs		Intermediate PCs		High PCs	
	Sm	**Zr**	**Sm**	**Zr**	**Sm**	**Zr**
Olivine (Ol)	0,0049	0,0035	0,0049	0,02	0,087	0,0005
Clinopyroxene (Cpx)	0,651	0,52	0,58	0,8	0,785	0,05
Plagioclase (Plag)	0,11	0,0009	0,036	0,0866	0,221	0,0094
Apatite (Ap)					12,4	0,636
Oxide (Ox)					0,08	0,25
Bulk D	0,316	0,209	0,250	0,374	0,566	0,037

Overview of estimated distribution coefficients applied in the melt modelling calculations (Figure 8.11). Low, Intermediate and High PCs refer to melts crystallising Al-salite, high-mg# Na-salite, and low-mg# Na-salite, respectively. Estimated proportions of minerals crystallising are set to Ol_{10}:Cpx_{40}:$Plag_{50}$ for basaltic/intermediate compositions and Ol_4:Cpx_{41}:$Plag_{52}$:Ap_1:Ox_2 for evolved compositions. Data on PCs are from Watson & Green (1981), Fujimaki (1986), Nabelek (1980), McKenzie & O'Nions (1991), Nagasawa (1973), Dunn & Sen (1994), Fujimaki et al. (1984), Adam & Green (1994), Dostal et al. (1983), Shimitzu (1980), Villemant (1988) and Forsythe et al. (1994).

From the data presented it is shown that Na- and Al-salites precipitate from liquids of different compositions leading to two distinct crystallisation trends (Figure 8.9). Within the trend of Na-salites there are also large differences in the concentrations of trace elements (Figure 8.1), seemingly as a result of decoupling due to processes such as magma mixing. The Al/Ti ratio combined with Zr/MREE variations (Figure 8.6) adds insight to the question of how many melts are involved in the formation of these lavas

[9] Very Incompatible Elements. Elements which are not readily substituted for any major ions and are segregated into the late residual liquids.
[10] W_A: weight% of mineral A in the rock; PC_{iA}: distribution coefficient of element i in mineral A.

and syenites. It is also shown that increasing polymerisation of the melt (Figure 8.3) is a plausible mechanism controlling the distribution of elements between melt and precipitating clinopyroxenes. The enrichment of incompatible element concentrations seen among the high-mg# Na-salites, compared to Al-salites, are thus not necessarily the product of fractionation from melts with higher content of incompatible elements, but rather a function of elevated mineral-melt distribution coefficients.

The mixing model of O'Hara (1977), based on estimated melt compositions of Sm vs. Zr was used to shed light on the complexity of DH lavas and syenites. Zr was used as an index mineral due to its high solubility in alkaline felsic liquids (Watson & Harrison, 1983), and shows extreme enrichments in late stage liquids (Wolff & Toney, 1993). In this calculation an assumed estimated parental melt l_0, with starting composition Sm = 2,2 ppm and Zr = 25 ppm, is fractionally crystallised using the steady-state equation of O'Hara (1977):

$$\frac{C_{ssl}}{C_0} = \frac{(F+T)(1-F)^{D-1}}{1-(1-F-T)(1-F)^{D-1}}$$

C_{ssl}: concentration in steady-state liquid
C_0: concentration in parental liquid
F: fraction of material crystallised
T: volume lost to eruption
D: distribution coefficient

From the estimated parental liquid three sets of steady-state liquids are estimated based on the bulk distribution coefficients presented in Table 8.2. Firstly, a mixing model for basaltic compositions, comprising the high-mg# clinopyroxenes of Group Three, is estimated using the low bulk distribution coefficients. Secondly, a mixing model for high-mg# Na-salites of Group Two is estimated using intermediate D's, and finally high D's are used on evolved compositions of Group Three.

The parameters regarding parental liquid (C_0), fractionation (F), volume loss (T), and mixing proportions between steady-state liquids are the same for any given distribution coefficient used.

The initially steady-state liquid for each D-value is determined directly from the parental liquid l_0, assuming a T-value (see equation above) of 0,15. The first cycle (first mixing) starts with injections of the parental liquid (l_0) mixed with the residual melt of the preceding steady-state liquid (l_e^1), which have been subjected to a 15% crystallisation, in proportions 0,4(l_0)/0,6(l_e^1). The mixed melt (l_m^2) is then fractionated 15%, forming the evolved melt l_e^2, which is subsequently mixed with the parental melt (l_0) in proportions 0,4(l_0)/0,6(l_e^2), forming the mixed melt l_m^3, etc.

The estimated steady-state liquids are presented in Figure 8.11, together with whole rock data, and melt compositions estimated from clinopyroxene and amphibole data combined with mineral/melt distribution coefficients presented in Table 8.2. Whole rock data present the compositional results of a combination of processes, and thus only distinguish between relatively primitive and evolved melts. Mafic whole rock compositions plot along the low and intermediate D steady-state mixing trends, while evolved whole rock plot along the high D mixing trends (Figure 8.11). Estimated melts obtained from mineral data will, on the other hand, trace incremental steps during melt evolution and thus enable us to distinguish between different crystallisation trends. The calculations made only support the formation of the clinopyroxenes and amphiboles located along the steady-state mixing lines. Examining Figure 8.11 it is evident that not all samples may be explained by the steady-state fractional crystallisation model presented. This may be caused either by default selection of distribution coefficients or wrong estimates of the parameters used in the steady-state equation. However, the samples deviating from the steady-state estimates correlate with the Trend 2 clinopyroxenes (see Table 8.1). Since these samples deviate from what seems to be the 'normal' geochemical trends, occupying an intermediate position between the steady-state mixing trends, an alternative model of formation will be discussed below.

On the other hand, the Trend 1 clinpyroxenes show good consistency with the steady-state liquids estimated. The basaltic Al-salites correlate well with the estimates based on the procedure described above and plot close to, or on, the low D mixing lines. High-mg# Na-salites show somewhat higher Zr content than what the intermediate D mixing lines indicate, but the Sm enrichment trend is in accordance

with computed estimations. The low-mg# Na-salites may also to a satisfying degree be computed according to the high D parameters given.

In summary, the Sm/Zr-plot (Figure 8.11) shows that liquids precipitating clinopyroxenes clearly define three separate trends, of which two correspond to the steady-state model trends:

1) Primary melt composition and evolution towards REE enrichment at relatively constant low Zr concentrations. Comprising low and intermediate partition coefficients used on high-mg# clinopyroxenes of the Trend 1 series.
2) Elevated starting concentrations in Zr, which increases at almost constant low Sm concentrations (high PC from low-mg# Na-salites of the Trend 1 series).
3) Slightly elevated starting concentrations in both Sm and Zr, which increases with positive correlations between the elements (Trend 2 series, not correlated with steady-state mixing trends).

Wolff & Storey (1984) concluded that the mineralogical and compositional variations within the mafic to intermediate components of the Tenerife magma system are mainly due to magma mixing. This is supported in this thesis by petrographical and petrological evidence, and also illustrated by magma mixing models. The two steady-state trends with low and intermediate D's are clearly capable of producing all estimated melt compositions crystallising Trend 1 clinopyroxenes with high-mg# (Figure 8.11).

Although it is possible to model the Trend 1 liquids based on low-mg# Na-salites from the initial steady-state liquid, it is unrealistic to treat these samples in the same manner as the Trend 1 liquids based on high-mg# clinopyroxenes. The spider diagram patterns (Figure 5.5 & 5.7), shows that these low-mg# clinopyroxenes are highly enriched in incompatible elements, depleted in MREEs, and have strong negative Sr anomalies, thus defining the low Group One series, found in syenites and including all lava analysis. Such behaviour implies that they are formed directly from evolved melts, and not through several mixing events of primitive magma. In addition,

Figure 8.11. Estimated melt compositions, steady-state liquids and mixing trends.

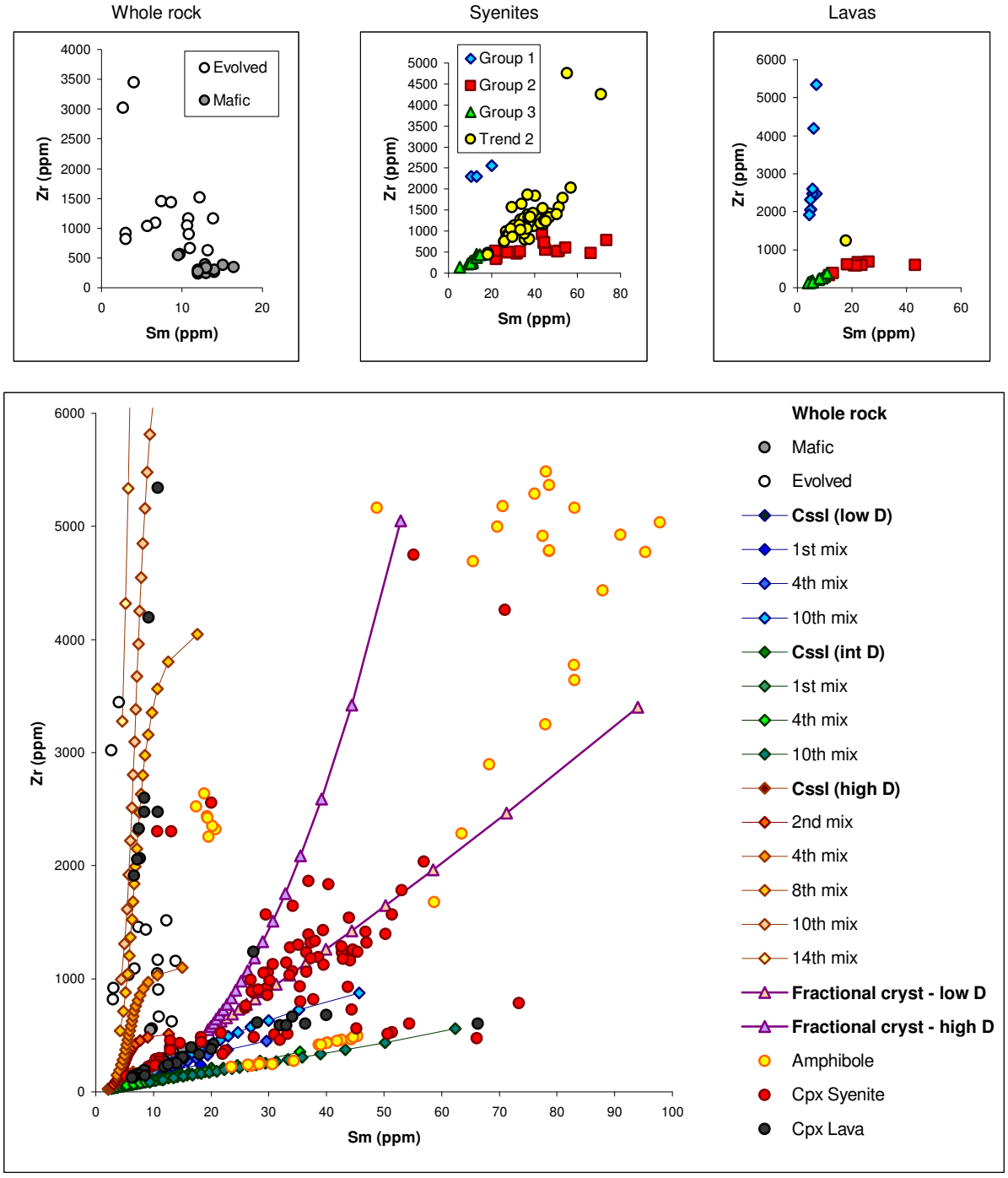

The figure shows variations in Sm vs. Zr concentrations for whole rock data, estimated melt compositions from clinopyroxenes, evolution of steady-state mixing trends with different bulk distribution coefficients and estimated fractional crystallisation trends of mixed magmas. See text for discussion.

whole rock data depict that more evolved products crystallise from highly polymerised melts (Figure 8.3). A solution may be that these low-mg# clinopyroxenes, crystallising from highly evolved melts, are the products of fractionation in the capping layer of a zoned magma chamber. A study on zoning in magma bodies by Wolff & Storey

(1984) concluded that the frequency of compositionally heterogeneous alkaline deposits in Tenerife strongly indicates that a large number of the pre-eruptive magma bodies were chemically zoned. Studies by Turner & Gustafson (1981) and Sparks et al. (1984) showed, based on laboratory experiments, that rapid generation of capping layers are possible through convective fractionation of intermediate magmas. Wall rock crystallisation of intermediate magma will create a low-density boundary layer of evolved magma, buoyantly rising due to density contrasts, forming a capping layer to the magma chamber. The average repose period between eruptions from zoned magma systems such as the Granadilla and Fasina members is in the order of<3000 years (Wolff & Storey, 1984). Such magma chamber dynamics can explain the formation of highly evolved clinopyroxenes, with high HFSE/MREE ratios, if the liquids which these crystals fractionated from were separated from parental melts, depleted in MREEs and enriched in HFSE, such as the liquids following the steady-state trend outlined by the high D's. Wolff & Storey (1984) also predict that 90-95% of total MREE depletion occurs during fractionation of phonolite in the presence of sphene, a phase which is virtually absent from basaltic to intermediate compositions.

If we accept that the Trend 1 clinopyroxenes of high-mg# represent pristine melts, in the sense that their chemical composition regarding major element content and trace element concentrations are derived, and then evolved, directly from the primitive liquids replenishing the shallow level magma chambers, what then about the Trend 2 clinopyroxenes?

Their overall major element content and trends are the same as for the pristine melts (Figure 5.1 & 5.4). However, in trace element concentrations the clinopyroxenes differ slightly, with elevated Zr and Hf concentrations among Group Two samples, and they also form the high Group One trend seen among syenitic samples (Figure 5.7), where the trace element concentrations are overall higher both for VICE and REE with respect to Low Group One samples. In Figure 8.12, Zr is plotted against Al and show that Trend 2 samples occupy an intermediate position between high-mg# and low-mg# clinopyroxenes of Trend 1. This is in accordance with the Zr/Gd plot (Figure 8.6), where Trend 2 samples define an intermediate evolutionary trend between the two Trend 1 samples. Amphibole data support the derivation of Trend 2 samples from more alkaline melt compositions (Figure 8.8).

Trend 2 clinopyroxenes are thus believed to be formed through mixing events between melts defining the low-intermediate PC steady-state trends and melts defining the high PC steady-state trends. Assuming that magma chamber dynamics separates the liquids in a magma chamber into two more or less immiscible liquids due to density contrasts. This forms a base of high density mafic to intermediate magma, precipitating, among other phases, high-mg# clinopyroxenes of Al- or Na-salite composition. The low density capping layer is then though to fractionate low Group One clinopyroxenes. If turbulence then disrupts the stability of the system, such as the entry of a new batch of magma at the base of the chamber, or venting of the chamber to form an eruption, the mixing of remaining liquids are evident. Pooling at the base may, or may not, cause enough upheave to mix the base layer with the capping layer. In the case of the latter, the clinopyroxenes will continue to crystallise

Figure 8.12. Clinopyroxene plot of Al_2O_3 vs. Zr.

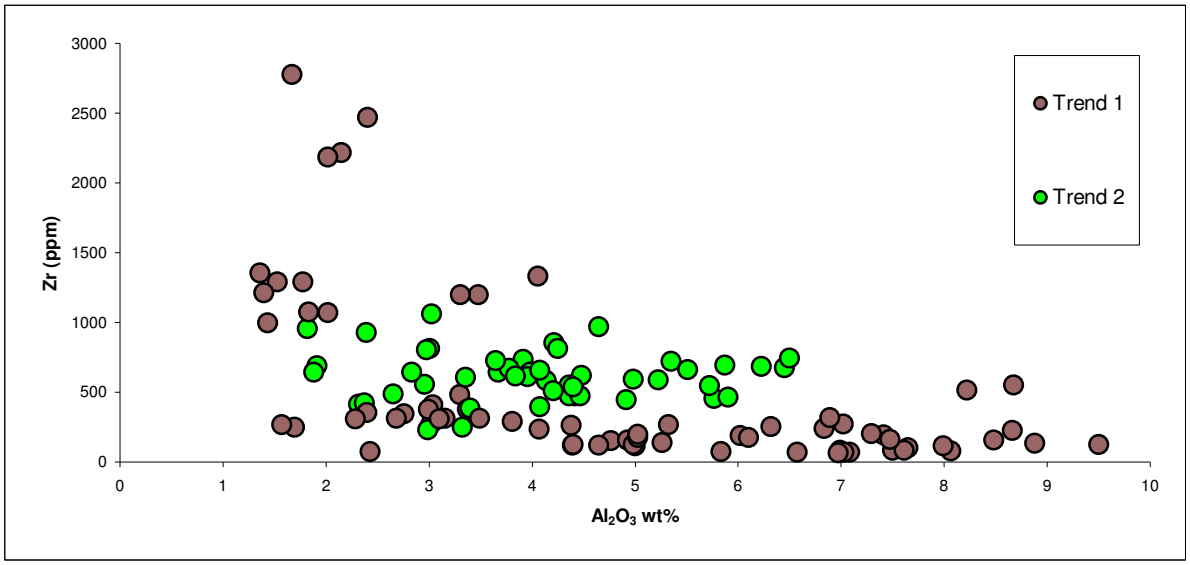

Clinopyroxene plot of lavas and syenites illustrating the intermediate position of Trend 2 samples between the mafic to intermediate (low Zr) and evolved (high Zr) compositions of Trend 1 samples.

along the low-intermediate PC steady-state trends (Figure 8.11), fractionating Trend 1 samples. However, based on the frequency of Trend 2 samples recorded in the syenitic samples, and the near absence of Group One samples, this mechanism seems not to occur very often.

To compute the evolutionary trend of the Trend 2 clinopyroxene samples in Figure 8.11, an assumed mixing between steady-state liquids of low-intermediate PC and high PC are used based on the following parameters: A 50/50 mix of the 7th steady-state mixing trends of the low and intermediate PC, which both have undergone 70% crystallisation, are mixed with the 7th steady-state mixing trend defined by the high PC, which also has been subjected to 70% crystallisation, in proportions 85^{primitive}/15^{evolved}. This new melt created then forms the basis for the evolution of the Trend 2 clinopyroxenes. Since this melt is formed indirectly from the primitive liquids thought to replenish the magma chamber, the fractional crystallisation equation[11] is used, instead of the steady-state equation applied on the pristine liquids, to calculate the evolutionary trend. In Figure 8.11 the two fractional crystallisation trends are based on the high and low bulk distribution coefficients of Table 8.2, and represent the possible melt compositions fractionating the Trend 2 clinopyroxenes.

Based on the mathematical calculations outlined above, estimated evolution of melt compositions may now be modelled to fit the fractionation of all the clinopyroxenes and amphiboles presented in this study (Figure 8.11), from the most primitive to the most evolved samples.

8.4 Compositional Differences Between Lavas and Syenites

Investigating the proposed melt modelling theory (Figure 8.11), clear differences in crystallisation trends between lavas and syenites are revealed:

1) Two primitive, compositionally different melts are suggested to fractionate Group Two and Three clinopyroxenes of Trend 1 composition. Both these clinopyroxenes are found in lavas and syenites.
2) Then the magma differentiates and forms a phonolitic capping layer, fractionating Trend 1 clinopyroxenes of Group 1. These are the only highly evolved clinopyroxenes found among lava analyses. The syenites are

[11] $\frac{C_l}{C_0} = (1-F)^{D-1}$, symbols are the same as for the steady-state fractionation equation.
C_l: concentration in the remaining liquid

overall scarce in Group One samples. Trend 1 samples of evolved compositions are only present in one sample (DH39.9).

3) When these two magmas are mixed, Trend 2 clinopyroxenes starts to fractionate. These samples are virtually absent from lava samples, but dominate the syenitic analyses.

It is thus clear that differences between lava and syenitic samples differ in terms of their ability to form the mixed melts crystallising Trend 2 samples.

Figure 8.13. PM normalised median trace patterns of clinopyroxenes.

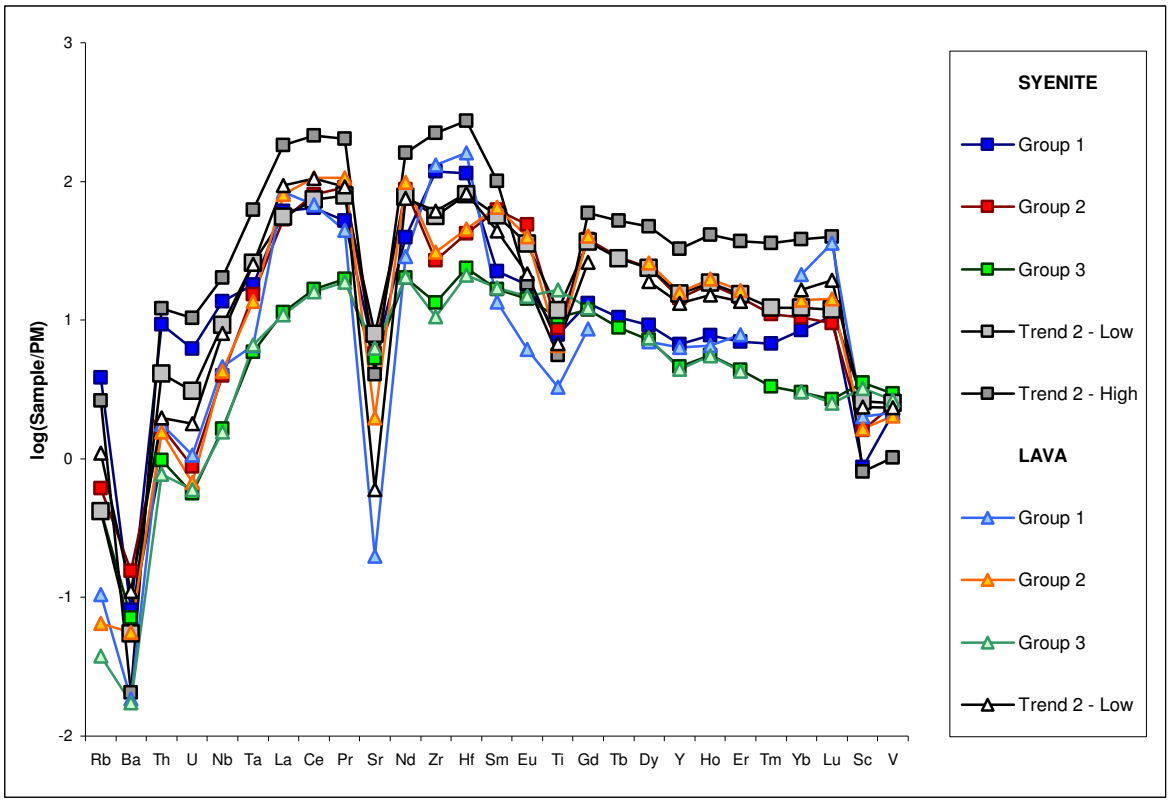

Trace element variations in spider diagram show that Trend 2 clinopyroxenes fractionally crystallising from the mixed magma have an overall affinity to Group 2 samples only deviating in Zr and Hf concentrations. However, the most evolved Trend 2 samples (High-series) mimic the behaviour of Group 1 samples, but their overall trace element concentrations are higher.

Trend 2 samples of mafic to intermediate clinopyroxene compositions have strong affinities to Group Two samples when trace element concentrations are compared (Figure 8.13), unrelated to whether they crystallise as Na- or Al-salites. The evolved compositions of Trend 2 samples deviate from the trace pattern exhibited by evolved Trend 1 samples (Figure 8.13). The most distinctive features of variations between the two trends are the overall higher trace element concentrations and the lack of

strong positive correlations in (LREE,HREE)/MREE among Trend 2 clinopyroxenes, implying that their crystallising conditions are different from Trend 1 samples. Such differences may be attributed to the crystallising assemblage. An accessory phase which may govern evolved clinopyroxenes to portray the two different crystallisation trends seen is sphene; $CaTiSiO_5$ (e.g. Wolff, 1984; Wolff et al., 2000). Through coupled substitutions of Ca^{2+} and Ti^{4+} a number of differently charged cations may be incorporated in the crystal lattice. (e.g. $Ca^{2+}+Ti^{4+}\leftrightarrow Fe^{3+}+REE^{3+}$; $Ca^{2}+Ti^{4+}\leftrightarrow Na^{+}+(Nb,Ta)^{5+}$). Sphene is thus a large repository for both HFSE and REE. The preferential fractionation of Ta/Nb into sphene (Green & Pearson, 1987) would cause the remaining liquid to be enriched in Nb with respect to Ta. Evolved clinopyroxene compositions of Trend 1 samples have significantly higher ratios of Nb/Ta than evolved Trend 2 compositions (Figure 8.14).

Figure 8.14. Variations in Nb/Ta ratios in clinopyroxenes.

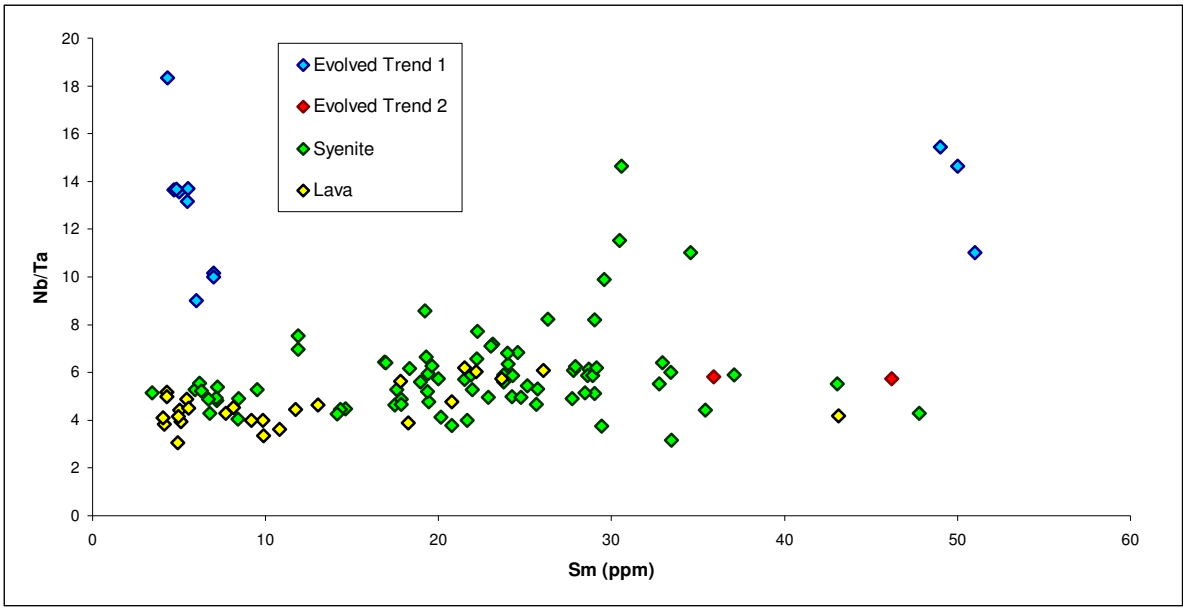

The Nb/Ta variations show that evolved clinopyroxenes of Trend 1 composition have higher ratios than evolved Trend 2 samples. This effect is believed to be caused by differences in the fractionating assemblage between the two trends, and is ascribed to the involvement of sphene. The evolved Trend 1 samples with unusually high Sm content is from the syenitic sample DH39.9. See text for discussion.

The much larger depletion of MREEs in evolved Trend 1 clinopyroxenes compared with evolved Trend 2 analyses may also be explained by the fractionation of sphene from these liquids. Other phases that would effectively fractionate MREE, such as apatite appears on the liquidus during the intermediate stage of melt evolution, and

do not show the pronounced effects in trace element patterns (Figure 8.13) among Group Two samples. The behaviour of MREE is therefore controlled by sphene once the phonolitic stage of fractionation has been reached. The crystallising conditions of lavas and syenites seems thus to have been of the same character during the basaltic and intermediate stage, but the absence of sphene in syenites and the presence of sphene in the lavas during fractionation of the phonolitic stage results in large compositional differences between evolved clinopyroxenes in lavas and syenites.

9 Summary and Conclusions

1. Whole rock composition of lavas and syenites plot within the basanite; tephrite/trachyte, phonolite fields of the TAS classification diagram (Le Bas et al., 1986).

2. Whole rock data of the lavas and syenites show general trends of increasing concentrations in lithophile elements, and decreasing content of elements compatible with olivine and clinopyroxene with decreasing MgO content in the range >4 wt% MgO (mafic compositions), and general trends of decreasing concentrations in Sr, P and Ti, and increasing agpitic index and concentrations in VICE with decreasing Mg content in the range <2 wt% MgO (evolved compositions). Trace element concentrations vary significantly for any given MgO content in the rocks.

3. Clinopyroxene phenocrysts from the Diego Hernández volcanics typically show normal, alternating and reverse zoning. Several cycles of zoning may be observed within a single crystal with abrupt changes in chemistry, often with signs of disequilibrium reactions in previously formed zones, such as incipient melting.

4. From major element variations the clinopyroxenes were divided into three different groups, corresponding to mafic-intermediate and evolved melt compositions. These groups are also recognised in trace element concentrations.

5. Among mafic-intermediate melt compositions clinopyroxenes crystallise as Al- or Na-salites, where Al-salites display the most mafic character, not related to mg#, but exhibited in trace element concentrations. Parameters concerning the ability for high-mg# Na-salites to incorporate trace elements in any significant way compared to Al-salites are negligible. Thus, such differences are attributed to fractionation from melts of different compositions.

6. Amphiboles fractionate from intermediate to evolved melt compositions and data show systematical variations in major element contents, giving rise to two different crystallisation trends, confined to specific samples. This is interpreted as precipitation from melts of different compositions.

7. The Al/Ti ratio in clinopyroxenes reveals two separate evolutionary trends where specific samples coincide with the two crystallisation trends described by amphiboles. These differences are not related to variations in other major element contents, but are recognised in Zr and Hf concentrations from trace elements.

8. Clinopyroxene data show two different trace element patterns among evolved compositions. Compared to each other, one trend has significant higher trace element concentrations and does not show the relatively large MREE depletion compared to LREE and HREE.

9. The compositional variations in whole rock and mineral data are interpreted as the results of fractional crystallisation (removal of ol+cpx and ol+cpx+ox from the most mafic compositions, ±ol+cpx+ox+plag+ap±amph from intermediate compositions and cpx+plag+alkfsp±neph+ap+ox±amph±sph from evolved compositions), repeatedly interrupted by mixing between mafic and more evolved melts (RTF processes, O'Hara, 1977; FCM processes, Neumann et al., 1999).

10. The processes from which pyroxenes of this study were formed occurred at temperatures ranging from about 1050 - 1250 ºC and pressures of about 2 - 11 Kb. This equals depths of about <5 – <15 km, placing the crustal magma chambers within the old oceanic crust and the overlying sequence of Canary Island lavas.

11. RTF processes working in the crustal magma chambers will progressively enrich the melts in incompatible elements, whereas compatible elements quickly will reach constant values, causing decoupling between major and trace elements. This feature is observed in whole rock and mineral data.

12. From variations in Zr/Sm concentrations in clinopyroxene and amphibole data a combination of steady-state fractional crystallisation, magmatic segregation and fractional crystallisation was used in modelling the complex evolution and mixing processes of Diego Hernández melts.

13. Different characteristics among clinopyroxenes in lavas and syenites are interpreted to be caused by differences in magma mixing properties and the fractionating assemblage.

Appendix I Petrography

Thin section	DH97-18A	DH97-18B	DH97-19A	DH97-19B
Rock type	Basaltic lava	Basaltic lava	Mafic lava	Mafic lava
Groundmass	Small fibrous feldspar (plag), cpx and ox.	As 18A, with higher content of larger (<X mm) plag matrix grains.	Fine grained needleshaped plag (<0,025 mm). Turbid textures.	Matrix as 19A.
Minerals	Ol>Plag>Cpx>Ox	Ol>Plag>Cpx>Ox	Plag>Cpx>Ol>Ox	Plag>Cpx>Ol>Ox
Mineral descriptions	Ol Dominating phenocryst phase. Subhedral (<3 mm). No clearly visible reaction rims.	Ol Slightly corroded (<4 mm) grains with small oxide inclusions along the rim.	Plag Common phenocryst phase. Found as individual grains or in aggregates. Largest grains (<2,3 mm) are highly corroded and fragmentated.	Plag Large (<2 mm) grains with reaction rims. Also found as huge (<5 mm) cummulat crystals totally corroded by the melt.
	Plag Found as fibrous, elongated grains or in corroded aggregates.	Plag As 18A, but in larger clusters with the same corrosion degree.	Cpx Large variations within single grains, displaying complex zoning patterns; olive-green to gray/pink colours. Subhedral where rim is gray/pink, and anhedral where rim is green. Contains abundant inclusions of oxides.	Cpx Sum- to almost euhedral grains with weak reaction rims. Hourglass and sector zoning; green to gray, and different shades of gray. Inclusions of oxides. Single green cpx's are highly corroded.
	Cpx Sub/anhedral zoned grains (hourglass), associated with or containing inclusions of oxides. Substantial corrosion and fragmentating.	Cpx Subhedral as phenocryst phase and anhedral as groundmass crystal. Several inclusions of oxides and slightly corroded rims.	Ol Decreasing apperance compared to 18-series. Found as small (<1 mm) subhedral grains with clearly visible reaction rims.	Ol Small (<0,75 mm) murky grains, highly corroded.
	Ox Associated with cpx or found as <1 mm corroded grains	Ox As 18A	Ox No common matrix or phenocryst phase. Associated with cpx in a corroded state.	Ox Only found associated with cpx.

Thin section	DH97-20	DH97-22A	DH97-22B	DH97-22C
Rock type	Phonolitic lava	Ignimbrite	Black glass	Blask pumice block
Groundmass	Almost aphyric. Murky matrix with needleshaped plag, cpx, ox and reaction minerals.	Glass; dominating white over black. Incomplete mixing.	Glass; dominating dark with flow structures. Mingled magma.	Glass; mingled magma. Dominantly white over black component.
Minerals	Cpx>Plag>Ox	Fsp>Ox>Cpx>Ol>(Amph)	Fsp>Cpx>Amph>Ox>(Ap)	Fsp>Amph>Ox>Cpx
Mineral descriptions	Cpx Varies in size (0,2-0,5 mm) and shape (sub/anhedral to euhedral). Occurs as single grains or in aggregates. Abundant oxide inclusions. Zoning in euhedral grains. Plag Scattered in the sample as <0,5 mm corroded grains. Ox Found scattered througout the sample. Associated with cpx or as small (<0,25 mm) individual grains.	Fsp Patchwork of different crystals (0,2-1,5 mm) in aggregates.Associated with cpx, ol and often encircle oxides. Zoned. Single grains are highly corroded. Ox Occurs as subhedral <0,5 mm grains in association with fragmented ol, and in corroded cpx. Cpx Euhedral <0,7 mm grains. Pink speciments either highly corroded or with clear reaction rims. Contains inclusions of ox. Ol Fragmentated (~0,2 mm) grains situated in white glass. No clear corrosion rims. Amph Anhedral, corroded grains in dark glass. Inclusions of ap. Zoned.	Fsp Occurs as two main types (0,1-1,5 mm); corroded plag and uncorroded alkfsp associated in white glass. Zoned without any inclusions. Cpx Associated in white glass. Gray cpx (0,3-2,0 mm) is in clear disequilibrium with the melt. Contains several inclusions of oxides. Amph Subhedral (0,5-1,2 mm), fragmentated and zoned. Inclusions of ap. Grows as laths around corroded cpx in dark glass. Ox Associated in dark glass. Anhedral (0,3-0,7 mm). Occurs as inclusions in cpx, and corroded amph. Ap Occurs as small inclusions in amph.	Fsp Fragmentated, sub/euhedral grains (0,3-2,5 mm) associated in dark glass as crystals or laths. Large grains are highly corroded. Homogenous crystallisation without inclusions. Amph Subhedral (1,0-1,5 mm), fagmentated and zoned grains in dark glass. Inclusions of ap. Ox Subhedral (0,1-0,6 mm), fragmentated and corroded grains associated with dark glass or as inclusions in cpx. Cpx Occurs as subhedral (~0,6 mm) grains in dark glass. Weak corrosion rims. Oxide inclusions. No visible zoning)

Thin section	DH97-22D	DH97-24	DH97-26A	DH97-26B
Rock type	Phonolitic pumice block	Phonolitic pumice	Phonolitic pumice	Welded ignimbrite
Groundmass	Glass; dominantly white 'patches' intwined with black flow structures.	Glass; white with a slightly dark component.	Glass: dominantly white with small blebs of a mafic component.	Glass: mixed black and white with flow textures. Trapped xenoliths with needle like plagioclase as groundmass crystals.
Minerals	Fsp>Cpx>Amph>Ox>(Ap)	Fsp>Amph>Cpx>Ox(Ap)	Near aphyric: Fsp>Cpx	Fsp>Cpx>Ox>Ol>Amph>(Ap)
Mineral descriptions	Fsp Fragmentated laths and corroded crystals (0,2-1,7 mm). Two types: Alkfsp (largest grains) - corroded in dark glass, plag – corroded in light glass. No inclusions.	Fsp Fragmented euhedral (Alkfsp) to subhedral (Plag) crystals (0,25-2 mm). Plag with reaction rims	Fsp Subhedral to anhedral grains (0,25-2 mm). Fragmented with reaction rims. Zoning occurs. Long prismatic crystals.	Fsp Subhedral to anhedral 0,025-2 mm grains. Plag: usually with defined crystals in dark glass as patchy laths defining domains, Found as individual crystals with reaction rims in white glass. Contains inclusions of ox and corroded (dissolved) cpx. Often zoned. Alkfsp: fragmented grains with clear signs of disequilibrium (corrosion). Exolution lamellae in some grains.
	Cpx Subhedral (0,3-0,9 mm) grains. Corroded in white glasss but preserve crystal form when associated with dark glass. Zoned, fragmentated and occurs with inclusions of oxides.	Amph Subhedral grains (0,5-1 mm). No visible reaction rims, but often fragmented. Contains inclusions of ap.	Cpx Anhedral, 1 mm grains. Light green crystals with reaction rims. Zoned.	Cpx Subhedral to anhedral 0,2-2 mm grains. Pink crystals associated with xenolitic domains contain inclusions of fsp and ox, and are zoned. Fragmented, zoned, greenish grains with reaction rims contain inclusions of ox and ap.
	Amph Occurs as subhedral, fragmented and zoned grains (0,6-0,9 mm) with small reaction rims when associated with dark glass. Larger grains are more corroded than smaller ones. Contain inclusions of ap.	Cpx Located in murky domains as highly corroded, almost disintegrated grains, clearly in disequilibrium.		Ox Found as inclusions in, or associated with, fsp and cpx. 0,01-0,25 mm anhedral grains.
	Ox Round corroded, anhedral grains. Found as two types in reflected light: Small yellow cores and gray rims.	Ox Found as small 0,05 mm anhedral grains scattered throughout the sample		Ol O,25-0,5 mm subhedral grains associated with dark glass. Weak reaction rims and signs of zoning.
		Ap Occurs as small inclusions in amph.		Amph Subhedral (0,5 mm) grains with reaction rims. Contains small inclusions of ap.

Thin section	DH97-26C	DH97-27A	DH97-27B	DH97-28B
Rock type	Phonolitic pumice	Phonolitic pumice	Phonolitic pumice	Basalt
Groundmass	Glass: mixed white and black. Flow structures. Xenolitic domains as 26B.	Glass: mixed white and black. Flow structures. Small xenolitic domains with plagioclase groundmass crystals.	As 27A	Plagioclase needles, some cpx, ox and dark glass.
Minerals	Near aphyric: Fsp>Cpx>Ox	Fsp>Neph>Cpx>(Ox)>(Ap)	As 27A	Cpx>Ox>Plag>Ol
Mineral descriptions	Fsp Highly corroded and fragmented anhedral grains (0,05-0,9 mm) scattered in the sample. Clearly in disequilibrium with host glass. Cpx Subhedral to anhedral 0,25-1 mm clear green grains. Reaction rims. Zoned. Inclusions of ox and ap. Ox Found as 0,05-0,5 mm grains scattered throughout the sample, often in association with cpx or as highly corroded grains in xenolitic material.	Fsp Subhedral (0,25-2 mm) alkfsp with reaction rims in black glass. Inclusions of ap. Plag define domains where long needle like crystals cluster together. Visible zoning towards rims. Corroded around edges. Neph Large (1 mm) subhedral grains with reaction rims against dark glass. Single crystals scattered throughout. Cpx Fragmented anhedral 0,25-0,5 mm green grains. Inclusions of ox and ap. Corroded. Ox Accessory phase associated with cpx as inclusions. Ap Accessory phase found as inclusions in cpx and fsp.	Fsp As 27A Neph As 27A Cpx As 27A, but also with fragmented pinkish grains. Corroded and Zoned. As 27A As 27A	Cpx 0,1-1,5 mm euhedral to subhedral grains. Zector and hourglass zoned. Corrosion along some rims. Found as single grains or in clusters. Inclusions of ox and plag. 'Greencores' with overgrowths of gray to pinkish zones. Ox Scattered 0,2-0,7 mm grains throughout the sample. Often associated with cpx. Plag Large (1 mm) higly corroded grains with signs of incipient melting. Ol Found as small (0,25 mm) subhedral grains in clusters with cpx. Slightly corroded.

Thin section	DH97-29A	DH97-29B	DH97-30A	DH97-30B
Rock type	Basalt	Basalt	Basalt	Basalt
Groundmass	As 28B, but with finer matrix crystals.	As 28B	As 28B	As 28B, with flow structures of finer grained matrix.
Minerals	Cpx>Ox	Cpx>Ox	Cpx>Ox	Cpx>Ox>(Ol)
Mineral descriptions	Cpx As 28B, but with the absence of 'greencores'. Ox As 28B, smaller grains (<0,5 mm).	Cpx As 28B, but does not form aggregate clusters. Missing 'greencores'. Ox As 28B, but with smaller grains (0,1-0,3 mm).	Cpx As 28B, but without clusters and hourglass zoning. No 'greencores'. Ox As 29B	Cpx Appearance as 28B, without clusters. Ox As 28B. Ol Small 0,25 mm grains associated with Cpx. Corrosion along rims.

Thin section	DH97-4	D97-12	DH97-13A	DH97-13B
Rock type	Mixed porphyritic fallout	Basalt	Basalt	Basalt
Groundmass	Dominantly white glass, with domains of dark xenolitic material in a groundmass of small needle like plagioclase.	Small (0,1-0,25 mm) needle shaped plag, cpx (<0,15 mm), ox and dark glass. Vesicular.	Fine grained matrix consisting of plag, cpx, ox and dark glass.	Needle shaped plag, cpx, ox and dark glass.
Minerals	Fsp >Amph>Cpx >Ox>(Ap)	Fsp>Cpx>(Ox)	Fsp>Cx>Ox	Fsp>Cpx>Ox
Mineral descriptions	Fsp Plag: occurs as euhedral to anhedral grains (0,1-2,5 mm). Zoned and corroded. Usually present associated with dark groundmass in aggregates with cpx, amph and ox. Contains inclusions of ox, amph, ap and cpx. Overgrowths on alkfsp. Alkfsp: Anhedral grains (0,2-1,5 mm). Fragmented and highly corroded in association with dark groundmass. Often rimmed with plag. Inclusions of ox, amph and remnants of cpx.	Fsp Plag: Occurs as subhedral (0,3-2,5 mm) grains. Slightly corroded along some rims. Zoned and fragmented. Alkfsp: found as 0,5-1,5 mm anhedral grains, with clear signs of disequilibrium to host rock. Corroded.	Fsp Plag: 0,2-1,25 mm grains of several types. May be fragmented and euhedral with no visible reaction rims, or anhedral with visible signs of incipient dissolution. Zoned. Alkfsp: 0,5-1 mm anhedral highly corroded grains in clear disequilibrium.	Fsp As 13A, but larger plag grains (<2,5 mm).
	Amph Subhedral (0,2-2,5 mm). Scattered throughout the sample. Inclusions of ox, ap and fsp. Fragmented. Corroded in the presence of dark domains.	Cpx 0,2-1 mm subhedral grains. Fragmented and often highly corroded. Zoned and forms cluster aggregates. Light green to grey/pink in colour.	Cpx 0,3-1,3 mm euhedral to subhedral grains. Cores may show signs of incipient melting while rims are uncorroded. Zoned (complex and hourglass) and often fragmented. Contains inclusions of ox.	Cpx Same textures as 13A, with the addition of light green cores in some grains.
	Cpx Occurs as corroded and fragmented greenish anhedral grains with inclusions of ox and ap, or as more subhedral pinkish grains in association with dark domains (0,1-2,5 mm).	Ox Found associated with or as inclusions in cpx.	Ox 0,2-0,5 mm grains scattered throughout the sample. Single grains or associated with cpx as inclusions.	Ox As 13A, but larger grains <1 mm.
	Ox Occurs as 0,05-0,5 mm grains scattered in the thin section. Often associated with other phenocryst phases.			
	Ap Mainly found as small inclusions in amph.			

Thin section	DH97-17	DH97-39.1	DH97-39.2	DH97-39.4
Rock type	Basalt	Syenite	Syenite	Syenitic
Groundmass	As 13B, with flow textures containind finer grained matrix.	Laths of alkalifeldspar and nepheline, subordinate plag, cpx. Secondary minerals. All highly corroded.	Large laths of plag (<3 mm), highly corroded.	Same as 39.2, with the addition of alkfsp in the matrix
Minerals	Fsp>Cpx>Ox	Amph>Neph>Cpx>Ox>(Ap)	Cpx>Ox>Amph>(Ap)	Cpx>Ox>Amph>Ol>(Ap)
Mineral descriptions	Fsp: As 13A, but with larger plag grains <2,5mm, and smaller Alkfsp grains <0,8 mm. Cpx: As 13B, with larger grains <3 mm, Inclusions of plag. Forms aggregates with ox. Ox: As 13A.	Amph: 0,25-3 mm grains, euhedral to subhedral. Some with reaction rims. Zoned. Inclusions of ap and ox. May form large aggregates. Neph: Occurs as large <3 mm higly corroded grains. Evidence of incipient melting Cpx: Occurs as highly corroded anhedral grains (0,1-0,6 mm). Inclusions of ox. Pale grey colour. Zoned. Ox: Scattered throughout the sample in association with other phases and ound as inclusions. Anhedral grains (0,1-1 mm). Ap: Found as inclusions in amph and occasionally in groundmass.	Cpx: Occurs as grey/pink and light green grains (0,25-5 mm). Varies from anhedral to subhedral. Zoned. Several cores show signs of disequilibrium (corrosion). Inclusions of ox and ap. Ox: Scattered throughout the sample. Anhedral to subhedral 0,1-2 mm grains. Forms large aggregates with cpx. Found as inclusions in cpx. Amph: Small <0,5 mm subhedral grains with reaction rims, and remnants of larger grains corroded to form secondary minerals. Ap: Found as inclusion inn all phenocryst phases.	Cpx: As 39.2, except smaller grains (<2 mm). Ox: As 39.2, but more and smaller grains (<1 mm) Amph: Only small <0,5 mm anhedral grains, with visible reaction rims against ox. Inclusions of ap. Ol: Small (0,1-0,2 mm) highly corroded anhedral grains found in association with cpx-ox aggregates. Ap: Accessory phase found as inclusions in all phases.

Thin section	DH97-39.5	DH97-39.7	DH97-39.8	DH97-39.9
Rock type	Syenitic	Syenitic	Syenitic	Syenitic
Groundmass	Gray murky matrix of secondary minerals formed from plag. Some highly corroded laths of plag.	Large laths of plag (<3 mm), corroded, with some visibly zoned towards rims. Alkfsp.	As 39.7	Framework of dominantly neph laths and some alkfsp. Murky domains with highly corroded groundmass grains.
Minerals	Cpx>Amph>Ox>(Ap)	Cpx>Amph>Ox>(Ap)	Cpx>Amph>Ox	Cpx>Amph>Ox>(Ap)
Mineral descriptions	Cpx 0,5-3 mm anhedral to subhedral grains with reaction rims against ox forming secondary minerals. Amph <1 mm corroded grains with signs of disequilibrium reactions. Anhedral. Ox Grains (0,3-2 mm) found in aggregates, growing along cpx rims. Ap Scattered throughout the sample, not in any association with other phases than amph.	Cpx Occurs as highly corroded grains (0,2-2 mm), with reaction rims and signs of melting. Corroded by the growth of ox. Amph Occurs as cpx. Contains inclusions of ap. Ox Grows as large aggregates around amph and cpx, forming large grains (0,3-3 mm). Inclusions of ap. Ap Scattered throughout. As inclusions in some amph, and engulfed where ox has reacted along amph rims.	Cpx As 39.7, but some larger grains (<4 mm). Also show more reaction with ox, especially in the cores, rather than the rims. Amph As 39.7. May show total replacement by ox. Ox Occurs as 0,3-3 mm grains scattered throughout the sample, replacing amph and cpx.	Cpx Found as pale green to grey anhedral 0,25-0,9 mm grains. Highly corroded. Inclusions of ap and ox. Fragmented. Disequilibrium reactions observed. Amph Fragmented and corroded grains (0,25-0,6 mm). Contains inclusions of ap. Reaction rims against groundmass and ox. Ox Scattered in the sample, growing around aggregates of cpx and amph. Totally replaces silicates in murky domains. Ap Scattered in the sample. Often found associated with, or as inclusions in amph.

Thin section	DH97-37.1	DH97-37.2	TF12.1	TF12.2
Rock type	Gabbro	Gabbro	Syenitic	Syenitic
Groundmass	Dark groundmass of dominantly secondary minerals, abundant dissolved plag, cpx and ox	As 37.1	Crystalline	Framework of large <2 cm plag grains.
Minerals	Amph>Plag>Cpx>Ox>(Ap)	Amph>Plag>Cpx>Ox>(Ap)	Cpx>Plag>Amph>Ox>(Ap)	Plag>Amph>Ox>Cpx>Ap
Mineral descriptions	Amph Euhedral to subhedral grains (0,25-2 mm). Reaction rims on some grains. Inclusions of ap and ox. Plag Large (6 mm) totally corroded grains. Melt disequilibrium, and formation of secondary minerals. Cpx Usually found as anhedral to subhedral (0,2-2 mm) greenish corroded grains, clearly in disequilibrium. Zoned. Inclusions of ox and ap. Ox Scattered in association with silicates. Subhedral (0,2-0,5 mm) grains. Ap Inclusions in cpx and amph.	Amph As 37.1, but amphiboles seems more corroded. Plag As 37.1 Cpx As 37.1 Ox As 37.1 Ap As 37.1	Cpx Pale greenish (0,2-1,2 mm) grains. Zoned. Inclusions of ap and ox. Fragmented. Subhedral. 'Greencores'. Reaction rims. Plag Lathlike framework of needle shaped grains (0,2-2 mm). Signs of incipient melting. Amph Anhedral (0,5-1 mm). Fragmented. Contains inclusions of ap and ox. Ox Grows interstitially, corroding associated mafic silicates. Found as inclusions I cpx and amph. Ap Scattered throughout. As inclusions in cpx, amph and ox.	Plag Framework of large, corroded and zoned grains. Inclusions of ap. Amph Large 1 cm anhedral grains with reaction rims. Corroded against ox. Fragmented. Inclusions of ap. Ox Forms large (<0,5 cm) grains in clusters associated with amph, and replacing cpx. Cpx Found as greenish anhedral (0,3 mm) remnants associated with amph. Replaced by ox. Corroded, with signs of melting. Ap Scattered as inclusions in silicates.

Thin section	**TF12.3**	**TDKS 17.3/4/5**	**TDKS 17.11**
Rock type	Syenitic	Syenitic	Syenitic
Groundmass	Crystalline (secondary minerals).	Crystalline framework of fibrous (1-1,5 mm) plag and secondary minerals.	Crystalline framework of Fsp
Minerals	Amph>Plag>Ox>Cpx>Ap	Plag>Cpx>Ox>Alkfsp>(Ol)>(Ap)	Plag>Alkfsp>Cpx>Ox>(Ap)
Mineral descriptions	Amph Patchwork of grains (<3 mm) defining domains. Anhedral with clear signs of disequilibrium. Inclusions of ap, plag and ox. Plag Framework of (<1,25 mm) grains, defining whith domains. Anhedral. Inclusions of ox. Disequilibrium, corrosion. Ox Growing in dark domains, replacing amph. Rounded 0,5 mm grains. Inclusions in plag. Cpx As 12.2 Ap As 12.2	Plag Elongated (<1,5 mm) grains. Subhedral with reaction rims. Zoned Cpx Pale grey to pink anhedral to subhedral grains (0,2-1,2 mm). Zoned. Reaction rims. Corroded. Inclusions of ox and ap. Forms clusters. Ox Scattered, often in association with cpx. Anhedral grains (0,25-0,5 mm). Alkfsp Large (1 mm) subhedral grains. Reaction rims. Corroded. Clear zoning. Ap Found as small inclusions in cpx. Ol Small anhedral(<0,2 mm) grains found in association with reaction rims of cpx and ox.	Fsp Plag: Fibrous elongated grains (<2,5 mm). Subhedral. Corrosion and evidence of incipient melting. Alkfsp: Subhedral (<1,5 mm) grains. Zoned. Signs of corrosion. Cpx As 17.3 Ox As 17.3

Appendix II Geochemical Data

Table A2.1. Clinopyroxene major element: lavas.

Sample	DH97-18A					
Grain core/int/rim	**4-1d core**	**4-1c int**	**4-1a rim**	**4-2d core**	**4-2b int**	**4-2a rim**
SiO2	50,65	48,22	43,48	47,53	45,15	50,10
TiO2	1,04	1,12	2,21	1,30	1,70	1,64
Al2O3	3,44	5,74	8,90	5,79	8,21	3,32
Cr2O3	0,01	1,00	0,00	0,01	0,11	0,00
FeO	7,11	7,00	8,33	7,38	7,81	8,63
MnO	0,30	0,16	0,21	0,25	0,17	0,32
MgO	13,84	12,99	10,89	12,69	11,86	12,67
NiO	0,00	0,00	0,00	0,09	0,00	0,00
CaO	22,42	22,85	22,67	22,49	22,83	21,76
Na2O	0,63	0,56	0,62	0,67	0,51	0,65
Sum	99,44	99,64	97,31	98,20	98,35	99,09
mg#	77,6	76,8	70,0	75,4	73,0	72,4

Sample	DH97-18B					
Grain core/int/rim	**3-1f core**	**3-1c int**	**3-1a rim**	**8-1f core**	**8-1e int©**	**8-1a rim**
SiO2	49,35	45,89	45,63	48,25	51,39	49,09
TiO2	2,00	3,09	4,18	2,34	1,14	2,36
Al2O3	4,72	7,98	6,63	5,48	2,78	4,41
Cr2O3	0,13	0,08	0,00	0,00	0,00	0,00
FeO	6,69	7,18	8,39	7,27	7,28	7,31
MnO	0,18	0,08	0,18	0,21	0,37	0,15
MgO	13,75	12,10	11,56	13,09	14,02	13,99
NiO	0,00	0,01	0,00	0,03	0,00	0,10
CaO	22,74	22,65	22,06	22,49	22,42	22,33
Na2O	0,43	0,57	0,64	0,64	0,70	0,44
Sum	99,99	99,63	99,27	99,80	100,10	100,18
mg#	78,6	75,0	71,1	76,2	77,4	77,3

Sample	DH97-19A					
Grain core/int/rim	**1-1e core**	**1-1b int**	**1-1a rim**	**5-1l core**	**5-1k core**	**5-1g int ->**
SiO2	51,90	51,10	51,64	51,93	51,66	51,14
TiO2	0,75	1,02	1,08	0,79	1,16	1,04
Al2O3	1,69	2,33	2,51	1,81	2,49	2,32
Cr2O3	0,00	0,06	0,00	0,00	0,00	0,02
FeO	12,05	10,07	9,05	9,96	8,22	10,08
MnO	1,21	0,85	0,67	1,09	0,69	0,86
MgO	9,46	10,97	12,04	11,11	12,16	10,84
NiO	0,00	0,06	0,05	0,00	0,00	0,00
CaO	20,47	21,91	22,09	21,56	22,07	21,68
Na2O	2,26	1,63	1,32	1,61	1,29	1,66
Sum	99,79	100,00	100,45	99,86	99,74	99,64
mg#	58,3	66,0	70,3	66,5	72,5	65,7

Table A2.1. Continued.

Sample	DH97-19A				DH97-19B	
Grain core/int/rim	5-1e int ->	5-1c int ->	5-1b int ->	5-1a rim	1-1e core	1-1i int
SiO2	48,85	47,02	46,93	43,77	48,20	47,23
TiO2	2,03	2,64	2,51	4,31	2,21	2,49
Al2O3	4,36	6,89	6,84	8,82	5,97	6,51
Cr2O3	0,00	0,41	0,50	0,05	0,47	0,26
FeO	8,36	6,92	6,64	8,45	6,51	6,70
MnO	0,34	0,11	0,09	0,12	0,11	0,10
MgO	12,09	12,78	12,66	11,03	13,23	12,91
NiO	0,02	0,03	0,11	0,00	0,00	0,00
CaO	22,69	22,74	22,78	22,09	22,85	22,83
Na2O	0,94	0,45	0,49	0,62	0,53	0,52
Sum	99,68	99,99	99,55	99,26	100,08	99,55
mg#	72,0	76,7	77,3	69,9	78,4	77,4

Sample	DH97-19B					
Grain core/int/rim	1-1k rim	2-1i core	2-1f int	2-1a rim	3-1e core	3-1f int
SiO2	44,74	45,41	44,98	44,04	51,65	50,87
TiO2	4,02	3,32	3,51	3,83	0,77	1,12
Al2O3	8,36	7,94	8,41	8,84	1,82	2,64
Cr2O3	0,03	0,37	0,09	0,10	0,00	0,00
FeO	8,38	7,45	7,82	7,70	9,56	9,07
MnO	0,15	0,10	0,13	0,18	0,85	0,76
MgO	11,15	11,87	11,64	11,46	11,26	11,65
NiO	0,01	0,04	0,02	0,00	0,00	0,01
CaO	22,39	22,68	22,74	22,58	22,47	22,23
Na2O	0,78	0,55	0,58	0,64	1,46	1,45
Sum	100,01	99,73	99,92	99,37	99,84	99,80
mg#	70,3	74,0	72,6	72,6	67,7	69,6

Sample	DH97-19B	DH97-20				
Grain core/int/rim	3-1h rim	1-1c core	1-1b int	1-1a rim	2-1j core	2-1k int©
SiO2	46,17	48,10	46,47	46,66	46,43	46,22
TiO2	3,21	2,35	3,03	3,46	3,02	3,01
Al2O3	6,74	5,30	5,81	5,88	6,88	7,04
Cr2O3	0,04	0,00	0,00	0,00	0,00	0,00
FeO	7,96	6,91	7,58	7,89	7,45	7,15
MnO	0,20	0,16	0,15	0,14	0,16	0,15
MgO	11,93	13,44	12,79	12,19	12,42	12,39
NiO	0,03	0,00	0,00	0,00	0,00	0,02
CaO	22,48	22,78	22,78	22,26	22,92	22,84
Na2O	0,72	0,41	0,45	0,65	0,63	0,58
Sum	99,48	99,45	99,06	99,13	99,91	99,40
mg#	72,8	77,6	75,0	73,4	74,8	75,5

Table A2.1. Continued.

Sample	DH97-22A					
Grain core/int/rim	2-1m int®	2-1p rim	2 core	2 rim	2 rim	5 core
SiO2	47,57	50,67	51,63	50,30	50,62	50,20
TiO2	2,48	1,65	0,49	0,96	0,75	1,18
Al2O3	5,52	2,93	1,29	2,08	2,06	2,17
Cr2O3	0,02	0,00	0,00	0,03	0,03	0,00
FeO	7,50	7,74	13,27	13,44	13,98	14,67
MnO	0,17	0,28	1,40	1,10	1,28	1,23
MgO	13,49	12,74	9,01	8,46	8,22	7,86
NiO	0,00	0,05	0,01	0,03	0,00	0,00
CaO	22,19	22,94	20,71	20,12	19,76	19,49
Na2O	0,41	0,73	2,19	2,57	2,68	2,79
Sum	99,35	99,73	100,00	99,09	99,38	99,59
mg#	76,2	74,6	54,8	52,9	51,2	48,8

Sample	DH97-22A					DH97-22B
Grain core/int/rim	5 rim	5 rim	9 core	9 rim	9 rim	3 core
SiO2	51,21	51,83	47,11	46,98	46,61	50,97
TiO2	0,72	0,41	2,72	2,91	2,88	0,50
Al2O3	1,83	1,37	6,27	6,38	6,68	1,16
Cr2O3	0,00	0,00	0,00	0,00	0,03	0,00
FeO	13,60	12,77	7,84	7,41	7,07	14,22
MnO	1,33	1,38	0,21	0,17	0,17	1,53
MgO	8,53	9,02	12,24	12,69	12,56	9,20
NiO	0,02		0,01	0,04	0,03	0,00
CaO	20,24	20,71	22,62	22,57	22,63	20,93
Na2O	2,61	2,12	0,67	0,61	0,58	1,49
Sum	100,09	99,61	99,69	99,76	99,24	100,00
mg#	52,8	55,7	73,6	75,3	76,0	53,6

Sample	DH97-22B					DH97-22C
Grain core/int/rim	3 int	3 rim	3 rim	4 core	4 rim	8 core
SiO2	48,73	50,84	46,41	46,15	47,47	46,46
TiO2	2,14	1,53	3,27	3,03	2,82	3,16
Al2O3	3,49	3,04	7,16	6,72	6,18	7,09
Cr2O3	0,00	0,00	0,01	0,00	0,00	0,00
FeO	10,01	7,67	7,22	8,49	7,15	7,34
MnO	0,66	0,47	0,13	0,16	0,08	0,17
MgO	11,57	13,07	12,68	11,84	12,76	12,51
NiO	0,00	0,00	0,00	0,04	0,00	0,00
CaO	22,10	22,22	22,87	22,34	22,43	22,91
Na2O	0,98	0,99	0,51	0,83	0,63	0,54
Sum	99,68	99,83	100,26	99,60	99,52	100,18
mg#	67,3	75,2	75,8	71,3	76,1	75,2

Table A2.1. Continued.

Sample	DH97-22C		DH97-22D			
Grain core/int/rim	8 core	8 rim	8 rim	1 core	1 rim	3 core
SiO2	47,85	44,82	46,05	51,39	51,28	50,81
TiO2	2,24	3,61	2,98	0,97	1,08	1,23
Al2O3	5,84	8,45	7,36	2,04	2,34	2,66
Cr2O3	0,00	0,00	0,00	0,02	0,04	0,02
FeO	6,87	7,73	7,36	7,70	7,76	8,01
MnO	0,10	0,14	0,14	0,58	0,55	0,54
MgO	13,34	11,93	12,32	12,91	13,22	12,77
NiO	0,01	0,00	0,00	0,00	0,00	0,01
CaO	22,80	22,58	22,55	22,43	22,36	22,34
Na2O	0,46	0,62	0,59	1,11	1,03	1,16
Sum	99,51	99,88	99,35	99,15	99,66	99,55
mg#	77,6	73,3	74,9	74,9	75,2	74,0

Sample	DH97-22D					DH97-26B
Grain core/int/rim	3 rim	3 rim	7 core	7 rim	7 rim	6A core
SiO2	50,21	50,31	45,06	45,42	44,83	44,57
TiO2	1,34	1,31	3,35	3,12	3,29	3,35
Al2O3	2,84	2,94	8,30	7,38	7,94	8,43
Cr2O3	0,02	0,00	0,00	0,00	0,01	0,02
FeO	7,86	8,16	7,56	7,25	7,56	7,58
MnO	0,48	0,59	0,15	0,12	0,20	0,07
MgO	12,82	12,50	11,55	11,87	11,90	11,61
NiO	0,00	0,00	0,00	0,03	0,05	0,01
CaO	22,32	22,26	22,48	22,85	22,68	23,12
Na2O	1,02	1,11	0,59	0,63	0,60	0,50
Sum	98,91	99,18	99,04	98,67	99,06	99,26
mg#	74,4	73,2	73,1	74,5	73,7	73,2

Sample	DH97-26B					
Grain core/int/rim	6A rim	6A rim	6B core	6B rim	6B rim	5 core
SiO2	44,82	44,06	49,52	51,21	51,07	49,21
TiO2	3,31	3,73	1,15	0,53	0,60	1,84
Al2O3	8,39	9,30	2,76	1,77	1,92	4,16
Cr2O3	0,00	0,00	0,00	0,00	0,00	0,02
FeO	7,44	7,58	14,61	12,94	12,93	9,28
MnO	0,15	0,10	1,36	1,28	1,29	0,48
MgO	11,66	11,43	7,67	9,18	8,87	11,45
NiO	0,05	0,02	0,01	0,02	0,01	0,00
CaO	22,90	23,12	20,12	20,92	20,43	22,66
Na2O	0,48	0,49	2,43	2,17	2,15	1,11
Sum	99,20	99,83	99,63	100,02	99,27	100,21
mg#	73,6	72,9	48,3	55,8	55,0	68,7

Table A2.1. Continued.

Sample	DH97-26B					
Grain core/int/rim	5 rim	5 rim	4 core	4 rim	4 rim	10 core
SiO2	50,24	48,86	50,83	50,09	50,75	49,21
TiO2	1,56	2,17	1,40	1,38	1,38	1,19
Al2O3	3,70	4,55	2,99	2,96	2,90	2,71
Cr2O3	0,00	0,01	0,00	0,00	0,01	0,01
FeO	8,10	8,88	8,37	8,75	8,53	14,96
MnO	0,54	0,36	0,56	0,67	0,60	1,31
MgO	12,31	12,20	12,36	12,00	12,18	7,58
NiO	0,00	0,00	0,01	0,00	0,02	0,00
CaO	22,25	22,07	22,60	22,04	22,24	20,05
Na2O	1,02	1,15	1,10	1,26	1,23	2,56
Sum	99,72	100,25	100,22	99,15	99,84	99,58
mg#	73,0	71,0	72,5	71,0	71,8	47,5

Sample	DH97-26B					DH97-26C
Grain core/int/rim	10 rim	10 rim	6 core	6 rim	6 rim	VI-4 core
SiO2	50,91	50,50	51,58	50,86	51,65	51,11
TiO2	0,70	0,81	0,47	1,34	1,12	0,43
Al2O3	1,92	2,14	1,40	2,81	2,47	1,38
Cr2O3	0,00	0,00	0,00	0,03	0,02	0,03
FeO	12,36	14,01	12,62	8,45	8,41	12,79
MnO	1,22	1,40	1,37	0,52	0,60	1,23
MgO	9,11	8,59	9,26	12,23	12,70	9,27
NiO	0,04	0,00	0,03	0,00	0,00	0,03
CaO	20,88	20,72	21,51	22,39	22,33	21,46
Na2O	2,16	2,24	1,74	1,18	1,06	1,81
Sum	99,30	100,41	99,95	99,81	100,36	99,54
mg#	56,8	52,2	56,7	72,1	72,9	56,4

Sample	DH97-26C					
Grain core/int/rim	VI-4 rim	VI-2 core	IV-3 core	IV-3 rim	VI-2 core	VI-7 core
SiO2	50,86	50,48	46,96	50,69	50,52	50,98
TiO2	1,12	0,75	2,45	1,11	0,67	1,02
Al2O3	2,57	2,14	5,27	2,71	2,07	2,36
Cr2O3	0,00	0,00	0,00	0,03	0,00	0,01
FeO	8,75	13,93	9,15	7,49	13,35	8,60
MnO	0,62	1,44	0,46	0,43	1,35	0,57
MgO	11,66	8,43	11,12	13,18	8,74	12,32
NiO	0,00	0,00	0,00	0,02	0,06	0,02
CaO	22,06	20,37	22,24	22,57	20,50	22,10
Na2O	1,24	2,19	1,10	0,87	2,20	1,07
Sum	98,88	99,73	98,75	99,10	99,46	99,05
mg#	70,4	51,9	68,4	75,8	53,9	71,9

Table A2.1. Continued

Sample	DH97-28B				DH97-29A	
Grain core/int/rim	2-1g core	2-1c int	2-1b int®	2-1a rim	3-1c core	3-1a rim
SiO2	48,32	44,17	43,57	42,67	45,76	45,74
TiO2	2,16	4,18	4,10	5,29	3,14	3,66
Al2O3	4,84	8,76	8,44	9,73	7,42	7,10
Cr2O3	0,00	0,00	0,05	0,00	0,18	0,07
FeO	6,90	7,99	7,73	8,32	7,43	7,84
MnO	0,16	0,13	0,25	0,15	0,12	0,25
MgO	13,57	11,35	11,56	10,53	12,39	11,88
NiO	0,04	0,00	0,00	0,00	0,00	0,06
CaO	22,84	22,39	22,66	22,13	22,94	22,77
Na2O	0,47	0,53	0,53	0,72	0,51	0,59
Sum	99,30	99,50	98,89	99,54	99,89	99,96
mg#	77,8	71,7	72,7	69,3	74,8	73,0

Sample	DH97-29B				DH97-30A	
Grain core/int/rim	5-1h core	5-1i int©	5-1m int®	5-1n rim	2-1c core	2-1e int
SiO2	47,22	45,84	48,49	47,20	42,92	42,74
TiO2	2,53	3,09	2,32	2,80	4,60	4,62
Al2O3	6,08	7,53	4,72	5,80	9,24	9,15
Cr2O3	0,00	0,00	0,09	0,10	0,02	0,08
FeO	6,38	6,90	6,60	7,20	7,71	7,87
MnO	0,09	0,15	0,18	0,10	0,15	0,18
MgO	13,09	12,31	13,79	13,00	11,10	10,97
NiO	0,08	0,03	0,00	0,00	0,03	0,00
CaO	23,30	22,99	22,97	22,90	22,96	23,08
Na2O	0,45	0,50	0,37	0,40	0,52	0,57
Sum	99,22	99,34	99,53	99,50	99,25	99,26
mg#	78,5	76,1	78,8	76,3	72,0	71,3

Sample	DH97-30A			DH97-30B		DH97-4
Grain core/int/rim	2-1f rim	5-1e core	5-1d rim	5-1o core	5-1q rim	2A
SiO2	41,31	48,88	48,60	48,80	46,24	48,93
TiO2	5,12	1,98	2,11	1,88	3,13	2,09
Al2O3	10,33	4,91	5,21	4,80	6,18	5,03
Cr2O3	0,17	0,15	0,01	0,41	0,07	0,00
FeO	8,27	6,03	6,22	5,87	7,63	7,69
MnO	0,17	0,09	0,14	0,15	0,12	0,34
MgO	10,34	13,78	13,50	14,03	12,80	12,52
NiO	0,00	0,00	0,04	0,00	0,09	0,09
CaO	22,68	23,19	23,35	23,65	22,59	21,93
Na2O	0,59	0,46	0,47	0,45	0,38	0,66
Sum	98,98	99,47	99,65	100,04	99,23	99,27
mg#	69,0	80,3	79,5	81,0	74,9	74,4

Table A2.1. Continued.

Sample	DH97-4					
Grain core/int/rim	2B	2C	1A	1B	1C	3A
SiO2	48,93	46,00	46,66	44,97	45,54	47,86
TiO2	2,09	3,09	3,27	3,65	3,33	2,34
Al2O3	5,03	6,89	7,99	8,48	7,47	5,84
Cr2O3	0,00	0,00	0,00	0,00	0,00	0,00
FeO	7,69	8,37	7,05	7,67	7,99	6,97
MnO	0,34	0,22	0,19	0,12	0,20	0,01
MgO	12,52	11,17	12,70	11,63	11,76	13,37
NiO	0,09	0,00	0,10	0,08	0,01	0,05
CaO	21,93	22,11	22,36	22,47	22,11	22,23
Na2O	0,66	0,75	0,58	0,53	0,62	0,51
Sum	99,27	98,59	100,92	99,59	99,04	99,19
mg#	74,4	70,4	76,3	73,0	72,4	77,4

Sample	DH97-4				DH97-12	
Grain core/int/rim	3B	8	9A	9B	3-1j core	3-1a rim
SiO2	44,46	51,22	46,49	43,58	46,61	44,09
TiO2	4,00	1,22	3,17	4,30	3,18	4,69
Al2O3	8,88	2,68	7,29	9,50	6,99	8,12
Cr2O3	0,00	0,00	0,00	0,00	0,00	0,06
FeO	7,28	8,30	7,30	7,60	6,79	8,01
MnO	0,21	0,66	0,05	0,10	0,12	0,06
MgO	11,54	12,27	12,29	11,06	12,44	11,07
NiO	0,00	0,00	0,00	0,00	0,04	0,00
CaO	22,64	21,95	22,77	22,36	23,13	22,50
Na2O	0,53	1,06	0,58	0,57	0,52	0,64
Sum	99,54	99,37	99,94	99,09	99,82	99,24
mg#	73,9	72,5	75,0	72,2	76,6	71,1

Sample	DH97-13A		DH97-13B		DH97-17	
Grain core/int/rim	core	rim	1-1f core	1-1n rim	2-1f core	2-1k rim
SiO2	46,91	43,52	50,47	44,50	46,96	43,00
TiO2	2,66	4,60	1,42	3,71	2,99	5,21
Al2O3	6,75	8,28	3,21	7,94	6,46	8,65
Cr2O3	0,01	0,00	0,04	0,03	0,00	0,04
FeO	7,00	8,19	7,82	7,61	6,91	8,47
MnO	0,15	0,20	0,48	0,09	0,17	0,14
MgO	12,74	11,26	13,25	12,10	12,95	10,80
NiO	0,02	0,00	0,00	0,00	0,04	0,00
CaO	23,03	22,47	22,32	22,47	22,86	22,44
Na2O	0,48	0,66	0,94	0,54	0,56	0,65
Sum	99,75	99,18	99,95	98,99	99,90	99,40
mg#	76,4	71,0	75,1	73,9	77,0	69,4

Table A2.2. Clinoyroxene major element data: syenites.

Sample	TDKS 17.2			TDKS 17.3		
Grain core/int/rim	1-4a core	1-4b rim	2-2a core	2-2b rim	2-1a core	2-1b rim
SiO2	49,84	50,62	49,85	47,96	45,12	47,10
TiO2	1,63	1,41	1,91	2,73	3,88	3,25
Al2O3	2,74	2,11	3,12	4,68	6,09	5,32
Cr2O3	0,04	0,02	0,06	0,04	0,03	0,03
FeO	7,95	7,97	7,22	7,70	8,33	7,82
MnO	0,21	0,31	0,20	0,24	0,26	0,21
MgO	13,37	13,38	13,84	12,66	11,45	12,05
CaO	22,25	21,87	21,99	22,09	22,05	22,32
Na2O	0,61	0,64	0,59	0,74	0,73	0,62
K2O	0,00	0,00	0,01	0,00	0,00	0,00
NiO	0,00	0,03	0,00	0,00	0,00	0,00
P2O5	na	na	na	na	0,03	0,03
Cl	0,02	0,00	0,01	0,00	0,00	0,00
F	0,04	0,02	0,05	0,08	0,06	0,03
Sum	98,68	98,37	98,83	98,91	98,03	98,79
mg#	75,0	74,9	77,4	74,5	71,0	73,3

Sample	TDKS 17.3	TDKS 17.4				
Grain core/int/rim	10-a core	1-1a core	1-1b int	1-1c rim	2-1a core	2-1b rim
SiO2	49,29	50,30	46,98	50,21	49,70	49,29
TiO2	0,58	1,71	3,08	1,90	2,02	2,09
Al2O3	0,94	2,51	5,06	3,02	2,97	3,34
Cr2O3	0,04	0,00	0,00	0,00	0,00	0,00
FeO	17,80	8,26	7,95	7,72	7,50	8,69
MnO	0,52	0,24	0,24	0,30	0,20	0,26
MgO	6,75	13,09	12,28	13,25	13,69	12,06
CaO	20,65	22,16	22,07	22,21	22,24	22,23
Na2O	1,32	0,60	0,75	0,69	0,53	0,75
K2O	0,03	0,00	0,00	0,02	0,02	0,01
NiO	0,04	0,00	0,04	0,00	0,03	0,00
P2O5	0,04	0,00	0,00	0,00	0,00	0,00
Cl	0,02	0,00	0,01	0,00	0,00	0,02
F	0,04	0,02	0,09	0,11	0,07	0,06
Sum	98,06	98,91	98,55	99,42	98,96	98,78
mg#	40,3	73,9	73,4	75,4	76,5	71,2

Table A2.2. Continued.

Sample	TDKS 17.4					TDKS 17.5
Grain core/int/rim	3-1a core	3-1b rim	11-1a core	11-1b int	11-1c rim	1-1a core
SiO2	50,52	48,01	49,72	46,51	48,69	46,15
TiO2	1,78	2,35	2,16	3,39	2,22	2,37
Al2O3	2,80	2,83	3,09	5,48	3,36	3,99
Cr2O3	0,00	0,03	0,00	0,00	0,04	0,00
FeO	8,03	14,11	7,69	8,03	8,94	7,32
MnO	0,23	0,41	0,23	0,24	0,30	0,21
MgO	13,58	8,34	13,64	12,13	11,88	12,46
CaO	22,35	21,33	22,35	22,21	22,29	20,93
Na2O	0,66	1,19	0,53	0,76	0,88	0,65
K2O	0,02	0,03	0,01	0,00	0,01	0,00
NiO	0,04	0,06	0,00	0,02	0,00	0,09
P2O5	0,00	0,00	0,00	0,00	0,00	0,00
Cl	0,01	0,00	0,01	0,03	0,02	0,02
F	0,08	0,10	0,06	0,10	0,05	0,00
Sum	100,09	98,79	99,50	98,90	98,67	94,20
mg#	75,1	51,3	76,0	72,9	70,3	75,2

Sample	TDKS 17.5					
Grain core/int/rim	2-1a core	2-1b rim	3-1a core	3-2a core	3-2b rim	5-1a core
SiO2	45,37	48,29	48,69	49,04	49,85	45,59
TiO2	2,81	1,70	1,85	1,51	1,30	3,22
Al2O3	5,75	2,85	2,85	2,57	2,01	5,36
Cr2O3	0,00	0,00	0,01	0,05	0,00	0,00
FeO	7,19	7,32	7,29	7,10	7,74	7,66
MnO	0,08	0,26	0,24	0,17	0,23	0,24
MgO	12,37	12,67	13,11	13,01	12,83	11,93
CaO	21,12	20,95	21,32	21,24	21,41	21,12
Na2O	0,70	0,65	0,60	0,59	0,63	0,72
K2O	0,00	0,00	0,01	0,00	0,00	0,00
NiO	0,04	0,05	0,00	0,00	0,06	0,07
P2O5	0,02	0,03	0,04	0,03	0,00	0,03
Cl	0,00	0,00	0,01	0,01	0,00	0,00
F	0,04	0,05	0,07	0,02	0,04	0,06
Sum	95,47	94,82	96,08	95,35	96,13	96,01
mg#	75,4	75,5	76,2	76,6	74,7	73,5

Table A2.2. Continued.

Sample	TDKS 17.5			TDSK 17.11		
Grain core/int/rim	5-1b rim	6-1a core	6-1b rim	7-1a core	1-1a core	1-1b rim
SiO2	48,52	45,25	48,23	48,32	49,68	47,27
TiO2	1,89	3,08	1,83	1,93	2,02	3,00
Al2O3	3,12	5,04	2,82	3,12	3,19	4,93
Cr2O3	0,05	0,00	0,00	0,00	0,00	0,00
FeO	7,17	7,65	8,21	7,46	7,69	7,97
MnO	0,22	0,15	0,24	0,22	0,32	0,28
MgO	13,19	11,73	11,96	13,03	13,09	12,16
CaO	21,37	21,14	21,20	21,22	22,39	22,15
Na2O	0,59	0,69	0,83	0,59	0,59	0,67
K2O	0,00	0,00	0,00	0,03	0,00	0,00
NiO	0,07	0,00	0,00	0,04	0,00	0,00
P2O5	0,02	0,03	0,01	0,01	na	na
Cl	0,00	0,01	0,01	0,00	0,01	0,00
F	0,04	0,05	0,09	0,07	0,06	0,04
Sum	96,24	94,81	95,44	96,03	99,02	98,46
mg#	76,6	73,2	72,2	75,7	75,2	73,1

Sample	TDSK 17.11					
Grain core/int/rim	1-2a core	1-2b rim	2-1a core	2-1b rim	2-2a core	2-2b rim
SiO2	49,69	49,81	49,80	49,90	49,52	49,39
TiO2	1,97	1,62	1,91	1,65	2,07	1,97
Al2O3	3,13	2,53	2,90	2,65	3,40	3,04
Cr2O3	0,00	0,00	0,01	0,06	0,00	0,02
FeO	7,77	8,97	7,76	9,27	7,53	7,62
MnO	0,19	0,26	0,24	0,26	0,19	0,21
MgO	12,74	11,96	13,33	11,98	12,98	13,20
CaO	22,52	22,27	22,38	22,22	22,37	22,25
Na2O	0,57	0,88	0,59	0,85	0,57	0,52
K2O	0,01	0,00	0,00	0,00	0,00	0,00
NiO	0,00	0,00	0,00	0,04	0,00	0,00
P2O5	na	na	na	na	na	na
Cl	0,00	0,01	0,01	0,00	0,00	0,01
F	0,05	0,08	0,02	0,04	0,09	0,04
Sum	98,63	98,39	98,95	98,92	98,72	98,28
mg#	74,5	70,4	75,4	69,7	75,4	75,5

Table A2.2. Continued.

Sample	TDSK 17.11		DH 39.1			
Grain core/int/rim	4-1a core	4-1b rim	5-3a core	5-3b rim	2-1a core	7-2a core
SiO2	46,94	50,27	51,07	48,06	47,49	47,98
TiO2	3,15	1,30	1,07	2,78	2,29	2,26
Al2O3	5,32	2,10	1,66	4,37	4,91	5,02
Cr2O3	0,04	0,00	0,00	0,03	0,00	0,02
FeO	7,65	9,22	9,00	7,83	6,64	6,20
MnO	0,20	0,31	0,33	0,24	0,10	0,20
MgO	12,46	12,13	12,41	12,30	13,30	13,84
CaO	22,39	22,67	22,13	22,14	23,14	22,92
Na2O	0,62	0,81	0,72	0,67	0,65	0,55
K2O	0,00	0,01	0,00	0,00	0,00	0,00
NiO	0,09	0,07	0,01	0,06	0,10	0,06
P2O5	na	na	na	na	na	na
Cl	0,01	0,00	0,00	0,00	0,00	0,02
F	0,05	0,08	0,07	0,07	0,05	0,07
Sum	98,93	98,96	98,47	98,55	98,67	99,14
mg#	74,4	70,1	71,1	73,7	78,1	79,9

Sample	DH 39.1	DH 39.2				
Grain core/int/rim	7-2b rim	8-2a core	1-3a core	1-3b int	1-3c rim	2-1a core
SiO2	47,42	49,36	49,59	48,45	50,56	46,92
TiO2	2,40	1,16	1,94	2,68	1,66	3,34
Al2O3	5,14	2,98	3,18	4,24	2,64	5,21
Cr2O3	0,00	0,00	0,00	0,01	0,08	0,00
FeO	7,98	11,16	8,09	8,34	7,46	8,31
MnO	0,31	0,69	0,19	0,28	0,39	0,22
MgO	11,97	10,32	13,32	12,13	13,31	11,89
CaO	22,64	22,08	22,54	22,10	21,93	22,35
Na2O	0,86	1,37	0,63	0,67	1,07	0,66
K2O	0,00	0,00	0,01	0,00	0,00	0,00
NiO	0,00	0,01	0,01	0,00	0,00	0,06
P2O5	na	na	na	na	na	na
Cl	0,00	0,00	0,00	0,00	0,00	0,00
F	0,07	0,07	0,00	0,06	0,04	0,02
Sum	98,79	99,20	99,50	98,96	99,14	98,99
mg#	72,8	62,2	74,6	72,2	76,1	71,8

Table A2.2. Continued.

Sample	DH 39.2					
Grain core/int/rim	2-1b rim	4-1a core	4-1b rim	5-4a core	5-4b int	5-4c rim
SiO2	50,16	49,56	47,86	50,26	48,66	49,89
TiO2	1,86	2,02	2,88	1,70	2,41	1,71
Al2O3	3,19	3,48	4,76	2,75	4,01	3,03
Cr2O3	0,00	0,00	0,06	0,01	0,06	0,00
FeO	8,08	7,95	7,50	7,89	8,61	7,94
MnO	0,25	0,27	0,32	0,32	0,31	0,41
MgO	13,05	13,20	12,36	12,75	12,01	12,68
CaO	22,56	22,27	22,38	22,63	22,21	22,23
Na2O	0,63	0,61	0,97	0,71	0,86	1,06
K2O	0,03	0,00	0,01	0,02	0,01	0,02
NiO	0,00	0,10	0,00	0,05	0,07	0,09
P2O5	na	na	na	na	na	na
Cl	0,00	0,00	0,00	0,00	0,00	0,01
F	0,00	0,07	0,12	0,04	0,07	0,09
Sum	99,80	99,54	99,22	99,14	99,29	99,15
mg#	74,2	74,8	74,6	74,2	71,3	74,0

Sample	DH 39.4					
Grain core/int/rim	1-1a core	1-1b int	1-1c rim	1-3a core	1-6a core	1-6bn int
SiO2	46,05	51,00	50,15	49,94	49,54	48,18
TiO2	3,62	1,19	1,69	1,80	2,02	2,46
Al2O3	6,21	2,11	2,68	3,17	3,61	4,19
Cr2O3	0,03	0,00	0,04	0,00	0,00	0,01
FeO	7,95	9,63	8,12	7,84	7,42	7,79
MnO	0,20	0,34	0,32	0,28	0,27	0,27
MgO	11,60	12,29	12,75	13,20	13,39	12,23
CaO	22,02	22,43	22,62	22,45	22,28	22,24
Na2O	0,84	0,82	0,87	0,69	0,70	0,81
K2O	0,00	0,00	0,00	0,00	0,00	0,00
NiO	0,00	0,00	0,00	0,00	0,00	0,09
P2O5	0,04	0,00	0,02	0,00	0,03	0,03
Cl	0,00	0,01	0,01	0,00	0,01	0,01
F	0,11	0,06	0,11	0,08	0,09	0,06
Sum	98,66	99,90	99,36	99,45	99,34	98,34
mg#	72,2	69,5	73,7	75,0	76,3	73,7

Table A2.2. Continued.

Sample	DH 39.4					
Grain core/int/rim	1-6c rim	2-1a core	2-1b rim	3-1a core	3-1b rim	4-2a core
SiO2	50,07	47,28	50,84	47,29	48,64	47,10
TiO2	1,48	3,10	1,22	3,04	2,41	3,08
Al2O3	2,67	5,28	2,18	5,05	3,99	5,34
Cr2O3	0,01	0,01	0,00	0,00	0,00	0,01
FeO	9,47	7,67	9,76	7,92	8,13	7,59
MnO	0,31	0,25	0,31	0,22	0,24	0,22
MgO	11,88	12,01	11,73	12,34	12,14	12,17
CaO	21,98	22,04	22,16	22,35	22,59	22,70
Na2O	0,99	0,81	0,93	0,86	0,84	0,77
K2O	0,00	0,00	0,00	0,03	0,00	0,00
NiO	0,03	0,00	0,04	0,00	0,01	0,00
P2O5	0,00	0,07	0,00	0,02	0,04	0,07
Cl	0,00	0,01	0,00	0,00	0,01	0,00
F	0,05	0,10	0,06	0,04	0,09	0,08
Sum	98,92	98,63	99,24	99,15	99,14	99,12
mg#	69,1	73,6	68,2	73,5	72,7	74,1

Sample	DH 39.4				DH 39.5	
Grain core/int/rim	4-2b rim	4-4a core	4-4b int	4-4c rim	1-1a core	1-1b rim
SiO2	50,09	49,83	47,57	50,89	43,36	47,97
TiO2	1,85	2,00	2,96	1,29	3,99	2,31
Al2O3	3,16	3,54	4,90	2,16	8,85	5,07
Cr2O3	0,00	0,01	0,02	0,00	0,02	0,00
FeO	7,66	7,58	7,76	8,82	7,54	6,99
MnO	0,24	0,22	0,28	0,27	0,06	0,09
MgO	12,80	13,25	12,35	12,35	11,35	13,51
CaO	22,31	22,27	22,10	21,96	22,43	22,67
Na2O	0,75	0,61	0,77	0,87	0,55	0,53
K2O	0,02	0,02	0,00	0,00	0,03	0,00
NiO	0,01	0,04	0,02	0,06	0,01	0,00
P2O5	0,01	0,06	0,04	0,01	na	na
Cl	0,00	0,00	0,01	0,01	0,00	0,00
F	0,07	0,08	0,06	0,11	0,06	0,05
Sum	98,99	99,52	98,84	98,79	98,24	99,17
mg#	74,9	75,7	73,9	71,4	72,9	77,5

Table A2.2. Continued.

Sample	DH 39.5				DH 39.7	
Grain core/int/rim	2-1a core	2-1b rim	4-2a core	4-2b rim	1-1a core	1-1b rim
SiO2	43,47	49,89	49,70	48,05	49,48	46,84
TiO2	4,06	1,38	1,27	1,88	1,75	2,68
Al2O3	8,46	3,34	3,39	4,47	3,70	6,03
Cr2O3	0,00	0,02	0,00	0,00	0,00	0,00
FeO	8,35	8,64	7,96	8,33	6,78	7,47
MnO	0,17	0,22	0,23	0,24	0,25	0,12
MgO	11,50	12,80	13,11	12,80	14,29	12,44
CaO	22,20	22,80	22,64	22,62	22,12	22,01
Na2O	0,59	0,75	0,60	0,58	0,58	0,61
K2O	0,00	0,00	0,04	0,02	0,00	0,00
NiO	0,00	0,02	0,07	0,01	0,00	0,00
P2O5	na	na	na	na	na	na
Cl	0,01	0,02	0,00	0,01	0,01	0,00
F	0,04	0,00	0,00	0,03	0,06	0,09
Sum	98,83	99,87	99,02	99,03	99,01	98,29
mg#	71,1	72,5	74,6	73,2	79,0	74,8

Sample	DH 39.7		DH 39.8			
Grain core/int/rim	3-2a core	3-2b rim	1-1a core	1-1b int ->	1-1c int ->	1-1d int ->
SiO2	49,31	49,41	46,57	46,94	49,14	49,03
TiO2	1,71	1,59	3,27	3,12	2,28	2,22
Al2O3	3,73	3,58	5,99	5,86	3,94	4,11
Cr2O3	0,00	0,02	0,01	0,01	0,00	0,01
FeO	7,77	7,37	7,62	7,74	7,37	7,45
MnO	0,18	0,30	0,19	0,24	0,22	0,17
MgO	12,97	13,21	12,07	12,08	13,24	13,19
CaO	22,30	21,94	22,06	22,00	22,27	22,24
Na2O	0,88	0,83	0,80	0,85	0,70	0,74
K2O	0,00	0,01	0,03	0,00	0,00	0,01
NiO	0,00	0,06	0,00	0,03	0,00	0,00
P2O5	na	na	0,10	0,00	0,03	0,08
Cl	0,00	0,00	0,02	0,01	0,02	0,00
F	0,02	0,00	0,06	0,04	0,01	0,05
Sum	98,88	98,32	98,79	98,91	99,21	99,29
mg#	74,9	76,2	73,9	73,6	76,2	75,9

Table A2.2. Continued.

Sample	DH 39.8					
Grain core/int/rim	1-1e int ->	1-1f int ->	1-1g rim	2-2a core	2-5a core	2-5b rim
SiO2	49,02	49,03	48,70	51,14	48,78	49,49
TiO2	2,26	2,23	2,18	0,93	2,22	2,25
Al2O3	4,12	4,03	4,04	1,82	3,95	3,82
Cr2O3	0,00	0,00	0,00	0,02	0,04	0,00
FeO	7,33	7,35	7,31	9,06	7,30	7,30
MnO	0,26	0,30	0,28	0,29	0,31	0,20
MgO	13,15	13,34	13,25	12,42	13,37	13,07
CaO	22,27	22,44	22,04	22,47	22,30	22,54
Na2O	0,84	0,74	0,82	0,80	0,70	0,69
K2O	0,02	0,00	0,00	0,02	0,01	0,01
NiO	0,00	0,04	0,10	0,12	0,02	0,08
P2O5	0,00	0,05	0,02	0,00	0,04	0,00
Cl	0,00	0,00	0,00	0,00	0,02	0,01
F	0,11	0,12	0,12	0,07	0,16	0,05
Sum	99,37	99,65	98,86	99,15	99,21	99,51
mg#	76,2	76,4	76,3	71,0	76,5	76,1

Sample	DH 39.8	DH 39.9				
Grain core/int/rim	3-1a core	1-1a core	1-4a core	1-4b rim	2-5a core	2-6a core
SiO2	50,42	47,23	48,41	47,47	47,95	49,56
TiO2	1,22	2,54	2,19	2,47	2,10	1,25
Al2O3	2,16	4,79	4,33	4,62	4,46	3,03
Cr2O3	0,00	0,03	0,00	0,04	0,00	0,00
FeO	8,96	8,80	8,57	8,69	8,82	10,43
MnO	0,32	0,46	0,39	0,48	0,49	0,63
MgO	12,12	11,13	11,46	11,52	11,50	11,08
CaO	22,30	21,70	21,93	22,17	22,25	22,07
Na2O	0,76	1,59	1,43	1,43	1,27	1,31
K2O	0,00	0,04	0,02	0,01	0,00	0,02
NiO	0,00	0,00	0,02	0,00	0,00	0,08
P2O5	0,05	0,04	0,04	0,01	0,00	0,00
Cl	0,00	0,00	0,00	0,00	0,00	0,00
F	0,02	0,11	0,06	0,10	0,05	0,09
Sum	98,32	98,46	98,84	98,99	98,89	99,55
mg#	70,7	69,3	70,4	70,3	69,9	65,4

Table A2.2. Continued.

Sample	DH 39.9	TF 12.1				
Grain core/int/rim	3-1a core	5-1a core	5-1b rim	1-10a core	1-10b rim	1-11a core
SiO2	48,82	49,21	49,33	44,90	45,57	43,63
TiO2	1,16	1,25	1,93	2,83	3,03	2,98
Al2O3	3,13	3,18	3,58	6,31	6,82	6,40
Cr2O3	0,00	0,00	0,05	0,00	0,00	0,03
FeO	10,58	11,02	8,65	7,07	7,21	7,99
MnO	0,58	0,65	0,54	0,22	0,16	0,24
MgO	10,78	10,36	11,88	12,61	12,86	12,03
CaO	22,37	22,31	21,56	22,31	22,41	22,19
Na2O	1,37	1,45	1,51	0,65	0,62	0,77
K2O	0,02	0,02	0,00	0,01	0,01	0,00
NiO	0,00	0,05	0,00	0,00	0,00	0,05
P2O5	0,01	0,00	0,03	na	na	na
Cl	0,01	0,00	0,01	0,00	0,00	0,00
F	0,06	0,11	0,08	0,02	0,02	0,03
Sum	98,89	99,60	99,15	96,92	98,72	96,31
mg#	64,5	62,6	71,0	76,1	76,1	72,8

Sample	TF 12.1			TF 12.2		TF 12.3
Grain core/int/rim	2-4a core	2-4b int	2-4c rim	4-3a core	4-5a core	3-2a core
SiO2	51,07	45,30	46,33	50,41	51,86	49,28
TiO2	1,05	2,80	3,10	1,24	0,80	1,57
Al2O3	2,37	6,48	7,01	2,76	1,55	4,14
Cr2O3	0,00	0,00	0,00	0,00	0,02	0,03
FeO	7,80	7,61	7,35	7,74	7,76	6,72
MnO	0,56	0,22	0,19	0,44	0,53	0,28
MgO	13,69	12,29	12,68	13,68	13,84	14,25
CaO	22,45	22,50	22,65	22,35	22,50	22,12
Na2O	0,83	0,67	0,61	0,72	0,84	0,61
K2O	0,01	0,01	0,00	0,00	0,01	0,00
NiO	0,02	0,03	0,01	0,00	0,03	0,00
P2O5	na	na	na	0,01	0,01	0,00
Cl	0,00	0,00	0,00	0,00	0,01	0,00
F	0,03	0,03	0,05	0,04	0,02	0,02
Sum	99,87	97,94	99,98	99,40	99,77	99,02
mg#	75,8	74,2	75,5	75,9	76,1	79,1

Table A2.2. Continued.

Sample	TF 12.3	TF 12.4			TF 16.1	
Grain core/int/rim	4-1a core	1-5a core	1-5b int	1-5c rim	1-1a core	1-1b int
SiO2	50,54	50,11	48,50	50,83	46,37	45,03
TiO2	1,18	1,27	1,87	0,82	2,90	3,32
Al2O3	3,50	3,06	4,44	1,85	6,88	7,66
Cr2O3	0,04	0,00	0,00	0,07	0,00	0,00
FeO	6,23	6,88	7,72	8,37	7,57	7,85
MnO	0,31	0,42	0,35	0,52	0,22	0,15
MgO	14,30	13,82	13,13	12,99	12,43	11,95
CaO	22,37	22,54	22,27	22,33	22,66	22,70
Na2O	0,73	0,86	0,66	1,20	0,58	0,50
K2O	0,00	0,02	0,01	0,01	0,00	0,01
NiO	0,02	0,00	0,03	0,00	0,01	0,03
P2O5	0,02	na	na	na	0,00	0,06
Cl	0,01	0,00	0,00	0,00	0,00	0,01
F	0,02	0,09	0,06	0,04	0,08	0,05
Sum	99,28	99,07	99,05	99,00	99,70	99,31
mg#	80,4	78,2	75,2	73,4	74,5	73,1

Sample	TF 16.1			DH 37.1	DH 37.2	
Grain core/int/rim	1-1c rim	3-2a core	3-2b rim	1-5a int	1-1a core	1-1b rim
SiO2	47,30	49,78	47,72	50,44	51,32	47,25
TiO2	2,70	1,63	2,37	1,25	0,85	2,47
Al2O3	6,16	4,18	5,27	2,82	2,11	6,27
Cr2O3	0,01	0,05	0,04	0,00	0,06	0,01
FeO	6,98	8,09	8,30	8,09	8,73	7,44
MnO	0,09	0,24	0,20	0,48	0,71	0,17
MgO	13,25	12,27	12,46	12,86	12,33	12,67
CaO	22,67	22,87	23,00	22,09	22,29	22,59
Na2O	0,58	1,15	0,65	1,03	1,19	0,71
K2O	0,00	0,00	0,00	0,01	0,03	0,02
NiO	0,04	0,04	0,03	0,00	0,11	0,00
P2O5	0,00	0,00	0,06	na	na	na
Cl	0,00	0,02	0,00	0,02	0,01	0,01
F	0,01	0,05	0,03	0,02	0,01	0,05
Sum	99,79	100,39	100,14	99,10	99,73	99,66
mg#	77,2	73,0	72,8	73,9	71,6	75,2

Table A2.2. Continued.

Sample	DH 37.2				
Grain core/int/rim	**3-1a core**	**5-1a core**	**5-1b rim**	**6-1a core**	**6-1b rim**
SiO2	48,75	50,53	50,59	50,13	46,18
TiO2	1,76	1,11	1,26	1,41	2,97
Al2O3	4,18	2,41	3,05	3,25	7,09
Cr2O3	0,00	0,00	0,00	0,05	0,02
FeO	7,31	8,26	7,39	7,24	7,73
MnO	0,25	0,62	0,41	0,46	0,14
MgO	13,28	12,35	13,81	13,48	12,01
CaO	22,17	21,95	22,44	22,23	22,20
Na2O	0,62	1,16	0,77	0,86	0,72
K2O	0,03	0,01	0,00	0,01	0,02
NiO	0,00	0,00	0,00	0,00	0,02
P2O5	na	na	na	na	na
Cl	0,01	0,02	0,00	0,02	0,00
F	0,01	0,05	0,01	0,02	0,04
Sum	98,37	98,46	99,72	99,15	99,13
mg#	76,4	72,7	76,9	76,8	73,5

Table A2.3. Amphibole Major Elements: lavas.

Sample	DH97-22B					
Grain core/int/rim	**5-1a core**	**5-1b core**	**3-1a core**	**3-2a core**	**3-3a core**	**8-1a core**
SiO2	41,32	41,05	40,48	39,04	38,12	40,13
TiO2	5,55	5,61	5,67	6,37	6,19	6,38
Al2O3	10,88	10,64	11,22	12,46	13,06	12,52
Cr2O3	0,01	0,00	0,06	0,10	0,00	0,00
FeO	11,89	11,88	11,91	12,66	13,29	10,91
MnO	0,41	0,36	0,42	0,28	0,28	0,11
MgO	12,63	12,39	12,42	11,60	10,97	13,01
CaO	11,44	11,37	11,73	11,53	11,59	12,20
Na2O	2,78	2,76	2,83	2,79	2,87	2,54
K2O	1,27	1,31	1,30	1,22	1,25	1,05
Cl	0,01	0,02	0,03	0,01	0,03	0,02
Total	98,18	97,38	98,06	98,05	97,66	98,87
mg#	65,44	65,03	65,02	62,01	59,53	68,00

Sample	DH97-22B					
Grain core/int/rim	**8-1b core**	**8-1c rim**	**8-2a core**	**8-2b rim**	**8-2c rim**	**9-1a core**
SiO2	39,82	40,02	40,54	39,94	40,66	40,15
TiO2	6,61	6,75	6,03	6,15	6,09	6,50
Al2O3	12,82	12,77	11,96	12,09	11,54	12,26
Cr2O3	0,00	0,00	0,01	0,00	0,00	0,00
FeO	10,19	10,13	11,56	11,97	11,74	10,74
MnO	0,18	0,11	0,30	0,25	0,29	0,22
MgO	13,23	13,17	12,50	12,26	12,51	13,16
CaO	11,98	12,18	11,80	11,95	11,82	11,76
Na2O	2,53	2,50	2,73	2,73	2,73	2,63
K2O	0,94	0,90	1,07	1,07	1,13	0,96
Cl	0,03	0,00	0,01	0,02	0,02	0,02
Total	98,34	98,53	98,53	98,44	98,54	98,41
mg#	69,82	69,86	65,84	64,62	65,51	68,60

Table A2.3. Continued.

Sample	DH97-22D					
Grain core/int/rim	**2-1a core**	**2-1b rim**	**2-1c rim**	**4-1a core**	**4-1b core**	**4-1c rim**
SiO2	39,53	40,08	39,37	39,59	39,15	39,31
TiO2	6,70	6,68	6,63	6,89	6,83	6,89
Al2O3	12,46	13,12	13,17	13,33	13,13	13,15
Cr2O3	0,00	0,00	0,00	0,01	0,00	0,00
FeO	10,93	10,23	9,80	10,32	9,84	10,12
MnO	0,16	0,08	0,11	0,14	0,08	0,11
MgO	12,81	13,28	13,15	13,20	13,11	12,99
CaO	12,26	12,25	12,20	12,19	12,35	11,97
Na2O	2,48	2,57	2,57	2,48	2,39	2,40
K2O	1,00	0,95	0,88	0,93	0,98	1,01
Cl	0,01	0,01	0,01	0,01	0,01	0,01
Total	98,34	99,26	97,89	99,10	97,87	97,94
mg#	67,63	69,82	70,52	69,50	70,37	69,59

Sample	DH97-22D				
Grain core/int/rim	**4-2a core**	**6-1a core**	**6-1b rim**	**6-1c rim**	**6-1d rim**
SiO2	39,43	39,44	40,15	39,96	39,87
TiO2	7,01	6,59	6,72	6,70	6,75
Al2O3	13,33	12,73	12,81	12,81	12,88
Cr2O3	0,00	0,01	0,00	0,00	0,03
FeO	9,55	10,40	9,97	10,38	9,96
MnO	0,06	0,13	0,14	0,13	0,12
MgO	13,17	13,13	13,37	13,05	13,16
CaO	12,43	12,22	12,50	12,03	12,35
Na2O	2,52	2,52	2,59	2,62	2,63
K2O	0,99	0,98	0,95	0,93	0,97
Cl	0,01	0,01	0,00	0,01	0,01
Total	98,50	98,16	99,20	98,63	98,73
mg#	71,08	69,23	70,50	69,14	70,21

Table A2.4. Amphibole major element data: syenites.

Sample	DH 39.1					
Grain core/int/rim	1-1a core	1-1b rim	1-2b core	1-2a rim	3-2a core	4-1a core
SiO2	38,42	37,09	38,66	38,24	39,38	38,60
TiO2	5,85	2,52	6,33	2,84	5,90	6,45
Al2O3	12,93	12,20	12,67	11,74	11,63	12,84
Cr2O3	0,04	0,00	0,00	0,00	0,00	0,00
FeO	12,01	22,46	10,49	21,53	13,47	11,72
MnO	0,26	0,51	0,22	0,64	0,37	0,24
MgO	11,11	5,96	12,06	7,21	10,35	11,19
CaO	11,68	10,51	12,16	10,86	11,38	11,85
Na2O	3,14	3,00	3,03	2,89	3,03	2,99
K2O	1,02	1,82	0,97	1,74	1,24	1,02
NiO	0,09	0,00	0,00	0,00	0,00	0,12
P2O5	na	na	na	na	na	na
Cl	0,02	0,01	0,03	0,04	0,04	0,01
F	0,30	0,15	0,30	0,16	0,28	0,31
Total	96,85	96,22	96,91	97,87	97,06	97,33
mg#	62,2	32,1	67,2	37,4	57,8	63,0

Sample	DH 39.1					
Grain core/int/rim	4-2a core	4-2b rim	4-3a core	5-1b int©	5-1c int®	5-1d rim
SiO2	38,62	38,38	38,41	39,06	39,10	39,02
TiO2	6,22	3,87	6,51	5,72	5,28	5,09
Al2O3	11,87	11,43	12,36	11,66	11,80	11,23
Cr2O3	0,00	0,00	0,03	0,00	0,00	0,00
FeO	12,99	17,59	12,73	13,83	14,88	15,90
MnO	0,33	0,53	0,32	0,33	0,36	0,51
MgO	10,42	8,63	10,68	10,42	9,64	8,90
CaO	11,21	11,22	11,59	11,33	11,18	11,43
Na2O	3,11	2,95	3,03	3,14	3,19	3,02
K2O	1,18	1,75	1,11	1,32	1,34	1,45
NiO	0,01	0,00	0,00	0,06	0,10	0,02
P2O5	na	na	na	na	na	na
Cl	0,03	0,04	0,03	0,03	0,02	0,03
F	0,20	0,18	0,23	0,28	0,28	0,13
Total	96,21	96,57	97,04	97,16	97,18	96,73
mg#	58,8	46,6	59,9	57,3	53,6	50,0

Table A2.4. Continued.

Sample	DH 39.1					DH 39.2
Grain core/int/rim	6-2b rim	7-1a core	7-1b rim	8-1a core	8-1b rim	2-4a core
SiO2	39,36	38,11	39,24	38,60	38,36	42,80
TiO2	5,36	6,42	4,20	3,70	2,79	4,88
Al2O3	11,51	13,15	11,44	11,53	11,49	8,87
Cr2O3	0,00	0,00	0,00	0,00	0,03	0,00
FeO	14,67	11,82	17,63	18,34	21,49	10,16
MnO	0,42	0,18	0,54	0,45	0,56	0,30
MgO	10,15	11,48	8,65	8,42	6,76	13,97
CaO	11,27	11,95	11,13	11,04	10,68	11,30
Na2O	3,08	2,99	2,96	2,94	2,92	3,22
K2O	1,45	1,04	1,64	1,68	1,70	1,36
NiO	0,00	0,00	0,03	0,04	0,01	0,01
P2O5	na	na	na	na	na	na
Cl	0,02	0,01	0,05	0,06	0,02	0,01
F	0,23	0,26	0,25	0,26	0,20	1,67
Total	97,53	97,40	97,75	97,06	97,00	98,55
mg#	55,2	63,4	46,6	45,0	35,9	71,0

Sample	DH 39.2			DH 39.4		
Grain core/int/rim	3-3a core	3-3b rim	4-4a core	5-3a core	1-2a core	1-2b rim
SiO2	43,26	43,49	43,09	42,99	41,77	41,13
TiO2	4,16	4,21	4,76	4,76	4,61	4,48
Al2O3	8,83	8,57	8,84	8,91	9,28	9,54
Cr2O3	0,00	0,00	0,04	0,00	0,02	0,00
FeO	8,85	9,30	9,22	9,22	12,53	14,61
MnO	0,29	0,28	0,28	0,33	0,25	0,34
MgO	15,01	14,59	14,44	14,71	12,35	10,81
CaO	11,31	11,43	11,36	11,22	11,22	11,39
Na2O	3,31	3,17	3,19	3,27	2,82	2,82
K2O	1,27	1,29	1,43	1,33	1,47	1,52
NiO	0,13	0,09	0,05	0,08	0,00	0,00
P2O5	na	na	na	na	0,00	0,01
Cl	0,00	0,01	0,00	0,00	0,00	0,06
F	1,84	1,92	1,72	1,76	1,45	1,52
Total	98,27	98,34	98,40	98,57	97,78	98,22
mg#	75,1	73,7	73,6	74,0	63,7	56,9

Table A2.4. Continued.

Sample	DH 39.4					DH 39.5
Grain core/int/rim	1-3b rim	2-2a core	2-2b rim	4-1a core	4-1b rim	3-1a core
SiO2	42,11	42,19	41,89	43,11	40,88	40,01
TiO2	4,63	4,56	4,31	4,02	4,34	5,68
Al2O3	9,16	9,28	8,72	8,71	9,57	12,35
Cr2O3	0,00	0,00	0,00	0,02	0,03	0,00
FeO	13,10	13,80	13,37	12,36	15,68	10,60
MnO	0,25	0,24	0,23	0,24	0,35	0,16
MgO	12,16	11,60	12,45	13,10	10,13	12,91
CaO	11,16	11,39	11,24	11,31	11,12	11,89
Na2O	2,84	2,91	2,92	3,01	2,90	3,22
K2O	1,52	1,45	1,43	1,43	1,58	0,79
NiO	0,11	0,00	0,00	0,00	0,00	0,02
P2O5	0,03	0,04	0,03	0,00	0,04	na
Cl	0,03	0,04	0,02	0,03	0,05	0,01
F	1,54	1,52	1,51	1,58	1,38	0,28
Total	98,64	99,01	98,11	98,90	98,05	97,91
mg#	62,3	60,0	62,4	65,4	53,5	68,5

Sample	DH 39.5					
Grain core/int/rim	3-1b rim	3-2b rim	4-1a core	4-1b rim	4-3a core	5-3a core
SiO2	39,56	39,94	39,38	39,89	39,61	39,51
TiO2	6,21	6,51	5,80	5,95	5,60	5,87
Al2O3	11,73	11,96	12,77	12,49	12,24	12,61
Cr2O3	0,00	0,06	0,00	0,00	0,04	0,06
FeO	10,48	10,13	11,11	9,84	10,53	11,17
MnO	0,19	0,11	0,15	0,10	0,16	0,16
MgO	12,14	12,56	12,56	12,68	12,81	12,08
CaO	11,98	11,98	11,89	11,88	11,71	11,91
Na2O	3,01	3,03	3,05	3,00	3,17	3,17
K2O	1,04	0,99	0,76	0,96	0,73	0,85
NiO	0,00	0,00	0,00	0,00	0,00	0,00
P2O5	na	na	na	na	na	na
Cl	0,03	0,02	0,00	0,02	0,01	0,02
F	0,30	0,26	0,40	0,31	0,32	0,33
Total	96,66	97,55	97,86	97,15	96,93	97,73
mg#	67,4	68,8	66,8	69,7	68,4	65,8

Table A2.4. Continued.

Sample	DH 39.7					DH 39.8
Grain core/int/rim	2-1a core	2-1b rim	3-1a core	3-1b rim	5-1a core	2-3a core
SiO2	40,80	40,65	40,36	40,12	40,50	43,23
TiO2	6,21	5,95	5,92	5,78	6,20	4,03
Al2O3	11,60	11,56	11,32	11,17	11,53	8,82
Cr2O3	0,00	0,04	0,00	0,01	0,00	0,02
FeO	10,01	10,44	11,23	11,99	9,89	11,06
MnO	0,19	0,23	0,24	0,29	0,23	0,25
MgO	12,69	12,68	12,21	11,89	13,07	13,69
CaO	11,63	11,56	11,50	11,47	11,46	11,30
Na2O	3,28	3,33	3,21	3,11	3,37	3,08
K2O	0,95	0,97	1,12	1,10	0,88	1,37
NiO	0,01	0,00	0,06	0,03	0,02	0,00
P2O5	na	na	na	na	na	0,00
Cl	0,00	0,01	0,02	0,03	0,01	0,02
F	0,30	0,23	0,30	0,25	0,31	1,41
Total	97,68	97,65	97,48	97,23	97,49	98,27
mg#	69,3	68,4	66,0	63,9	70,2	68,8

Sample	DH 39.8					DH 39.9
Grain core/int/rim	2-3b rim	2-6a core	2-6b rim	3-2a core	3-2b rim	1-2a core
SiO2	41,28	42,49	42,03	42,66	42,01	39,85
TiO2	4,52	4,47	4,79	4,65	4,78	4,69
Al2O3	9,72	8,94	9,34	9,33	9,52	9,96
Cr2O3	0,00	0,01	0,00	0,00	0,00	0,00
FeO	13,82	11,37	12,06	11,30	12,65	14,25
MnO	0,36	0,29	0,23	0,23	0,27	0,58
MgO	11,39	13,30	12,53	13,36	12,04	10,80
CaO	11,30	11,13	11,34	11,33	11,31	11,29
Na2O	2,89	3,00	3,06	3,00	2,98	3,12
K2O	1,40	1,42	1,45	1,37	1,42	1,48
NiO	0,04	0,02	0,00	0,01	0,04	0,00
P2O5	0,02	0,04	0,03	0,04	0,03	0,00
Cl	0,08	0,05	0,05	0,03	0,03	0,04
F	1,03	1,45	1,22	1,30	1,03	0,60
Total	97,84	97,97	98,12	98,62	98,10	96,66
mg#	59,5	67,6	64,9	67,8	62,9	57,5

Table A2.4. Continued.

Sample	DH 39.9			TF 12.1		
Grain core/int/rim	1-5a core	1-5b rim	2-4a core	4-1a core	1-7a core	1-7b rim
SiO2	40,22	39,56	39,58	40,51	39,11	38,59
TiO2	4,63	3,60	3,60	4,82	6,66	6,43
Al2O3	10,27	10,42	10,74	10,36	12,68	12,75
Cr2O3	0,05	0,00	0,00	0,00	0,02	0,00
FeO	13,54	17,93	16,47	12,58	10,36	10,25
MnO	0,58	0,78	0,66	0,49	0,14	0,13
MgO	11,20	8,97	9,69	12,02	13,01	13,12
CaO	11,45	11,22	11,24	11,21	12,25	12,36
Na2O	3,05	2,97	2,94	3,03	2,58	2,75
K2O	1,57	1,59	1,69	1,64	0,94	0,84
NiO	0,00	0,00	0,02	0,00	0,00	0,02
P2O5	0,03	0,02	0,00	0,00	na	na
Cl	0,03	0,03	0,01	0,04	0,01	0,03
F	0,62	0,56	0,63	0,78	0,27	0,25
Total	97,24	97,64	97,29	97,47	98,03	97,50
mg#	59,6	47,1	51,2	63,0	69,1	69,5

Sample	TF 12.1					TF 12.2
Grain core/int/rim	1-8a core	2-1a core	2-1b rim	3-1a core	3-2a core	1-1a core
SiO2	38,92	38,53	38,17	38,83	39,02	40,44
TiO2	6,47	6,53	6,40	6,59	6,71	5,42
Al2O3	13,02	12,58	12,35	12,82	12,89	11,59
Cr2O3	0,00	0,00	0,02	0,02	0,00	0,00
FeO	10,74	10,62	10,35	10,15	10,25	11,49
MnO	0,20	0,10	0,19	0,12	0,23	0,34
MgO	13,05	12,89	12,90	13,03	13,11	12,65
CaO	12,16	12,37	12,01	12,06	12,23	11,55
Na2O	2,79	2,63	2,55	2,63	2,77	3,37
K2O	0,87	0,92	0,86	0,88	0,87	0,85
NiO	0,00	0,00	0,00	0,03	0,02	0,00
P2O5	na	na	na	na	na	0,04
Cl	0,00	0,01	0,04	0,01	0,01	0,02
F	0,27	0,25	0,22	0,23	0,24	0,26
Total	98,49	97,42	96,04	97,40	98,35	98,01
mg#	68,4	68,4	69,0	69,6	69,5	66,3

Table A2.4. Continued.

Sample	TF 12.2					
Grain core/int/rim	1-1b rim	2-2a core	2-2b int	2-2c rim	4-1a core	4-1b int
SiO2	39,98	40,04	40,34	40,35	40,41	40,70
TiO2	5,44	6,03	5,59	5,68	5,93	4,92
Al2O3	11,16	11,80	11,47	11,73	11,69	11,45
Cr2O3	0,02	0,02	0,04	0,00	0,01	0,01
FeO	12,63	11,37	11,62	11,38	11,10	12,93
MnO	0,41	0,28	0,35	0,34	0,41	0,38
MgO	11,43	12,68	12,62	12,57	12,39	11,50
CaO	11,65	11,75	11,81	11,61	11,57	11,14
Na2O	3,39	3,16	3,15	3,49	3,54	3,39
K2O	0,89	0,82	0,85	0,73	0,81	1,17
NiO	0,00	0,00	0,00	0,00	0,02	0,01
P2O5	0,00	0,07	0,02	0,04	0,04	0,01
Cl	0,01	0,02	0,00	0,03	0,02	0,07
F	0,23	0,31	0,36	0,27	0,23	0,29
Total	97,26	98,35	98,22	98,21	98,17	97,98
mg#	61,7	66,5	65,9	66,3	66,5	61,3

Sample	TF 12.2	TF 12.3				
Grain core/int/rim	4-1c rim	2-1a core	2-1b rim	3-3a core	3-3b rim	5-1a core
SiO2	40,66	40,67	41,57	41,02	40,58	41,24
TiO2	5,43	4,69	4,27	5,38	5,04	4,20
Al2O3	11,49	11,70	11,10	11,41	11,76	11,31
Cr2O3	0,02	0,11	0,02	0,09	0,08	0,09
FeO	12,01	10,28	10,76	10,69	10,89	10,71
MnO	0,34	0,24	0,25	0,23	0,20	0,33
MgO	11,92	13,72	13,82	13,19	13,09	13,65
CaO	11,78	11,57	11,51	11,69	11,68	11,26
Na2O	3,51	2,95	3,01	3,02	3,08	3,14
K2O	0,84	1,06	1,15	1,09	1,11	1,06
NiO	0,00	0,10	0,04	0,02	0,00	0,01
P2O5	0,02	0,04	0,02	0,02	0,05	0,00
Cl	0,01	0,02	0,03	0,01	0,04	0,03
F	0,23	0,25	0,23	0,19	0,20	0,19
Total	98,24	97,38	97,76	98,03	97,79	97,23
mg#	63,9	70,4	69,6	68,7	68,2	69,4

Table A2.4. Continued.

Sample	TF 12.3	TF 12.4		TF 16.1		
Grain core/int/rim	5-1b rim	1-6a core	6-1a core	6-5a core	2-3a core	3-3a rim
SiO2	40,40	40,03	39,72	39,52	38,87	38,99
TiO2	4,75	3,55	3,53	3,22	6,37	5,69
Al2O3	11,54	10,65	11,09	11,27	13,23	12,26
Cr2O3	0,15	0,08	0,05	0,00	0,01	0,04
FeO	10,76	16,37	16,14	16,52	9,96	14,03
MnO	0,25	0,61	0,61	0,70	0,11	0,24
MgO	13,24	10,04	10,06	9,79	13,31	10,83
CaO	11,72	11,24	10,95	10,73	12,25	12,00
Na2O	3,06	3,07	3,00	3,12	2,81	3,00
K2O	1,01	1,48	1,38	1,51	1,08	1,24
NiO	0,04	0,10	0,00	0,02	0,01	0,08
P2O5	0,00	na	na	na	0,02	0,02
Cl	0,03	0,04	0,03	0,03	0,02	0,03
F	0,17	0,27	0,27	0,27	0,24	0,14
Total	97,12	97,52	96,84	96,70	98,27	98,57
mg#	68,7	52,2	52,6	51,4	70,4	57,9

Sample	TF 16.1					
Grain core/int/rim	4-4a core	4-4b rim	6-1a core	6-1b int©	6-1c int®	6-1d rim
SiO2	38,80	38,58	39,35	39,06	39,63	39,51
TiO2	6,24	6,11	6,20	5,89	5,98	5,53
Al2O3	13,19	13,53	12,91	12,96	12,79	11,59
Cr2O3	0,01	0,02	0,02	0,09	0,02	0,00
FeO	10,28	11,60	10,24	9,52	9,85	13,59
MnO	0,15	0,14	0,08	0,07	0,11	0,24
MgO	12,69	11,74	13,51	13,56	13,30	11,40
CaO	12,13	12,34	12,07	12,30	12,31	11,70
Na2O	2,83	2,86	2,70	2,45	2,78	2,81
K2O	1,13	1,01	1,15	1,19	1,07	1,32
NiO	0,00	0,04	0,04	0,00	0,06	0,00
P2O5	0,06	0,01	0,04	0,03	0,09	0,00
Cl	0,01	0,02	0,00	0,00	0,00	0,03
F	0,16	0,18	0,25	0,24	0,19	0,19
Total	97,67	98,19	98,54	97,36	98,17	97,91
mg#	68,8	64,3	70,2	71,8	70,6	59,9

Table A2.4. Continued.

Sample	DH 37.1					
Grain core/int/rim	1-3a core	2-3a core	2-3b rim	2-5a core	3-1a core	3-1b rim
SiO2	38,89	39,70	39,46	39,20	38,76	39,87
TiO2	6,40	6,26	6,17	6,72	6,63	6,20
Al2O3	12,82	12,45	12,73	12,77	12,92	12,61
Cr2O3	0,00	0,07	0,00	0,07	0,00	0,00
FeO	10,73	10,53	10,40	10,19	11,51	11,38
MnO	0,14	0,21	0,19	0,12	0,10	0,20
MgO	12,83	12,74	12,50	12,77	12,23	12,47
CaO	12,04	11,98	12,07	11,83	11,90	11,95
Na2O	2,69	2,69	2,65	2,63	2,52	2,73
K2O	0,97	1,00	0,94	1,01	1,07	0,95
NiO	0,00	0,01	0,01	0,07	0,00	0,03
P2O5	na	na	na	na	na	na
Cl	0,02	0,00	0,00	0,02	0,02	0,02
F	0,19	0,27	0,22	0,22	0,15	0,22
Total	97,70	97,91	97,35	97,63	97,81	98,63
mg#	68,1	68,3	68,2	69,1	65,4	66,2

Sample	DH 37.1				DH 37.2	
Grain core/int/rim	4-3a core	5-4a core	5-5a core	5-5b rim	2-1a core	2-1b rim
SiO2	38,73	39,05	38,88	38,53	39,28	39,10
TiO2	6,41	6,56	6,64	5,03	6,16	6,39
Al2O3	12,74	12,84	12,99	12,72	12,39	12,63
Cr2O3	0,00	0,01	0,01	0,00	0,02	0,01
FeO	11,36	10,66	10,94	13,14	11,31	10,57
MnO	0,20	0,13	0,15	0,21	0,20	0,18
MgO	12,29	12,52	12,43	11,64	12,36	12,39
CaO	11,75	11,89	12,05	11,93	11,92	11,95
Na2O	2,66	2,85	2,75	2,69	2,49	2,79
K2O	1,02	0,99	0,98	0,90	1,04	0,94
NiO	0,00	0,00	0,01	0,03	0,00	0,04
P2O5	na	na	na	na	na	na
Cl	0,01	0,02	0,03	0,02	0,04	0,01
F	0,20	0,16	0,24	0,27	0,23	0,23
Total	97,36	97,67	98,11	97,10	97,44	97,21
mg#	65,8	67,7	66,9	61,2	66,1	67,6

Table A2.4. Continued.

Sample	DH 37.2				
Grain core/int/rim	**3-2a core**	**4-1a core**	**4-1b rim**	**4-2a core**	**4-2b rim**
SiO2	39,22	39,20	39,23	38,84	39,33
TiO2	6,44	6,31	6,09	6,59	6,15
Al2O3	12,37	12,54	12,53	12,62	12,50
Cr2O3	0,07	0,07	0,06	0,00	0,00
FeO	10,94	11,21	10,77	10,13	11,11
MnO	0,21	0,19	0,22	0,21	0,21
MgO	12,24	12,47	12,51	12,37	12,59
CaO	11,83	11,77	11,64	11,93	11,89
Na2O	2,71	2,80	2,64	2,69	2,77
K2O	0,99	1,03	0,95	0,97	0,96
NiO	0,00	0,02	0,04	0,00	0,00
P2O5	na	na	na	na	na
Cl	0,03	0,02	0,04	0,01	0,03
F	0,24	0,21	0,31	0,22	0,24
Total	97,28	97,83	97,02	96,57	97,78
mg#	66,6	66,5	67,4	68,5	66,9

Table A2.5. Clinopyroxene trace element data: lavas.

Sample	DH97-22C	DH97-22D		DH97-24		
Grain	**21**	**III 6**	**VII 5**	**VII 8**	**IV 2**	**V 4**
Li	3,95	11,40	1,34	11,63	12,88	3,28
P	36,51	11,60		56,45	52,22	29,12
Sc	38,11	33,71	24,88	28,12	28,70	26,39
V	191	177	133	147	187	164
Cr	0,80					
Co	8,67	8,50	8,89	10,25	10,04	8,65
Ni	2,49	1,00	1,30	1,27	0,91	0,69
Cu	10,50	0,60	0,60	0,63	0,41	0,88
Zn	248,52	223,40	271,84	282,77	322,45	149,67
Ga	11,87	12,61	8,39	10,25	11,56	8,76
As	1,37	0,60	0,60	0,53	0,71	1,09
Rb	0,66	0,02	0,15	0,10	0,11	
Sr	11,9	4,8	5,3	4,3	4,4	29,7
Y	56,60	31,11	23,88	27,17	33,36	68,54
Zr	642,4	1287,1	1073,2	1286,8	2777,2	351,7
Nb	5,27	5,90	1,90	2,32	6,49	2,59
Cs	0,01					
Ba	0,73					
La	60,70	55,92	47,05	53,07	74,22	56,60
Ce	175,04	128,05	100,60	106,98	151,49	184,81
Pr	23,28	13,91	10,09	10,78	14,91	27,48
Nd	94,25	45,32	30,37	36,15	48,47	123,39
Sm	17,80	7,00	5,00	5,50	7,00	26,06
Eu	3,31	1,16	1,00	0,94	1,22	5,58
Gd	14,15	6,00	4,50	4,86	5,98	21,57
Dy	12,78	5,80	4,40	4,65	5,88	17,41
Ho	2,26	1,15	0,81	0,99	1,26	2,92
Er	5,96	4,00	2,90	3,49	4,36	7,34
Yb	7,30	8,20	8,69	9,62	12,57	6,46
Lu	1,30	1,96	2,20	2,59	3,24	1,02
Hf	19,63	34,11	28,57	34,46	85,48	11,93
Ta	0,94	0,58	0,14	0,17	0,65	0,43
Pb	0,9813	0,3702	0,2997	0,3594	0,5374	0,3066
Th	0,1575	0,1701	0,0799	0,2220	0,2839	0,1095
U	0,0365	0,0210	0,0200	0,0254	0,0355	0,0120

Table A2.5. Continued

Sample	DH97-24	DH97-26A				DH97-26C
Grain	VI 2	IV 2	IV 6	II 5	III6	VI 1
Li	8,13	0,62	12,21	4,37	2,66	3,73
P	62,98	45,59	28,91	24,81	24,18	24,82
Sc	26,82	103,18	31,71	25,57	21,48	24,93
V	153	282	206	174	170	162
Cr		237,41				
Co	9,24	35,35	10,10	9,73	10,04	10,43
Ni	1,12	134,56	0,62	0,87	0,94	0,99
Cu	0,51	10,02	0,40	0,76	0,76	0,66
Zn	296,42	28,19	273,52	119,33	106,87	116,10
Ga	9,55	12,00	13,91	9,18	8,85	8,79
As	0,51	0,34	0,40	0,98	0,86	0,99
Rb	0,03	0,11		0,04		
Sr	4,7	84,7	2,6	32,2	45,7	38,6
Y	26,21	12,33	31,71	61,20	61,42	58,10
Zr	1350,9	68,4	2181,4	344,6	312,0	306,2
Nb	2,54	0,68	7,20	3,17	2,91	2,31
Cs						
Ba	0,36	1,87		0,66		0,05
La	57,19	4,40	74,03	49,50	46,53	43,28
Ce	122,51	15,75	145,66	165,01	160,41	138,83
Pr	11,58	2,73	13,91	23,49	24,18	20,76
Nd	36,67	14,76	41,92	103,92	109,35	94,90
Sm	5,49	4,29	6,00	22,18	23,64	20,76
Eu	0,92	1,40	1,01	4,70	5,51	4,28
Gd	4,57	4,29	5,00	18,91	19,43	17,46
Dy	4,67	3,08	5,20	15,19	15,44	14,17
Ho	0,92	0,52	1,13	2,62	2,67	2,53
Er	3,45	1,28	4,10	6,56	6,15	6,15
Yb	9,85	0,89	10,70	5,79	5,61	5,71
Lu	2,54	0,11	2,70	1,02	0,87	0,90
Hf	37,99	3,41	60,73	11,47	10,58	9,78
Ta	0,19	0,13	0,80	0,52	0,51	0,48
Pb	0,4470		0,4202	0,1639	0,2159	0,1318
Th	0,4165	0,0584	0,2601	0,1311	0,1295	0,1098
U	0,0406	0,0110	0,0190	0,0153	0,0151	0,0099

Table A2.5. Continued

Sample	DH97-26C					DH97-27A
Grain	**VI 2**	**VI 3**	**VI 4**	**VI 7**	**III 1**	**VII7**
Li	10,20	9,27	2,84	2,13	0,56	0,50
P	10,00	12,39	27,04	32,80	44,62	42,02
Sc	30,91	28,12	28,30	25,07	92,31	102,04
V	159	138	143	165	297	295
Cr					62,83	666,89
Co	10,40	11,20	11,15	10,75	34,72	36,50
Ni	1,02	0,87	0,88	1,01	58,05	134,58
Cu	0,61	0,65	0,42	0,78	1,94	2,76
Zn	241,74	260,08	251,37	120,33	25,16	28,93
Ga	10,61	8,94	8,94	9,18	12,52	12,49
As	0,41	0,32	0,42	1,34		0,54
Rb				0,06		
Sr	3,2	3,3	3,9	40,4	101,3	99,2
Y	25,30	24,89	23,04	62,01	14,46	14,17
Zr	1067,8	1208,7	994,7	305,4	78,9	83,6
Nb	2,37	1,77	1,74	2,50	0,72	0,64
Cs						
Ba			0,04			
La	46,61	46,54	42,61	45,45	4,89	4,68
Ce	95,27	98,90	89,02	145,85	19,24	17,53
Pr	9,38	9,80	8,73	22,05	3,53	3,11
Nd	29,78	31,68	28,30	101,97	18,44	17,89
Sm	4,69	4,85	4,31	21,49	5,12	5,04
Eu	0,77	0,84	0,78	4,81	1,75	1,67
Gd	4,08	4,09	3,68	18,81	5,12	5,04
Dy	4,18	4,31	3,68	15,45	3,87	3,72
Ho	0,93	0,91	0,81	2,59	0,63	0,59
Er	3,16	3,12	2,84	6,60	1,56	1,40
Yb	8,47	8,94	8,10	5,93	1,08	0,94
Lu	2,21	2,41	2,10	0,91	0,14	0,12
Hf	27,85	35,23	26,73	9,74	3,98	4,20
Ta	0,17	0,13	0,09	0,40	0,18	0,14
Pb	0,2142	0,3232	0,3683			
Th	0,0714	0,0528	0,0621	0,1231	0,0444	0,0372
U		0,0075		0,0146	0,0114	

Table A2.5. Continued

Sample	DH97-27A		DH97-27B			
Grain	**V7**	**V9**	**III4**	**III6**	**IV7**	**V3**
Li	0,50	0,56	0,64	0,59	0,55	0,62
P	50,13	54,56	45,23	47,74	42,70	36,62
Sc	103,84	102,69	114,08	112,93	127,39	119,16
V	287	307	298	311	296	292
Cr	781,91	380,57	981,23	133,56	688,61	3099,06
Co	34,93	37,34	38,38	38,08	38,53	37,93
Ni	122,86	136,88	179,97	104,21	184,05	179,28
Cu	2,39	2,79	2,36	2,12	3,34	2,50
Zn	28,35	29,22	27,99	30,18	29,10	26,36
Ga	12,20	13,94	12,87	13,44	12,88	12,05
As	0,36	0,48	0,32	0,58	0,68	0,44
Rb						
Sr	98,6	108,3	88,2	94,9	86,6	87,9
Y	13,28	14,91	12,40	14,74	12,88	12,64
Zr	84,5	99,2	68,6	80,6	70,9	65,7
Nb	0,62	0,89	0,54	0,68	0,56	0,49
Cs					0,05	
Ba	0,10	0,96	0,13		0,07	0,13
La	4,67	5,46	4,25	4,95	4,17	4,06
Ce	18,06	20,49	15,47	18,27	15,39	14,91
Pr	3,11	3,64	2,75	3,77	2,73	2,56
Nd	17,83	19,52	14,64	17,92	14,55	14,31
Sm	4,90	5,46	4,13	4,95	4,29	4,06
Eu	1,63	1,84	1,38	1,66	1,40	1,34
Gd	4,67	5,21	4,25	4,83	4,29	4,17
Dy	3,59	3,88	3,19	4,01	3,46	3,46
Ho	0,59	0,68	0,57	0,66	0,54	0,55
Er	1,32	1,48	1,17	1,43	1,28	1,19
Yb	0,89	0,99	0,77	1,04	0,89	0,98
Lu	0,12	0,12	0,12	0,13	0,11	0,10
Hf	4,07	4,49	3,42	4,01	3,82	3,34
Ta	0,20	0,18	0,14	0,17	0,11	0,12
Pb					1,0616	
Th	0,0383	0,0630	0,0272	0,0542	0,0477	0,0453
U					0,0119	0,0131

Table A2.5. Continued

Sample	DH97-4					
Grain	**2A**	**2B**	**2C**	**1A**	**1B**	**1C**
Li	2,39	2,35	2,34	0,65	0,64	0,64
P	67,86	48,56	88,87	74,34	77,86	70,65
Sc	27,74	25,10	31,50	66,63	60,56	57,16
V	164	179	220	243	255	243
Cr	0,66	0,77	0,77	7,27	1,24	1,11
Co	12,72	12,06	12,16	25,49	23,15	21,12
Ni	0,36	0,46	0,44	17,44	4,61	2,65
Cu	0,93	1,40	1,88	2,01	2,25	1,99
Zn	61,83	64,68	69,20	32,87	37,41	35,60
Ga	10,85	12,39	16,80	12,41	14,04	13,38
As	0,69	0,88	1,11	0,56	0,64	0,55
Rb			0,02		0,01	
Sr	180,7	196,0	216,7	147,3	170,2	166,8
Y	29,93	32,01	45,10	20,12	25,39	25,54
Zr	172,2	196,7	318,8	113,9	154,9	158,9
Nb	1,66	2,24	3,87	1,15	1,66	1,68
Cs						
Ba	0,12	0,09	0,13	0,04	0,03	0,06
La	14,25	16,66	25,98	7,38	10,34	10,39
Ce	51,74	62,71	93,07	28,51	39,32	39,58
Pr	9,10	10,74	15,81	5,14	7,08	6,97
Nd	46,37	53,94	79,14	28,51	38,09	38,03
Sm	11,73	13,05	18,24	7,71	9,89	9,84
Eu	3,73	4,17	5,86	2,57	3,26	3,21
Gd	10,30	11,07	16,14	7,27	9,44	9,18
Dy	7,67	8,55	11,72	5,25	6,74	6,74
Ho	1,28	1,38	1,90	0,85	1,09	1,12
Er	2,96	3,29	4,42	2,01	2,42	2,54
Yb	2,23	2,40	3,43	1,43	1,79	1,79
Lu	0,32	0,34	0,45	0,18	0,21	0,23
Hf	6,47	7,02	12,27	4,92	6,74	6,52
Ta	0,37	0,48	0,99	0,27	0,49	0,42
Pb	0,0767	0,0767	0,0884	0,0447		
Th	0,0735	0,0910	0,1857	0,0593	0,0764	0,0907
U	0,0077	0,0143	0,0210	0,0078	0,0112	0,0122

Table A2.5. Continued

Sample	DH97-4				
Grain	**3A**	**3B**	**8**	**9A**	**9B**
Li	0,76	0,79	1,84	0,69	0,70
P	63,25	101,42	38,09	83,55	68,42
Sc	80,04	86,25	18,00	74,10	64,73
V	238	301	201	288	247
Cr	36,24	4,87	0,99	1,94	2,46
Co	30,68	27,96	6,15	23,45	23,92
Ni	63,70	19,47	0,68	6,37	7,60
Cu	1,73	2,38	0,97	2,73	2,12
Zn	30,01	33,28	127,11	34,26	32,42
Ga	10,23	14,83	9,88	15,82	12,19
As	0,49	0,57	2,09	0,61	0,63
Rb	0,01		0,02	0,01	
Sr	109,5	139,5	53,3	168,5	150,8
Y	15,79	24,22	92,31	28,57	22,14
Zr	73,8	132,8	312,6	203,3	125,0
Nb	0,57	1,31	2,93	2,14	1,26
Cs					
Ba	0,03	0,08	0,21	0,11	
La	4,56	8,38	65,09	10,81	7,94
Ce	18,79	32,60	243,79	41,09	30,41
Pr	3,45	5,89	40,83	7,40	5,48
Nd	19,34	32,71	196,81	40,52	30,30
Sm	5,56	9,17	43,14	10,81	8,16
Eu	1,92	3,17	12,51	3,53	2,68
Gd	5,56	8,94	34,58	10,36	7,94
Dy	4,22	6,45	25,91	7,28	5,59
Ho	0,68	1,00	4,17	1,23	0,94
Er	1,48	2,30	9,77	2,73	2,19
Yb	1,09	1,64	7,03	1,98	1,51
Lu	0,13	0,20	1,01	0,23	0,18
Hf	3,56	5,89	10,65	8,65	5,48
Ta	0,13	0,33	0,70	0,59	0,28
Pb	0,0333		0,1976	0,0569	
Th	0,0456	0,0781	0,1251	0,1013	0,0660
U	0,0033	0,0057	0,0121	0,0137	0,0089

Table A2.6. Clinopyroxene trace element data: syenites.

Sample	DH97-39-1					
Grain core/int/rim	2-1a outer	2-1b pale rim	2-1c pink c	2-1d pink internal	2-1e pale r	2-1f inner
Li	7,19	7,44	15,78	14,17	4,67	9,27
Be	0,521	0,543	2,39	2,31	0,292	1,18
B	1,18	1,05	1,48	1,45	0,437	0,699
P	31,88	32,12	25,25	27,77	17,17	13,41
Sc	72,02	70,84	21,1	21,17	33,58	10,15
V	171,73	177,71	196,2	196,36	91,68	102
Co	24,17	23,19	14,25	12,98	13,38	7,84
Ni	79,1	75,52	7,94	1,82	43,51	3,28
Ga	9,05	9,15	19,43	19,53	5,73	9,98
Rb	<0.034	<0.032	0,249	0,045	0,1192	0,214
Sr	172,33	175,84	257,85	264,49	89,02	127,63
Y	17,13	17,1	44,66	47,03	8,01	20,73
Zr	149,93	155,25	513,26	548,25	72,11	235,01
Nb	0,948	1,008	5,39	5,49	0,513	2,603
Cs	<0.0163	<0.0158	<0.0136	<0.0154	<0.0073	<0.0065
Ba	<0.039	0,142	0,5	0,245	0,31	0,697
La	8,15	8,57	24,91	28,21	4,16	12,29
Ce	28,33	29,65	88,19	96,83	16,38	45,21
Pr	5,02	5,33	15,35	16,71	2,83	7,9
Nd	26,34	26,92	74,24	80,56	13,61	36,37
Sm	6,77	7,18	17,47	19,45	3,46	8,44
Eu	2,26	2,36	5,32	5,89	1,127	2,62
Gd	6,73	6,45	14,81	16,18	3,1	6,81
Tb	0,87	0,832	2,02	2,19	0,384	0,964
Dy	4,41	4,55	11,13	11,91	2,05	5,09
Ho	0,758	0,729	1,899	2,05	0,342	0,886
Er	1,62	1,671	4,55	4,7	0,69	2,06
Tm	0,175	0,172	0,565	0,566	0,0759	0,263
Yb	1,047	0,934	3,37	3,45	0,479	1,443
Lu	0,1439	0,1378	0,47	0,505	0,0569	0,211
Hf	6,44	6,5	17,34	18,83	2,92	7,9
Ta	0,221	0,209	1,162	1,153	0,0996	0,531
Pb	<0.121	0,116	0,19	<0.110	0,129	0,099
Th	0,0797	0,0951	0,191	0,212	0,0338	0,0914
U	0,0045	0,0089	0,0237	0,027	0,0059	0,0146

Table A2.6. Continued.

Sample	DH97-39-2					
Grain core/int/rim	2-2d c	3-1a c small	2-2b pale c	2-2a pale outer	3-1b c/out	2-2c pale r
Li	20,18	37,29	16,43	15,5	39,67	23,93
Be	1,36	1,42	1,34	2,3	1,33	1,16
B	1,06	<0.37	<0.40	0,85	0,4	<0.43
P	124,77	65,14	57,97	48,95	61,17	43,04
Sc	25,01	51,11	27,82	34,02	52,79	32,3
V	101,57	188,93	86,39	95,35	185,72	128,17
Co	17,21	20,95	13,02	12,55	22,89	21,32
Ni	1,6	2,63	1,47	1,52	2,79	2,06
Ga	14,47	14,31	13,55	15,14	14,01	12,65
Rb	0,712	0,063	0,086	1,38	<0.033	0,296
Sr	158,41	175,43	149,78	139,46	186,4	186,24
Y	87,26	73,67	85,58	92,72	68,01	93,49
Zr	641,71	617,57	640,08	735,51	640,87	813,91
Nb	7,88	5,81	6,25	17,75	4,83	5,89
Cs	<0.0133	<0.0140	<0.0151	<0.0136	<0.024	<0.0163
Ba	4,25	0,146	0,231	1,327	0,137	0,526
La	40,25	33,46	36,03	43,86	30,82	48,64
Ce	154,34	117,8	134,55	162,17	109,64	171,67
Pr	24,43	20,05	22,42	26,16	18,77	28,54
Nd	118,98	100,49	109,97	122,5	93,1	136,85
Sm	29,02	25,12	27,81	30,48	23,77	33,44
Eu	6,92	6,03	7,02	7,07	5,58	6,79
Gd	25,2	21,74	24,19	25,87	20,33	28,36
Tb	3,58	3,08	3,5	3,76	2,82	3,93
Dy	20,12	17,27	20,21	21,76	15,55	22,51
Ho	3,57	3,02	3,53	3,81	2,77	3,95
Er	8,57	7,17	8,48	9,31	6,49	9,36
Tm	1,08	0,896	1,098	1,23	0,816	1,21
Yb	6,76	5,45	6,65	7,72	5,09	7,64
Lu	0,997	0,777	0,966	1,132	0,734	1,188
Hf	20,53	21,96	21,17	23,57	22,24	27,79
Ta	0,96	1,07	1,029	1,54	0,82	0,982
Pb	0,161	0,076	0,06	0,14	0,078	0,132
Th	0,351	0,26	0,297	0,38	0,216	0,252
U	0,141	0,0528	0,0507	0,0656	0,041	0,0516

Table A2.6. Continued.

Sample	DH39-2	DH39-4				
Grain core/int/rim	3-1c rim	6-1a outer c	6-1b r	4-3a c	4-3b pink outer	2-1a r
Li	22,33	8,98	11,12	9,24	8,53	9,88
Be	1,45	6,41	10,86	4,78	2,7	3,51
B	1,62	<0.35	1,48	1,22	0,96	1,6
P	57,22	31,24	19,18	501,75	149,26	37,51
Sc	45,85	19,55	8,81	35,92	35,1	40,15
V	170,6	101,58	68,47	134,79	136,65	175,45
Co	21,19	21,07	23,77	25,73	25,14	21,02
Ni	2,15	3,91	4,37	5,07	4,77	4,2
Ga	14,12	13,13	13,38	8,38	8,87	10,93
Rb	2,24	<0.053	1,58	0,314	3,33	1,99
Sr	181,59	79,85	81,08	86,12	81,64	86,64
Y	70,51	150,19	130,01	88,55	87,72	112,08
Zr	612,5	2215,26	2469,72	686,69	643	1058,24
Nb	5,81	13,08	13,57	12,87	5,91	9,71
Cs	0,0154	<0.0189	0,099	0,0243	0,061	0,08
Ba	0,872	0,0473	0,39	0,377	4,52	0,196
La	32,35	123,33	114,47	66,93	61,96	83,42
Ce	112,91	368,61	351,74	211,45	199,31	250,55
Pr	19,19	54,32	48,52	32,07	30,72	38,27
Nd	95,24	221,52	181,83	136,63	133,19	166,99
Sm	24,28	46,2	35,92	30,59	29,58	37,08
Eu	5,61	3,19	2,53	4,82	4,22	5,88
Gd	21	37,2	27,78	25,02	23,96	30,66
Tb	2,94	5,9	4,46	3,62	3,53	4,48
Dy	16,53	36,1	28,28	21,69	20,89	26,21
Ho	2,89	6,97	5,4	3,9	3,71	4,67
Er	6,84	17,84	14,84	9,79	9,23	11,93
Tm	0,86	2,54	2,32	1,35	1,24	1,57
Yb	5,33	17,64	16,23	9,08	8,54	10,37
Lu	0,794	2,85	2,56	1,48	1,39	1,58
Hf	21,5	64,92	64,91	20,32	18,13	32,54
Ta	0,99	2,28	2,33	0,88	0,597	1,65
Pb	0,11	0,347	0,397	0,212	0,248	0,123
Th	0,31	0,914	1,01	0,445	0,257	0,596
U	0,0618	0,19	0,23	0,086	0,073	0,111

Table A2.6. Continued.

Sample	DH39-4			DH97-39-5		
Grain core/int/rim	2-1b interm	2-1c c	2-1d outer	4-1a large out	4-1b c	4-1c r
Li	11,21	13,99	9,19	13,57	21,78	20,77
Be	4,04	1,05	0,95	0,357	0,329	0,651
B	1,37	0,74	0,52	1,68	1,49	1,26
P	55,51	50,15	32,88	44,44	57,55	43,28
Sc	79,78	72,83	44,81	69,87	73,85	55,34
V	269,67	226,81	164	297,37	309,61	306,98
Co	22,41	24,83	22,97	34,13	36,53	29,73
Ni	5,91	7,44	5,22	49,06	62,41	28,88
Ga	15,01	10,11	9,14	9,44	9,5	11,01
Rb	0,98	0,124	0,035	<0.038	0,139	0,223
Sr	169,84	153,18	146,35	89,4	83,99	102,95
Y	67,79	47,64	64,98	19,88	21,26	23,05
Zr	722,3	385,73	485,08	113,3	118	138,72
Nb	10,82	3,67	4,5	0,878	0,789	1,246
Cs	<0.0185	<0.0153	<0.0158	<0.0198	<0.0178	<0.0150
Ba	0,221	0,174	0,142	0,244	0,453	0,689
La	41,66	26,35	42	5,91	5,8	7,93
Ce	137,49	91,82	140,06	22,48	23,12	30,32
Pr	22,03	14,85	22,29	4,07	4,21	5,46
Nd	101,99	70,32	100,29	20,86	21,88	27,53
Sm	24,01	16,86	23,02	5,94	6,18	7,21
Eu	5,86	4,33	5,2	1,953	2,046	2,315
Gd	20,55	14,31	19,01	5,82	6,25	7,1
Tb	2,81	2,02	2,68	0,823	0,838	0,961
Dy	16,21	11,36	15,86	4,78	5,07	5,5
Ho	2,84	1,97	2,78	0,827	0,881	0,972
Er	6,8	4,83	6,83	2,03	2,08	2,18
Tm	0,85	0,597	0,89	0,238	0,26	0,264
Yb	5,53	3,92	5,74	1,406	1,462	1,605
Lu	0,82	0,574	0,89	0,196	0,182	0,216
Hf	23,45	12,83	14,55	4,77	4,78	5,43
Ta	1,7	0,57	0,633	0,166	0,142	0,231
Pb	0,083	0,08	0,089	<0.137	0,128	0,259
Th	0,679	0,217	0,228	0,0714	0,0617	0,0794
U	0,138	0,042	0,05	0,0096	0,0109	0,0129

Table A2.6. Continued.

Sample	DH39-5					DH39-8
Grain core/int/rim	4-1d r	5-1a	5-1b	5-2c	5-2d	1-1a
Li	18,26	18,49	23,16	18,28	22,47	8,3
Be	0,546	0,316	0,307	0,553	0,85	4
B	1,2	1,45	1,41	0,94	1,46	0,49
P	44,7	58,62	71,4	63,73	62	21,47
Sc	55,26	76,8	79,41	83	88,56	29,46
V	308,3	291,28	309,33	396,65	443,27	117,96
Co	32,67	33,66	39,23	33,81	37,89	19,55
Ni	32,02	55,91	66,1	58,22	60,79	3,19
Ga	10,7	8,36	9,73	13,91	18,45	8,28
Rb	0,181	<0.034	0,178	0,222	3,19	0,128
Sr	101,3	86,3	83,01	94,72	96,87	65,28
Y	22,01	21,35	22,31	26,07	29,13	95,94
Zr	124,34	117,4	122,81	191,62	224,17	954,9
Nb	1,04	0,705	0,678	1,775	2,579	5,47
Cs	<0.0170	<0.0177	<0.0140	<0.0141	0,084	<0.0152
Ba	0,562	0,066	0,489	0,365	1,264	0,0285
La	7,33	6,05	6,21	9,07	10,58	54,31
Ce	29,42	23,62	24,51	35,89	40,24	172,22
Pr	5,18	4,46	4,58	6,25	6,92	26,07
Nd	26,07	22,87	23,57	31,43	34,96	112,7
Sm	7,16	6,3	6,7	8,41	9,5	26,3
Eu	2,176	2,161	2,144	2,72	3,09	3,12
Gd	6,74	6,43	6,75	8,22	8,98	22,37
Tb	0,938	0,896	0,95	1,082	1,267	3,38
Dy	5,25	5,02	5,23	6,26	6,9	20,94
Ho	0,898	0,897	0,913	1,065	1,238	3,9
Er	2,08	2,11	2,19	2,64	2,83	10,32
Tm	0,25	0,257	0,273	0,303	0,354	1,44
Yb	1,627	1,472	1,553	1,76	2,1	9,97
Lu	0,208	0,217	0,215	0,261	0,284	1,56
Hf	4,76	5,05	5,37	8,09	8,77	24,76
Ta	0,211	0,135	0,139	0,439	0,489	0,664
Pb	0,222	<0.126	0,206	<0.105	0,138	0,204
Th	0,0748	0,0503	0,0685	0,132	0,184	0,374
U	0,0147	0,0103	0,0124	0,0216	0,0266	0,0739

Table A2.6. Continued.

Sample	DH39-8					
Grain core/int/rim	1-1a pale c	1-1b	1-1c pale c	1-1d pale c	1-1h pink inter	1-1b r
Li	24,16	9,69	29,31	20,35	40,17	25,86
Be	0,86	2,52	0,87	1,22	1,29	1,58
B	<0.49	0,89	<0.41	0,57	0,93	1
P	44,16	26,87	38,12	54,82	63,16	52,28
Sc	33,36	40,01	30,67	28,82	45,03	42,21
V	107,91	156,17	112,23	99,09	195,46	154,28
Co	19,89	18,22	22,49	17,93	25,97	21,75
Ni	2,08	3,17	2,14	1,83	2,77	2,26
Ga	8,23	7,88	9,68	14,53	17,22	13,44
Rb	<0.038	5,44	0,042	0,075	0,141	0,042
Sr	169,23	136,53	171,17	152,66	183,08	185,02
Y	67,91	62,84	69,13	82,65	71,61	76,3
Zr	413,64	552,98	423,77	604,12	584,8	668,99
Nb	2,72	5,91	3	5,83	5,29	5,86
Cs	<0.0166	<0.0128	<0.0146	0,0131	<0.0138	<0.0144
Ba	0,113	0,172	0,33	0,245	0,187	0,121
La	29,09	38,9	31,24	36,25	32,59	35,54
Ce	102,56	139,26	115,36	140,86	124,14	127,2
Pr	18,34	21,02	19,91	23,79	21,48	22,19
Nd	91,08	93,95	97,76	112,18	101,3	108,36
Sm	23,13	22,2	24,57	28,7	25,72	27,72
Eu	5,23	5,01	5,46	7,07	6,1	6,34
Gd	20,6	17,94	21,75	25,23	22,64	23,8
Tb	2,9	2,56	3,01	3,55	3,11	3,38
Dy	16,52	14,99	17,03	20,39	17,21	18,94
Ho	2,92	2,68	3	3,67	3,08	3,33
Er	6,81	6,68	7,28	8,92	7,32	7,86
Tm	0,856	0,915	0,913	1,127	0,912	0,997
Yb	5,43	5,99	5,85	7,03	5,58	6,12
Lu	0,865	0,852	0,925	1,014	0,826	0,958
Hf	14,22	15,63	14,72	21,13	21,8	25,24
Ta	0,378	0,901	0,438	0,949	0,997	1,195
Pb	0,059	0,187	0,121	0,118	0,108	0,082
Th	0,128	1,212	0,143	0,282	0,25	0,247
U	0,034	0,149	0,0353	0,051	0,058	0,0546

Table A2.6. Continued.

Sample	DH39-8					
Grain core/int/rim	1-1e r	1-1f r	3-1a out	3-1c c	3-1d out	3-1e r
Li	15,13	32,13	11,97	14,52	17,78	10,52
Be	1,63	1,35	1,46	1,85	1,83	2,78
B	1,01	0,51	<0.46	1	1,27	1,5
P	53,35	59,73	128,62	207,54	201,09	56,01
Sc	33,08	43,17	70,23	67,9	67,72	43,83
V	92,91	167,65	246,98	255,24	272,56	166,29
Co	14,61	21,47	20,85	21,39	26,08	20,7
Ni	1,67	2,27	5,18	5,81	6,45	4,3
Ga	14,23	14,51	14,55	16,44	21,42	11,84
Rb	1,75	0,17	<0.039	0,218	0,196	3,09
Sr	144,27	185,16	174,33	168,46	179,71	106,98
Y	85,23	81,62	59,22	61,96	67,3	81,91
Zr	612,18	654,25	662,06	675,11	743,57	800,5
Nb	6,62	5,79	7,29	8,6	9,84	6,92
Cs	<0.0146	<0.0167	<0.0171	<0.0137	<0.0125	<0.019
Ba	0,364	0,288	5,9	0,457	1,029	0,864
La	37,75	37,73	35,52	35,26	40,25	53,14
Ce	139,1	135,69	119,2	122,83	142,42	177,14
Pr	23,11	23,1	19,02	19,61	22,6	27,28
Nd	112,32	113,09	89,23	91,92	106,15	120,13
Sm	27,9	29,01	21,94	22,86	25,64	28,6
Eu	6,92	6,57	5,91	6,05	6,89	5,51
Gd	24,39	25	18,58	19,17	21,88	23,56
Tb	3,48	3,45	2,52	2,58	2,99	3,49
Dy	20,36	19,93	15,06	15,07	17,19	21,05
Ho	3,53	3,54	2,63	2,67	2,99	3,83
Er	8,54	8,25	6,36	6,36	7,35	9,54
Tm	1,094	1	0,792	0,811	0,908	1,34
Yb	6,83	6,24	5,09	4,98	5,76	8,84
Lu	0,997	0,95	0,716	0,722	0,806	1,4
Hf	20,12	24,43	23,47	22,45	25,92	26,1
Ta	1,062	1,129	1,38	1,73	2,11	1,18
Pb	0,113	0,125	0,082	0,12	0,259	0,247
Th	0,322	0,27	0,487	0,571	0,68	0,797
U	0,0764	0,0576	0,092	0,095	0,131	0,228

Table A2.6. Continued.

Sample	DH39-8			DH39-9		
Grain core/int/rim	3-1f r	3-1h c	3-1i c/interm	3-1a c (messy)	3-1b c (good)	3-1c outer
Li	15,11	19,13	21,68	18,57	23,44	23,94
Be	1,32	1,99	1,78	3,41	6,43	7,14
B	0,54	1,37	1,53	1,05	1,88	0,97
P	101,63	753,03	522,08	134,08	264,46	185,31
Sc	60,07	64,71	62,53	16,61	11,49	14,12
V	215,92	270,39	291,02	163,25	162,08	182,52
Co	25,37	26,7	28,53	10,24	10,71	12,59
Ni	8,05	6,85	8,02	1,4	1,54	1,45
Ga	13,37	20,85	19,44	12,96	13,85	18,1
Rb	0,093	0,445	0,79	0,206	0,961	2,24
Sr	160,28	174,03	176,12	162,93	150,81	161,29
Y	51,91	64,37	64,41	60,77	54,61	64,93
Zr	474,19	685,4	694,27	855,12	813,65	969,25
Nb	5,64	8,75	8,8	10,15	8,29	11,35
Cs	<0.0146	0,021	0,0301	<0.013	0,0156	0,0215
Ba	3,28	0,925	1,18	0,202	0,277	0,742
La	29,32	41,43	41,74	58,03	55,46	66,37
Ce	100,77	147,86	147,72	191,92	170,45	210,4
Pr	16,5	22,08	22,71	27,74	24,59	30,12
Nd	79,19	101,4	104,53	111,3	101,04	123,99
Sm	19,38	24,26	24,77	22,23	19,21	24
Eu	5,3	6,43	6,58	6,13	5,5	6,63
Gd	16,98	20,31	20,25	17,8	15,25	18,97
Tb	2,34	2,8	2,86	2,392	2,083	2,61
Dy	13,96	16,21	16,37	14,21	12,22	15,17
Ho	2,35	2,78	2,84	2,509	2,076	2,618
Er	5,77	6,76	6,96	6,36	4,94	6,39
Tm	0,708	0,839	0,844	0,767	0,661	0,797
Yb	4,68	5,31	5,62	5,43	4,41	5,33
Lu	0,676	0,764	0,754	0,724	0,692	0,831
Hf	16,83	23,01	23,32	22,12	19,33	25,51
Ta	0,949	1,75	1,77	1,315	0,965	1,67
Pb	0,113	0,264	0,306	0,145	0,206	0,269
Th	0,348	0,679	0,655	0,455	0,464	0,552
U	0,069	0,151	0,149	0,071	0,0879	0,0998

Table A2.6. Continued.

Sample	DH39-9		TDKS-17-3			
Grain core/int/rim	5-1a c	5-1b r	1-2a c	1-1a pink outer	1-1b pink interm	1-1c pale c
Li	19,22	23,08	23,16	8,11	13,48	7,71
Be	11,16	9,42	10,57	1,16	1,05	1,48
B	1,88	1,01	1,65	0,7	0,83	0,63
P	38,8	15,23	16,39	50,77	91,11	55,94
Sc	14,87	15,79	11,76	48,23	77,04	54,06
V	172,31	176,42	173,35	292,93	494,84	308,76
Co	14,17	14,14	13,55	20,86	23,3	21,62
Ni	1,83	1,89	1,79	3,15	4,54	3,58
Ga	16,07	16,35	18,19	13,1	15,71	12,02
Rb	1,98	2,39	2,63	<0.031	0,08	0,398
Sr	94,1	98,06	142,17	195,05	169,35	198,2
Y	24,82	27,37	34,85	71,04	51,21	58,73
Zr	1197,3	1196,71	1329,26	551,18	453,43	474,49
Nb	5,48	6,82	19,5	5,8	4,73	4,64
Cs	0,021	0,031	0,0396	<0.0131	<0.0121	0,0186
Ba	0,115	0,775	1,7	0,163	0,284	0,163
La	33,39	39,05	46,94	35,69	23,5	28,28
Ce	87,45	105,54	134,92	112,37	78,23	90,76
Pr	10,56	12,79	17,35	19,21	13,56	15,22
Nd	37,91	46,09	69,13	97,63	71,21	78,33
Sm	6,92	8,52	13,07	23,78	17,84	19,28
Eu	2,06	2,55	4,07	5,88	4,93	5,01
Gd	5,45	6,52	10,42	21,03	16,24	17,22
Tb	0,8	0,945	1,45	2,83	2,106	2,32
Dy	4,81	5,8	8,6	16,78	12,14	13,61
Ho	0,943	1,085	1,5	2,82	2,06	2,27
Er	2,57	2,93	3,78	6,9	4,91	5,55
Tm	0,396	0,453	0,543	0,819	0,561	0,677
Yb	3,27	3,65	4,29	5,29	3,56	4,33
Lu	0,659	0,719	0,79	0,769	0,503	0,615
Hf	24,33	27,21	30,15	18,15	15,9	15,6
Ta	0,355	0,466	1,77	1,036	0,968	0,699
Pb	0,467	0,456	0,505	0,132	0,143	0,611
Th	0,493	0,734	1,13	0,296	0,276	0,235
U	0,0924	0,0752	0,287	0,051	0,0394	0,0582

Table A2.6. Continued.

Sample	TDKS-17-3					
Grain core/int/rim	1-1d pink inner r	2-1a pale c	2-1b c	2-1c dark pink r	2-1d r	2-1e pink inner r
Li	14,94	7,16	7,23	8,79	9,38	9,96
Be	1,03	1,01	0,86	1,41	1,3	1,37
B	0,48	0,8	0,99	0,79	0,49	0,51
P	98,93	54,13	68,17	52,63	50,41	56,69
Sc	81,13	54,89	62,07	54,82	51,87	67,41
V	517,61	318,82	382,19	360,5	353,1	415,64
Co	24,67	20,32	23,3	22,32	23,31	21,43
Ni	5,02	3,39	3,82	3,89	3,58	3,71
Ga	17,61	11,58	13,64	16,2	17,43	15,37
Rb	0,087	<0.033	0,037	0,031	0,141	<0.032
Sr	172,31	190,03	188,13	185,85	190,8	180,45
Y	52,1	61,3	55,54	62,96	63,82	57,62
Zr	462,2	510,82	470,47	586,42	593,87	547,49
Nb	4,75	4,45	4,16	6,72	7,28	6,31
Cs	<0.0112	<0.0134	<0.0130	<0.0119	<0.0130	<0.0136
Ba	0,303	0,144	0,161	0,179	0,186	0,128
La	23,4	28,93	25,94	28,72	31,54	25,51
Ce	81,21	92,41	87,81	96,56	107,48	84,69
Pr	13,32	15,49	14,53	16,07	17,47	14,56
Nd	69,92	80,75	75,06	81,63	87,7	75,42
Sm	17,59	19,63	18,33	19,97	21,52	18,95
Eu	4,83	5	4,77	5,05	5,47	4,98
Gd	16,15	17,41	16,43	17,71	19,1	17,07
Tb	2,07	2,3	2,2	2,37	2,57	2,26
Dy	11,97	13,77	12,7	14,12	15,14	13,39
Ho	2,02	2,37	2,14	2,38	2,54	2,22
Er	4,8	5,82	5,23	5,73	6,32	5,46
Tm	0,569	0,668	0,589	0,689	0,753	0,647
Yb	3,48	4,41	4,05	4,59	4,93	4,25
Lu	0,524	0,651	0,58	0,652	0,7	0,58
Hf	15,71	16,17	15,14	18,16	19,63	18,47
Ta	0,9	0,71	0,674	1,17	1,277	1,128
Pb	0,146	0,089	0,109	0,126	0,308	0,087
Th	0,247	0,234	0,223	0,252	0,306	0,262
U	0,0424	0,0409	0,0355	0,0467	0,0624	0,0397

Table A2.6. Continued.

Sample	TDKS-17-3					
Grain core/int/rim	2-1f pale c	3-1a pale c	3-1b pale c	3-1c interm (pink)	3-1f interm (pink)	3-1d r
Li	8,16	4,86	5,47	7,7	10,49	7,39
Be	0,89	0,55	0,54	1,02	1,06	3,17
B	0,61	0,76	1,04	0,74	0,28	4,3
P	50,81	68,1	67,41	60,13	75,78	39,57
Sc	49,6	67,42	63,48	47,37	63,62	15,78
V	328,12	361,02	353,2	319,89	416,74	115,22
Co	23,2	21,87	23,11	24,21	25,08	25,24
Ni	3,8	4,12	4,42	3,69	4,28	2,78
Ga	12,21	8,65	8,53	14,26	15,35	12,04
Rb	<0.029	0,106	0,029	0,05	0,126	2,97
Sr	186,09	142,26	147,03	192,07	184,09	69,66
Y	52,1	37,43	37,59	66,35	54,65	98,89
Zr	393,89	249,75	228,87	535,91	444,69	926,73
Nb	3,77	1,962	1,656	5,77	4,59	13,67
Cs	<0.0116	<0.0156	<0.0115	<0.0110	<0.0101	0,045
Ba	0,135	1,43	0,126	0,251	0,362	1,61
La	23,93	13,63	13,76	32,93	26,81	82,63
Ce	82,29	47,25	49,52	110,88	95,02	244,08
Pr	13,59	8,33	8,72	18,04	15,57	36,28
Nd	69,24	45,4	45,63	90,96	79,19	160,68
Sm	16,96	11,87	11,9	21,86	19,37	34,56
Eu	4,45	3,34	3,24	5,43	5,15	4,32
Gd	15,37	11,32	11,03	19,37	17,37	28,42
Tb	2,02	1,46	1,46	2,57	2,3	3,92
Dy	11,96	8,79	8,49	15,08	13,56	23,94
Ho	2,01	1,45	1,44	2,53	2,23	4,06
Er	4,93	3,49	3,43	6,35	5,51	10,81
Tm	0,588	0,427	0,41	0,741	0,639	1,43
Yb	3,88	2,67	2,6	4,74	4,19	10,96
Lu	0,532	0,382	0,38	0,698	0,585	1,83
Hf	12,42	8,66	7,69	16,85	16,06	23,93
Ta	0,588	0,282	0,22	0,977	0,884	1,24
Pb	0,114	0,067	0,098	0,136	0,181	1,45
Th	0,186	0,115	0,114	0,274	0,272	1,89
U	0,0384	0,0208	0,0219	0,0488	0,0499	0,267

Table A2.6. Continued.

Sample	TDKS-17-3	DH97-37-2				
Grain core/int/rim	3-1e inner r (pink)	1-1a c	1-1b outer	5-1a c	4-1a pale c	4-1b pale c
Li	6,13	0,582	0,787	0,652	0,585	0,712
Be	1,44	0,59	0,545	0,437	0,57	0,64
B	0,81	0,56	0,76	<0.24	0,5	0,63
P	47,5	38,37	30,38	27,33	18,28	18,21
Sc	31,48	26,32	17,83	16,3	12,14	15,71
V	219,41	195,83	194,92	186,71	159,28	159,23
Co	24,56	13,92	13,47	14,72	4,72	4,94
Ni	2,89	2,25	2,17	2,03	1,019	1,055
Ga	14,58	10,29	10,94	10,06	7,35	7,52
Rb	0,256	<0.025	0,419	<0.027	<0.025	0,19
Sr	180,27	223,79	204,55	142,95	23,65	22,53
Y	88,81	52,03	68,66	73,43	92,12	75,97
Zr	726,32	262,58	290	272,5	245,5	265,16
Nb	7,69	2,183	2,48	1,74	1,736	1,768
Cs	<0.0123	<0.0101	<0.0100	<0.0076	<0.0095	0,0086
Ba	0,786	0,221	2,64	0,29	0,264	2,36
La	55,25	24,93	36,94	37,91	61,21	58,5
Ce	183,97	103	154,26	157,98	237,5	220,28
Pr	28,98	18,15	27,24	28,97	40,98	35,95
Nd	139,82	85,4	130,39	142,5	193,38	159,85
Sm	32,76	20,15	29,43	33,47	43,03	32,95
Eu	7,2	6,83	10,17	10,53	11,11	7,89
Gd	28,27	16	22,71	27,51	34,33	25,73
Tb	3,8	2,097	3,12	3,68	4,64	3,5
Dy	22,66	12,38	17,77	21,19	27,44	21,1
Ho	3,81	2,04	2,97	3,49	4,54	3,66
Er	9,62	4,65	6,86	7,94	10,67	8,93
Tm	1,17	0,53	0,802	0,914	1,301	1,105
Yb	7,9	3,19	4,93	5,64	8,15	7,56
Lu	1,18	0,438	0,654	0,76	1,218	1,189
Hf	24	8,09	9,57	10,74	9,09	9,28
Ta	1,39	0,53	0,663	0,549	0,315	0,276
Pb	0,318	0,089	0,183	0,129	0,238	0,293
Th	0,414	0,0644	0,0886	0,0683	0,0944	0,152
U	0,084	0,0085	0,0179	0,0064	0,0102	0,0198

Table A2.6. Continued.

Sample	DH97-37-2					
Grain core/int/rim	4-1c interm	4-1e interm	1-1c pink inner r	1--1d dark outer r	4-1f out r	4-1d outer r
Li	0,911	1,062	0,709	0,708	0,854	0,714
Be	0,69	1,16	1,05	0,86	0,81	0,78
B	0,76	0,38	0,85	<0.33	0,6	0,54
P	33,6	25,57	50,74	49,29	62,69	51,98
Sc	19	13,64	27,48	46,13	31,76	45,68
V	209,15	217,85	213,11	246,2	227,86	241,46
Co	9,39	6,74	14,8	17,02	17,11	18,35
Ni	1,45	1,17	2,24	2,62	2,14	2,81
Ga	11,35	12,72	12,07	14,76	14,68	14,44
Rb	0,64	0,745	<0.029	0,483	0,521	0,515
Sr	148,73	50,04	209,32	247,09	219,06	217,87
Y	82,85	108,11	38,51	43,09	51,56	33,61
Zr	312,44	407,41	189,81	239,31	266,69	173,85
Nb	2,565	4,59	2,112	2,87	2,81	2,193
Cs	0,0092	0,008	<0.0120	<0.0144	<0.0063	<0.0063
Ba	2,52	2,81	0,286	2,87	6,92	1,121
La	46,55	66,44	16,3	21,5	24,3	14,56
Ce	192,98	276,02	69,07	96,22	106,19	63,67
Pr	33,55	46,27	12,38	17,13	18,32	11,23
Nd	158,95	218,74	61,07	85,6	91,85	57,02
Sm	35,43	47,8	14,61	20,76	21,66	14,32
Eu	10,79	12,78	4,84	7,09	7,15	4,76
Gd	28,3	36,65	12,3	16,92	18,04	12,27
Tb	3,74	4,94	1,67	2,27	2,34	1,6
Dy	21,57	28,64	9,44	13,06	13,59	9,22
Ho	3,6	4,63	1,545	2,16	2,26	1,51
Er	8,41	10,82	3,6	4,84	5,41	3,47
Tm	0,977	1,27	0,415	0,564	0,614	0,381
Yb	5,9	7,6	2,34	3,49	3,67	2,33
Lu	0,813	1,071	0,319	0,429	0,478	0,298
Hf	10,78	13,79	6,37	10,49	9,99	7,21
Ta	0,581	1,071	0,471	0,761	0,705	0,493
Pb	0,366	0,364	0,07	0,2	0,29	0,276
Th	0,1058	0,225	0,1065	0,156	0,124	0,0998
U	0,0159	0,0278	0,0168	0,0243	0,023	0,0157

Table A2.6. Continued.

Sample	DH97-37-2				
Grain core/int/rim	1-1e r green	3-1a r	3-1b core greenish	3-1c r	3-1d c/inner
Li	1,281	1,352	1,168	1,423	1,415
Be	1,53	0,977	1,31	0,92	1,22
B	1,29	0,97	1,13	0,93	1,57
P	79,7	76,2	65,26	88,79	171,55
Sc	26,65	63,17	25,96	57,77	28
V	165,73	242,1	169,91	231,82	180,39
Co	9,04	18,27	9,76	18,1	11,48
Ni	2,76	2,89	2,82	3,06	2,94
Ga	10,66	13,11	9,98	12,96	11,81
Rb	0,472	<0.025	0,106	0,091	0,739
Sr	68,43	158,04	81,79	154,53	97,87
Y	81,39	40,15	80,75	48,34	80,44
Zr	482,4	271,74	376,76	252,07	378,08
Nb	4,13	2,88	3,18	2,53	3,68
Cs	<0.0106	<0.0114	0,0127	<0.0108	<0.0097
Ba	1,908	0,086	0,39	0,575	9,19
La	57,83	18,3	53,85	26,47	55,82
Ce	188,42	65,35	182,92	93,24	187,65
Pr	29,71	11,28	28,88	15,67	29,34
Nd	133,74	57,17	130,43	74,87	132,73
Sm	28,45	14,13	28,92	17,85	29,14
Eu	6,82	4,62	7,83	5,35	8,02
Gd	23,63	13,06	23,88	15,44	24,26
Tb	3,41	1,742	3,31	2,096	3,4
Dy	19,18	9,67	18,68	11,79	19,09
Ho	3,45	1,677	3,31	2,015	3,39
Er	8,19	3,87	7,9	4,76	8
Tm	1,09	0,442	0,983	0,564	1,005
Yb	6,8	2,78	6,33	3,29	6,48
Lu	1,035	0,374	0,989	0,462	0,918
Hf	15,3	9,84	11,93	9,68	12,05
Ta	0,801	0,677	0,542	0,541	0,595
Pb	0,362	0,126	0,289	0,115	0,339
Th	0,229	0,211	0,188	0,194	0,264
U	0,0229	0,0193	0,0213	0,0199	0,0409

Table A2.7. Amphibole trace element data

Sample	DH97-39-2					DH97-39-4
Grain core/int/rim	2-1a	2-1b	2-1c	2-1d r	2-3a r	5-1a r
Li	10,33	10,2	9,08	13,96	18,16	4,33
Be	6,98	6,19	4,41	4	3,11	5,84
B	2,18	1,93	1,11	1,39	0,8	0,64
P	57,29	103,37	129,02	184,47	159,76	46,01
Sc	12,82	11,58	10,17	10,01	18,36	14,14
V	59,86	70,96	76,48	75,35	93,37	79,97
Co	13,99	16,14	15,79	16,23	18,7	27,5
Ni	1,078	1,26	1,23	1,33	1,52	5,71
Ga	26,92	30,69	28,72	28,27	19,49	22,02
Rb	3,66	5,85	4,42	5,68	3,73	4,75
Sr	181,9	192,4	200,81	202,77	176,63	169,29
Y	190,37	178,03	164,73	140,38	112,72	165,31
Zr	2305,85	1892,97	1689,11	1505,99	870,72	2485,78
Nb	1234,77	1146,34	1005,58	901,23	605,09	1783,96
Cs	0,041	0,0521	0,0129	0,0148	0,0191	<0.024
Ba	80,46	88,97	94,41	105,38	68,76	28,65
La	152,15	141,71	126,18	110,49	95,07	226,54
Ce	463,87	450,23	410,92	358,26	318,09	561,67
Pr	67,13	64,59	58,43	50,83	45,79	76,72
Nd	272,5	259,49	239,23	213,13	183,44	281,97
Sm	57,21	54,05	50,75	44,45	38,2	51,23
Eu	5,98	5,96	6,27	6,33	6,04	3,71
Gd	45,93	42,61	39,83	35,15	30,07	39,92
Tb	7,1	6,63	6,1	5,36	4,4	6,13
Dy	42,87	39,1	36,01	31,08	25,76	37,66
Ho	8,03	7,36	6,83	5,8	4,69	7,07
Er	20,72	18,75	17,25	14,33	11,39	18,39
Tm	2,81	2,51	2,31	2	1,57	2,52
Yb	18,74	16,24	15	12,39	10,05	16,28
Lu	2,75	2,35	2,06	1,76	1,37	2,3
Hf	58,86	46,39	40,58	38,78	20,73	68,03
Ta	48,45	40,89	36,02	31,15	20,06	79,34
Pb	0,6	0,67	0,64	0,57	0,72	0,8
Th	1,52	1,29	1,14	0,93	0,685	1,75
U	0,237	0,248	0,223	0,197	0,161	0,319

Table A2.7. Continued.

Sample	DH97-39-4					DH97-39-8
Grain core/int/rim	5-1b c	5-1c r	4-1a c	4-1b c	4-1c r	1-2a
Li	5,37	4,88	5,73	5,92	6,07	2,47
Be	7,51	6,52	6,23	8,27	6,57	8,33
B	3,01	1,29	0,44	2,65	0,68	2,12
P	52,99	45,12	49,27	45,63	44,39	1447,7
Sc	14,85	13,6	13,03	12,72	13,38	15,58
V	100,86	97,78	94,39	94,19	102,72	129,41
Co	29,31	31,84	28,21	30,71	31,09	31,41
Ni	5,98	6,93	5,92	6,31	6,52	4,78
Ga	25,55	28,28	25,02	25,77	28,18	24,86
Rb	9,33	6,64	4,8	7,38	5,97	11,3
Sr	192,35	178,01	179,33	169,61	186	161,19
Y	183,08	166,61	159,93	146,35	169,1	121,64
Zr	2481,65	2750,04	2691,95	2439,49	2489,71	2684,67
Nb	1542,16	1591,01	1611,6	1618,16	1545,68	1331,67
Cs	0,266	0,246	0,0441	0,124	0,0192	0,0531
Ba	36,25	29,51	30,73	28,18	32,83	35,04
La	288,98	247,49	233,24	216,62	248,45	168,14
Ce	714,87	610,86	558,72	540,91	641,82	408,27
Pr	93,63	78,29	71,02	66,64	80,13	49,3
Nd	341,38	276,72	257,34	237,45	288,17	177,49
Sm	62,07	49,55	45,98	42,62	51,21	31,75
Eu	4,29	3,49	3,47	3,28	3,73	3,71
Gd	47,1	38,03	35,32	32,27	39,53	25,1
Tb	7,16	5,83	5,54	5,09	6,06	3,76
Dy	43,15	35,42	34,05	31,22	37,04	23,89
Ho	7,99	6,76	6,49	5,95	7,08	4,6
Er	21,07	17,85	17,19	15,5	18,58	12,7
Tm	2,8	2,47	2,39	2,16	2,53	1,8
Yb	17,58	15,86	15,55	14,15	16,15	12,16
Lu	2,53	2,28	2,22	2,02	2,29	1,71
Hf	70,5	62,19	67,59	60,1	59,34	59,7
Ta	66,85	66,54	67,46	63,22	64,47	55,22
Pb	1,04	1,01	0,8	1,01	1,03	1,18
Th	2,98	2,08	2,11	1,84	2,4	3,36
U	0,501	0,428	0,369	0,37	0,455	0,676

Table A2.7. Continued.

Sample	DH97-39-8					DH97-39-9
Grain core/int/rim	1-2b	2-1a r	2-1b r	2-1c r	2-1d r	2-1a c
Li	2,98	3,8	3,27	2,15	1,28	4,27
Be	5,63	4,67	3,8	4,78	6,06	4,46
B	1,54	2,09	0,98	0,47	1,81	1,42
P	67,62	50,36	54,04	54,42	51,03	30,81
Sc	22,26	16,27	19,69	15,5	18,79	15,83
V	144,99	113,81	134,62	139,71	134,43	228,73
Co	25,73	25,83	25,99	29,38	30,82	20,11
Ni	3,79	3,87	3,8	4,33	4,71	1,67
Ga	21,19	23,53	25,13	28,04	27,86	26,48
Rb	4,26	4,41	4,65	5,25	10,14	10,79
Sr	194,38	200,54	240,32	222,66	199,92	263,77
Y	157,71	164,36	179,71	169,87	162,63	43,47
Zr	2598,09	2790,1	2618,85	2561,28	2852,92	1172,29
Nb	1339,97	1568,03	1642,02	1584,78	1762,3	511,33
Cs	<0.022	0,0415	0,0236	0,0271	0,0461	<0.0176
Ba	49,99	55,72	83,11	72,35	56,77	199,35
La	190,74	192,08	214,44	200,38	198,89	86,58
Ce	478,94	502,77	585,77	571,25	548,33	187,9
Pr	61,94	67,78	79,52	76,11	69,44	22,04
Nd	237,75	266,46	321,28	298,15	264,66	75,89
Sm	45,34	51,21	63,71	59,24	50,84	12,71
Eu	4,52	4,91	6,36	6,03	4,81	3,45
Gd	36,73	40,95	50,74	47,18	40,58	10,39
Tb	5,38	6,02	7,29	6,91	5,97	1,472
Dy	33,77	36,82	43,96	42,52	37,03	8,61
Ho	6,39	6,89	7,99	7,75	7,01	1,63
Er	16,54	18,21	20,28	19,91	18,61	4,37
Tm	2,32	2,44	2,67	2,72	2,54	0,627
Yb	15,47	15,81	17,26	17,39	16,45	4,61
Lu	2,15	2,3	2,51	2,5	2,41	0,777
Hf	63,77	66,01	65,38	67,37	69,66	26,55
Ta	56,51	66,85	68,16	70,27	75,4	6,63
Pb	0,76	1,01	1,1	1,28	1,42	1,037
Th	2,87	2,62	2,77	2,73	2,8	0,814
U	0,553	0,428	0,469	0,493	0,542	0,137

Table A2.7. Continued.

Sample	DH97-39-9					TF12-1
Grain	2-1b	2-1c	2-1d	4-1b	4-1a	2-1a
core/int/rim	c	r	r	r	c	c
Li	5,35	7,78	8	6,73	6,06	0,494
Be	4,66	4,26	4,32	5,42	4,66	0,83
B	0,75	1,27	1,04	1,76	1,41	0,67
P	28,96	34,61	37,99	52,19	207,63	115,28
Sc	16,29	16,13	16,24	15,09	15,93	32,43
V	231,31	236,96	230,97	247,58	223,83	319,53
Co	21,03	21,17	23,51	24,86	21,91	29,53
Ni	1,71	1,91	1,97	2,27	1,78	4,51
Ga	26,41	27,68	28,08	32,47	27,25	53,31
Rb	11,41	10,88	10,54	22,72	9,83	3,11
Sr	273,74	265,99	260,54	273,29	272,81	1605,94
Y	42,3	46,11	44,63	39,07	42,67	47,44
Zr	1266,09	1207,24	1222,48	1311,69	1370,76	141,91
Nb	496,33	504,12	491,06	473,17	485,08	108,64
Cs	<0.0134	0,0289	0,0215	0,0557	0,0161	<0.0159
Ba	207,84	197,14	192,11	214,03	196,36	1496,8
La	90,48	88,08	89,78	83,58	94,01	29
Ce	195,71	198,4	204,95	183,22	193,88	99,57
Pr	22,35	23,15	23,44	20,06	21,77	18,52
Nd	76,83	79,95	80,24	68,5	74,61	96,47
Sm	12,54	13,53	13,18	11,36	12,23	22,36
Eu	3,5	3,58	3,44	3,21	3,35	7,63
Gd	10,23	10,9	10,66	9,3	10,26	19,27
Tb	1,425	1,492	1,462	1,278	1,407	2,44
Dy	8,49	9,05	8,82	7,41	8,33	13,43
Ho	1,588	1,687	1,624	1,415	1,554	2,18
Er	4,3	4,43	4,39	3,84	4,14	4,86
Tm	0,601	0,638	0,618	0,549	0,607	0,53
Yb	4,52	4,65	4,37	4,03	4,29	2,98
Lu	0,752	0,784	0,731	0,713	0,738	0,377
Hf	27,96	25,51	25,73	26,87	29,1	5,55
Ta	6,1	6,43	6,34	5,14	5,8	6,88
Pb	1,26	1,15	1,21	1,46	1,015	0,408
Th	0,956	0,843	0,877	0,893	1,123	0,1244
U	0,166	0,172	0,169	0,186	0,166	0,0181

Table A2.7. Continued.

Sample	TF12-1					
Grain core/int/rim	2-1b r	2-1c r	2-2a c	2-2b c	3-1a c	3-1b c
Li	0,513	0,49	0,453	0,565	0,487	0,558
Be	0,76	0,8	0,71	0,75	0,88	0,9
B	0,54<0.45	<0.45		0,45	0,48	0,59
P	119,89	128,58	122,83	128,28	126,67	127,33
Sc	34,37	34,43	35,02	34,01	35,71	32,9
V	324,77	318,41	319,79	327,72	320,8	318,98
Co	30,62	29,11	29,24	32,18	28,86	27,17
Ni	4,54	4,31	4,17	4,54	4,27	4,42
Ga	42,54	43,74	39,88	46,89	43,05	39,5
Rb	3,47	3,14	3,32	3,42	3,02	2,72
Sr	1594,66	1619,33	1738,72	1535,16	1609,97	1491,75
Y	41,49	42,05	39,82	37,97	38,44	36,65
Zr	126,94	132,16	130,37	119,47	124,77	114,8
Nb	88,79	83,06	76,92	83	76,98	74,12
Cs	<0.0141	<0.0181	<0.0181	<0.0141	<0.0180	<0.0137
Ba	1260,49	1116,11	1069,77	1241,72	1064,93	868,33
La	23,23	22,36	20,98	22,32	21,17	17,69
Ce	85,11	79,01	73,48	81,72	72,89	65,03
Pr	15,76	14,45	13,81	14,55	13,48	11,67
Nd	81,65	75,76	74,83	74,99	71,14	61,62
Sm	19,95	18,55	18,39	17,54	17,16	15,28
Eu	6,83	6,39	6,4	6,12	5,86	5,11
Gd	16,7	15,98	16,34	15,05	15,11	12,92
Tb	2,116	2,055	2,07	1,88	1,907	1,61
Dy	11,89	11,5	11,73	10,78	10,8	9,15
Ho	1,97	1,95	1,93	1,7	1,78	1,55
Er	4,41	4,33	4,25	3,88	4,13	3,47
Tm	0,481	0,483	0,493	0,418	0,463	0,372
Yb	2,73	2,83	2,86	2,43	2,77	2,19
Lu	0,352	0,338	0,357	0,287	0,333	0,272
Hf	5,02	4,8	5,18	4,48	4,88	3,9
Ta	5,69	5,17	5,09	4,95	4,81	4,07
Pb	0,496	0,378	0,44	0,43	0,367	0,294
Th	0,1077	0,105	0,13	0,0974	0,1097	0,0917
U	0,0186	0,0191	0,0245	0,0189	0,0117	0,0113

Table A2.7. Continued.

Sample	TF12-2					
Grain core/int/rim	3-1a	3-1b c	3-1c c	2-1a	2-1b c	2-1c c
Li	9,62	9,16	13,98	7,21	11,11	9,87
Be	1,56	1,33	1,39	1,35	1,28	1,32
B	0,37	0,56	0,55	0,9	0,94	1,05
P	112,04	112,25	116,46	114,46	113,29	121,66
Sc	20,92	22,06	19,71	22,49	21,96	21,87
V	157,59	170,42	161,72	170,95	175,76	181,53
Co	10,79	12,77	11,32	12,73	12,76	14,27
Ni	0,494	0,6	0,658	0,495	0,565	0,567
Ga	37,53	37,67	39,22	37,18	36,59	38,67
Rb	2,95	3,01	3,14	2,83	2,86	3,23
Sr	1180,15	1164,33	1108,77	1119,63	1107,13	1116,54
Y	76,05	76,41	74,04	71,49	68,81	70,16
Zr	237,86	239,97	226,94	223,33	216,46	216,74
Nb	158,25	160,11	154,87	148,37	148,63	149,42
Cs	<0.0132	0,0167	<0.0105	<0.0183	<0.0104	0,0117
Ba	694,38	695,09	661,96	640,22	629,11	655,99
La	38,8	40,05	37,08	35,54	34,78	35,19
Ce	124,5	130,52	120,66	115,9	114,46	120,89
Pr	22,6	22,93	20,87	20,5	19,96	20,72
Nd	115,64	119,29	106,58	105,72	103,01	107,01
Sm	27,74	28,86	26,12	26,08	25,2	25,44
Eu	9,12	9,48	8,51	8,38	8,24	8,41
Gd	24,87	25,35	23,01	22,93	22,42	22,53
Tb	3,33	3,41	3,08	3,02	2,95	3,03
Dy	19,05	19,6	17,91	17,35	16,89	17,14
Ho	3,35	3,43	3,12	3,01	2,91	2,96
Er	7,77	8,08	7,31	7,18	6,91	6,93
Tm	0,921	0,94	0,847	0,826	0,808	0,817
Yb	5,34	5,46	5,15	4,75	4,65	4,79
Lu	0,743	0,756	0,697	0,628	0,627	0,616
Hf	9	9,17	7,73	7,79	7,41	7,48
Ta	7,89	8,2	7,11	6,83	7,16	6,88
Pb	0,518	0,497	0,556	0,418	0,466	0,518
Th	0,18	0,204	0,175	0,162	0,158	0,155
U	0,0264	0,0346	0,0316	0,026	0,0292	0,032

Table A2.7. Continued.

Sample	TF12-2	
Grain core/int/rim	1-1a	1-1b c
Li	7,82	8,84
Be	1,56	1,5
B	0,6	0,83
P	96,56	104,12
Sc	18,22	17,94
V	159,11	168,8
Co	12,16	13,02
Ni	0,546	0,589
Ga	40,35	42,18
Rb	2,95	3,17
Sr	1047,35	1031,62
Y	78,06	75,5
Zr	256,99	250,3
Nb	179,68	180,39
Cs	<0.0123	<0.0110
Ba	691,51	695,39
La	44,07	43,78
Ce	146,71	149,53
Pr	25,03	24,77
Nd	124,97	124,56
Sm	29,59	29,06
Eu	9,65	9,7
Gd	25,19	24,9
Tb	3,38	3,35
Dy	19,6	19,13
Ho	3,41	3,34
Er	8,1	7,83
Tm	0,948	0,917
Yb	5,64	5,5
Lu	0,755	0,731
Hf	9,43	9,1
Ta	8,37	8,23
Pb	0,512	0,59
Th	0,191	0,18
U	0,0359	0,0309

Table A2.8. Whole rock major and trace element data.

Unit	El Abrigo					
Sample	**DH97-38a**	**DH97-38d**	**DH97-38e**	**DH97-38f**	**DH97-38b**	**DH97-38c**
SiO2	60,26	60,57	61,05	60,56	60,44	60,54
TiO2	0,67	0,72	0,75	0,72	0,67	0,72
Al2O3	19,24	18,85	19,35	19,34	19,47	19,59
FeO	3,45	3,63	3,16	2,91	3,54	3,32
MnO	0,270	0,242	0,237	0,251	0,243	0,214
MgO	0,48	0,17	0,41	0,30	0,45	0,50
CaO	0,68	0,56	0,74	0,58	0,62	0,74
Na2O	9,51	9,71	8,59	9,70	9,05	8,65
K2O	5,43	5,51	5,63	5,59	5,48	5,65
P2O5	0,027	0,033	0,081	0,044	0,032	0,074
SUM	100,00	100,00	100,00	100,00	100,00	100,00
mg#	24,80	10,09	23,68	19,79	23,20	26,30
XRF traces						
Ni	6	7	7	7	4	6
Cr	2	2	3	0	1	0
Sc	1	1	2	3	0	3
V	49	44	45	34	41	44
Rb	203	205	173	193	204	174
Sr	34	26	34	22	50	64
Zr	1513	1455	1165	1157	1434	1045
Y	58	37	46	64	47	42
Nb	447	427	332	340	402	308
Ga	38	35	34	33	35	31
Cu	0	4	0	1	0	0
Zn	156	64	59	89	100	53
ICP-MS traces						
La	199	142,27	165,43	207,14	153	154
Ce	304	219,62	268,49	321,09	235	255
Pr	25,9	18,81	22,91	27,59	20,0	22,3
Nd	77,6	53,94	68,90	84,68	57,6	67,5
Sm	12,23	7,43	10,78	13,89	8,66	10,67
Eu	2,00	1,15	1,73	2,23	1,47	1,72
Gd	8,99	5,42	8,34	10,97	6,62	7,38
Tb	1,77	0,99	1,43	1,85	1,28	1,32
Dy	11,31	5,94	8,49	10,89	8,19	7,97
Ho	2,48	1,29	1,72	2,21	1,77	1,59
Er	7,38	3,79	4,86	6,11	5,26	4,53
Tm	1,20	0,65	0,76	0,92	0,88	0,70
Yb	7,63	4,53	4,88	5,79	5,85	4,65
Lu	1,18	0,75	0,78	0,87	0,93	0,72
Ba	38	29	71	29	64	42
Th	29,5	23,30	27,94	33,27	24,4	24,4
Nb	465	414,79	338,28	346,42	398	307
Y	65,5	35,34	47,59	66,79	48,0	42,3
Hf	34,3	30,32	25,56	26,29	29,8	22,5
Ta	23,69	22,05	19,10	18,90	19,63	18,33
U	11,03	9,06	7,48	7,55	10,00	6,97
Pb	21,49	17,11	13,35	15,69	15,10	11,88
Rb	203	199,0	169,9	191,7	202	173
Cs	3,40	2,09	1,10	2,40	2,01	1,37
Sr	34	25	35	22	50	64
Sc	1,6	1,0	1,1	0,9	1,4	0,9

Table A2.8. Continued.

Unit	Bandas del Sur			(Gabbro)	DH evolved	
Sample	**DH97-33d(i)**	**DH97-33d(iii)**	**DH97-33d(ii)**	**DH97-37**	**DH97-22d**	**DH97-2e**
SiO2	57,52	58,56	61,35	45,99	57,35	58,91
TiO2	0,33	0,41	0,70	4,18	0,93	0,62
Al2O3	20,94	22,03	18,84	17,43	20,35	21,08
FeO	4,23	2,72	2,81	10,78	3,74	3,03
MnO	0,241	0,218	0,186	0,187	0,176	0,181
MgO	0,81	0,27	0,50	4,51	0,71	0,44
CaO	2,99	0,82	3,01	10,12	2,03	1,29
Na2O	6,73	8,94	6,81	3,31	8,98	8,87
K2O	6,13	5,99	5,68	1,82	5,55	5,48
P2O5	0,072	0,049	0,103	†1,67	0,180	0,108
SUM	100,00	100,00	100,00	100,00	100,00	100,00
mg#	31,37	19,26	29,94	49,86	31,19	25,54
XRF traces						
Ni	4	10	7	0	8	7
Cr	1	0	2	9	1	3
Sc	0	2	2	23	7	3
V	19	21	37	306	60	35
Rb	317	†333	151	41	191	191
Sr	111	58	81	1312	287	144
Zr	3443	3018	902	345	1089	1034
Y	50	38	44	40	32	33
Nb	636	400	219	101	231	238
Ga	56	†47	26	22	32	33
Cu	25	0	0	2	1	1
Zn	118	164	56	118	115	118
ICP-MS traces						
La	181	107,75	128	88,85	105,64	113,35
Ce	186	114,28	204	167,83	151,73	153,32
Pr	11,3	7,18	19,3	19,64	12,71	12,35
Nd	27,9	18,21	65,0	81,18	39,82	36,68
Sm	4,01	2,70	10,89	16,47	6,70	5,73
Eu	0,84	0,58	2,67	5,10	1,78	1,30
Gd	3,26	2,44	8,08	13,72	5,35	4,83
Tb	0,69	0,49	1,37	1,91	0,87	0,80
Dy	5,26	3,63	7,96	9,46	5,01	4,81
Ho	1,40	0,93	1,56	1,62	1,04	0,99
Er	5,70	3,42	4,34	3,83	3,04	3,02
Tm	1,22	0,67	0,65	0,47	0,49	0,51
Yb	9,88	5,20	4,01	2,61	3,39	3,45
Lu	1,71	0,90	0,61	0,39	0,55	0,59
Ba	43	24	333	728	472	189
Th	117,9	65,54	18,4	5,90	31,03	30,18
Nb	654	376,20	215	96,61	226,11	229,57
Y	50,7	30,88	44,4	44,01	30,71	31,03
Hf	63,5	55,22	17,4	6,37	21,43	20,18
Ta	12,62	8,70	13,50	6,21	9,50	9,68
U	35,95	16,55	38,37	3,09	8,90	8,53
Pb	29,79	31,36	6,68	3,93	16,33	17,99
Rb	314	317,6	139	44,7	185,5	180,8
Cs	5,70	7,03	0,65	0,38	2,53	2,50
Sr	106	52	79	1379	271	142
Sc	2,0	1,5	0,9	16,6	3,0	1,8

Table A2.8. Continued.

Unit	DH evolved				DH-mafic	
Sample	**DH97-2d**	**DH97-4a**	**DH97-5a**	**DH97-9b**	**DH97-12**	**DH97-7**
SiO2	57,70	56,55	60,96	60,96	43,35	47,62
TiO2	1,24	1,67	0,54	0,56	4,00	†3,23
Al2O3	19,87	19,47	21,63	20,75	16,32	16,34
FeO	3,93	5,15	2,61	2,73	11,52	11,14
MnO	0,164	0,175	0,166	0,159	0,19	0,205
MgO	1,11	1,63	0,36	0,42	5,36	5,56
CaO	2,96	3,72	1,16	1,18	11,01	9,36
Na2O	7,88	6,49	5,79	6,92	3,47	4,02
K2O	4,86	4,73	6,69	6,22	1,50	1,68
P2O5	0,301	0,417	0,082	0,085	1,06	†0,84
SUM	100,00	100,00	100,00	100,00	97,78	100,00
mg#	40,19	42,86	24,89	26,88	52,52	†54,26
XRF traces						
Ni	6	5	8	9	33	55
Cr	8	9	0	3	103	113
Sc	6	8	6	4		22
V	86	112	31	38	287	236
Rb	122	113	190	177		35
Sr	491	567	89	91		†1032
Zr	663	622	919	815	270	392
Y	36	42	20	20		35
Nb	195	200	180	159	88	108,3
Ga	28	25	32	30		25
Cu	0	0	1	2	53	23
Zn	99	108	101	98	87	125
ICP-MS traces						
La	113,26	115,32	89,03	84,67	66	79,23
Ce	183,58	200,22	101,26	107,35	135	154,05
Pr	18,34	20,35	7,69	7,61	16,3	16,64
Nd	62,46	73,87	20,90	20,82	67	65,28
Sm	10,98	13,20	3,04	3,04	13	12,89
Eu	3,00	3,67	0,71	0,72	4,16	4,11
Gd	9,06	10,80	2,63	2,35	10	11,18
Tb	1,34	1,62	0,43	0,39	1,5	1,60
Dy	7,16	8,57	2,57	2,49	7,3	8,07
Ho	1,37	1,60	0,58	0,55	1,3	1,45
Er	3,53	3,98	1,82	1,77	3,3	3,40
Tm	0,51	0,56	0,33	0,32	0,41	0,43
Yb	3,09	3,22	2,44	2,25	2,3	2,54
Lu	0,49	0,49	0,41	0,40	0,31	0,38
Ba	858	875	137	242	537	537
Th	17,96	16,35	27,75	21,90	5,1	7,88
Nb	196,37	191,82	166,26	153,97	88	108,35
Y	37,79	42,20	18,43	17,67	36	36,44
Hf	13,78	13,00	16,85	15,52	6,4	9,26
Ta	11,39	12,17	5,48	5,32	5,27	6,96
U	4,93	4,61	7,72	6,23	1,2	2,04
Pb	12,11	10,81	17,42	15,29	-5	4,39
Rb	124,6	105,5	177,4	172,6	32	37,6
Cs	1,51	1,24	2,18	2,08	-0,5	0,42
Sr	494	582	95	90	1271	1012
Sc	3,2	5,3	1,1	1,3		17,3

Table A2.8. Continued.

Unit	DH-mafic					
Sample	**DH97-13A**	**DH97-13B**	**DH97-17**	**DH97-18A**	**DH97-18B**	**DH97-18C**
SiO2	43,68	43,59	43,76	44,66	44,81	45,29
TiO2	4,02	4,00	4,04	3,21	3,36	3,58
Al2O3	16,37	16,31	16,48	14,89	15,62	16,83
FeO	11,52	11,54	11,60	11,56	11,19	10,74
MnO	0,19	0,19	0,19	0,20	0,20	0,21
MgO	5,41	5,47	5,39	8,81	7,15	4,84
CaO	11,09	11,07	10,95	9,64	9,75	9,80
Na2O	3,85	3,84	3,56	3,69	4,07	4,43
K2O	1,49	1,47	1,38	1,38	1,47	1,68
P2O5	1,06	1,06	1,05	0,85	0,94	1,08
SUM	98,68	98,54	98,40	98,89	98,56	98,48
mg#	52,75	52,98	52,48	64,42	60,29	51,71
XRF traces						
Ni	39	36	28	157	88	10
Cr	71	54	55	350	271	47
Sc						
V	292	275	278	237	231	221
Rb						
Sr						
Zr	270	236	272	270	249	260
Y						
Nb	90	83	90	92	93	102
Ga						
Cu	55	47	53	57	47	27
Zn	91	77	91	108	85	27
ICP-MS traces						
La	66	62	66	66	69	78
Ce	134	127	135	131	138	153
Pr	16,2	15,3	16,3	15,4	16,4	18,2
Nd	67	63	66	63	67	74
Sm	13	12	13	12	13	14
Eu	4,16	3,97	4,16	3,84	4,07	4,41
Gd	10	9,8	10	9,3	9,8	11
Tb	1,5	1,4	1,5	1,4	1,5	1,6
Dy	7,3	7	7,5	6,7	7,1	7,7
Ho	1,3	1,2	1,3	1,2	1,2	1,3
Er	3,3	3,1	3,3	3,1	3,2	3,5
Tm	0,41	0,38	0,41	0,39	0,39	0,44
Yb	2,3	2,1	2,3	2,2	2,2	2,4
Lu	0,3	0,29	0,32	0,3	0,31	0,35
Ba	548	505	538	556	605	643
Th	5,1	4,8	5,2	5,3	5,2	5,6
Nb	90	83	90	92	93	102
Y	36	34	36	33	35	38
Hf	6,3	5,6	6,4	6,2	5,8	6,1
Ta	5,31	4,98	5,27	5,43	5,6	6,38
U	1,2	1,2	1,3	1,3	1,3	1,4
Pb	-5	-5	-5	-5	-5	-5
Rb	32	31	31	31	31	36
Cs	-0,5	-0,5	-0,5	-0,5	-0,5	-0,5
Sr	1319	1215	1277	1101	1202	1291
Sc						

Table A2.8. Continued.

Unit	DH-mafic					
Sample	**DH97-19A**	**DH97-19B**	**DH97-20**	**DH97-28A**	**DH97-28B**	**DH97-29A**
SiO2	50,28	50,33	42,82	44,45	44,75	43,37
TiO2	2,43	2,41	4,09	4,04	3,61	3,88
Al2O3	17,1	16,95	15,86	16,16	15,66	14,77
FeO	8,13	8,06	11,91	12,36	10,88	11,40
MnO	0,18	0,18	0,20	0,214	0,19	0,19
MgO	4,93	4,84	5,67	4,86	6,02	6,64
CaO	7,05	7,07	11,18	10,46	10,36	11,55
Na2O	5,69	5,49	4,00	4,19	4,15	3,93
K2O	2,11	2,92	1,55	1,80	1,67	1,53
P2O5	0,47	0,46	1,18	1,47	0,99	0,87
SUM	98,37	98,71	98,46		98,28	98,13
mg#	59,05	58,79	53,08	48,29	56,81	58,06
XRF traces						
Ni	80	64	22	0	48	75
Cr	158	164	41	8	157	165
Sc				16		
V	173	173	284	278	267	315
Rb				39		
Sr				1256		
Zr	558	545	298	380	323	295
Y				38		
Nb	162	160	106	116	100	92
Ga				26		
Cu	41	45	54	11	57	72
Zn	108	103	106	128	104	99
ICP-MS traces						
La	91	89	78	78,34	74	66
Ce	155	154	156	155,76	146	131
Pr	15,7	15,6	18,3	17,60	17,1	15,7
Nd	55	55	74	72,32	68	62
Sm	9,7	9,5	14	15,11	13	12
Eu	2,84	2,78	4,39	4,70	4,08	3,84
Gd	7,5	7,4	11	12,65	11	9,7
Tb	1,2	1,2	1,6	1,75	1,6	1,4
Dy	6,2	6,1	7,9	8,84	7,6	7,1
Ho	1,1	1,1	1,4	1,52	1,3	1,2
Er	3,3	3,2	3,6	3,54	3,4	3,2
Tm	0,47	0,48	0,44	0,44	0,44	0,4
Yb	2,9	2,8	2,5	2,46	2,4	2,3
Lu	0,41	0,41	0,35	0,34	0,33	0,31
Ba	449	453	588	523	574	533
Th	13	13	6,3	6,20	6,7	6,1
Nb	162	160	106	107,02	100	92
Y	34	34	38	37,68	36	34
Hf	12	12	7	8,25	7,5	7
Ta	8,73	8,85	6,13	6,93	5,86	5,45
U	3,3	3,2	1,4	1,62	1,6	1,6
Pb	8	8	-5	3,64	-5	-5
Rb	52	79	36	38,7	38	36
Cs	0,9	0,8	-0,5	0,57	-0,5	-0,5
Sr	647	698	1331	1181	1145	1044
Sc				14,3		

Table A2.8. Continued.

Unit	DH-mafic		
Sample	**DH97-29B**	**DH97-30A**	**DH97-30B**
SiO2	43,94	44,43	43,68
TiO2	3,78	3,74	3,95
Al2O3	15,71	15,75	14,67
FeO	10,97	10,80	11,66
MnO	0,19	0,19	0,19
MgO	6,09	6,04	6,88
CaO	10,79	10,78	11,62
Na2O	4,01	4,19	3,72
K2O	1,11	1,86	1,56
P2O5	0,98	1	0,84
SUM	97,57	98,78	98,77
mg#	56,89	57,07	58,37
XRF traces			
Ni	58	52	10
Cr	139	117	184
Sc			
V	284	279	320
Rb			
Sr			
Zr	336	333	269
Y			
Nb	107	106	94
Ga			
Cu	58	56	68
Zn	104	102	76
ICP-MS traces			
La	76	76	60
Ce	150	150	144
Pr	17,6	17,4	14,6
Nd	69	69	60
Sm	13	13	12
Eu	4,11	4,07	3,69
Gd	10	10	8,7
Tb	1,5	1,5	1,3
Dy	7,5	7,4	6,8
Ho	1,3	1,3	1,2
Er	3,4	3,4	3
Tm	0,42	0,43	0,37
Yb	2,4	2,4	2
Lu	0,34	0,33	0,28
Ba	610	612	500
Th	7,5	7,5	5,7
Nb	107	106	94
Y	36	36	33
Hf	7,6	7,6	6,3
Ta	6,33	6,38	4,96
U	2	1,8	1,4
Pb	-5	5	-5
Rb	46	46	32
Cs	0,5	-0,5	-0,5
Sr	1208	1199	936
Sc			

Acknowledgements

I particularly would like to thank my trusted professor, Dr. Else-Ragnhild Neumann for being an excellent supervisor during my work on this thesis. Without her guidance, I would never have learned the meaning and mechanics behind the most difficult words of all – 'shallow level processes'. Her patience, easy-going nature and encouraging support have saved my day far too many times to be counted.

Thanks to the friendly staff at GEMOC, Macquarie University, Sydney, Australia, for all their help and making my stay run smoothly during the analytical part of the thesis, especially Dr. Norm Pearson for his help and hints when times were hard using the microprobe.

A special thanks to my wife, Sissel, who has taken care of me through times of great ordeals, and for pushing me to finally finish this thesis. Without her kindly support, I do not think it would have been possible. My now two-year-old son, Simon, also deserves a big hug, for in his own way, I would like to think, cheering me along.

My parents deserve the utmost recognition. Although I suspect no one of them actually never quite knew what I was studying, they have supported me – in all ways possible – during these long years.

References

Ablay, G.J., Carrol, M.R., Palmer, M.R., Martí, J. & Sparks, R.J.S., 1998. Basanite-phonolite lineages of the Teide-Pico Viejo volcanic complex, Tenerife, Canary Islands. In: Davidson, J.P. & Bohrson, W.A. (eds.). Shallow level processes in oceanic island magmatism.
Journal of Petrology **39**, 905-936.

Adam, J. & Green, T.H., 1994. The effects of pressure on the partitioning of Ti, Sr and REE between amphibole, clinopyroxene and basanitic melts.
Chemical Geology **117**, 219-233.

Ancochea, E., Fúster, J.M., Ibarrola, E., Cendrero, A., Coello, J., Hernan, F., Cantagrel, J.M. & Jamond, C., 1990. Volcanic evolution of the island Tenerife (Canary Islands) in the light of new K-Ar data.
Journal of Volcanology and Geothermal Resarch **44**, 231-249.

Borley, G.D., Suddaby, P. & Scott, P., 1971. Some xenoliths from the alkalc rocks of Tenerife, Canary Islands.
Contributions to Mineralogy and Petrology **31**, 102-114.

Borley, G.D., 1974. Aspects of the volcanic history and petrology of the island Tenerife, Canary Islands.
Proceedings of the Geologists' Association **85**, 259-279.

Colson, R.O., McKay, G.A. & Taylor, L.A., 1989. Charge balancing trivalent trace elements in olivine and low-Ca pyroxene: A test using experimentalpartitioning data.
Geochimica et Cosmochimica Acta **53**, 643-648.

Cox, K.G., Bell, J.D. & Pankhurst, R.J., 1979. The interpretation of igneous rocks.
London: George Allen & Unwin, 450 pp.

Dostal, J., Dupuy, C., Carron, J.P., Le Guen de Kerneizon, M. & Maury, R., 1983. Partition coefficients of trace element application to volcanic rocks of St. Vincent, West Indies.
Geochimica et Cosmochimica Acta **47**, 525-533.

Dunn, T. & Sen, C., 1994. Mineral/Matrix Partition-Coefficients for Ortho-Pyroxene, Plagioclase, and Olivine in Basaltic to Andesitic Systems - a Combined Analytical and Experimental-Study.
Geochimica et Cosmochimica Acta **58**, 717-733.

Edgar, C.J., Wolff, J.A., Nichols, H.J., Cas, R.A.F. & Martí, J., 2002. A complex Quarternary ignimbrite-forming phonolitic eruption: the Poris Member of the Diego Hernández Formation (Tenerife, Canary Islands).
Journal of Volcanology and Geothermal Resarch **118**, 99-130.

Foley, S.F., Jackson, B.J., Greenough, J.D. & Jenner, G.A., 1996. Trace element partition coefficients from clinopyroxene and phlogopite in an alkaline lamprphyre from Newfoundland by LAM-ICP-MS.
Geochimica et Cosmochimica Acta **60**, 629-638.

Forsythe, L.M., Nielsen, R.L. & Fisk, M.R., 1994. High-Field-Strength Element Partitioning between Pyroxene and Basaltic to Dacitic Magmas.
Chemical Geology **117**, 107-125.

Francalancini, L., 1989. Trace element partition coefficients for minerals in shoshonite and calc-alkaline rocks from Stromboli Island.
Jahrbuch für Mineralogie, Abhandlungen **160**, 229-247.

Fujimaki, H., Tatsumoto, M. & Aoki, K.-I., 1984. Partition coefficients of Hf, Zr, and REE between phenocrysts and groundmasses.
Journal of Geophysical Research **89**, 662-672.

Fujimaki, H., 1986. Partition-Coefficients of Hf, Zr, and Ree between Zircon, Apatite, and Liquid.
Contributions to Mineralogy and Petrology **94**, 42-45.

Fúster, J.M., Araña, V., Brandle, J.L., Navarro, M., Alonso, U. & Aparicio, A., 1968. Geología y volcanología de las islas Canarias: Tenerife.
Madrid: Institutio "Lucas Mallada", CSIC, 218 pp.

Fúster, J. M., Ibarrola, E., Snelling, N., Cantagrel, J.M., Huertas, M., Coello, J. & Ancochea, E., 1994. Cronología K-Ar de la formación Cañadas en el sector Suroeste de Tenerife: implicaciones de los episodios piroclásticos en la evolución volcánica.
Sociedad Española de Historia Natural, Madrid, Boletin, Seccion Geologica **89**, 25-41.

Gaetani, G.A. & Groove, T.L., 1991. Partitioning of Ce and Yb between pyroxene and basaltic to andesitic melts: Influence of mineral chemistry vs. melt structure.
EOS **72**, 547-548 (abstract).

Gaetani, G.A. & Grove, T.L., 1995. Partitioning of rare earth elements between clinopyroxene and silicate melt: Crystal-chemical controls.
Geochimica et Cosmochimica Acta **59**, 1951-1962.

Gallahan, W.E. & Nielsen, R.L., 1992. The partitioning of Sc, Y and the rare earth elements between high-Ca clinopyroxene and natural mafic to intermediate lavas at 1 atmosphere.
Geochimica et Cosmochimica Acta **56**, 2387-2404.

Green, T.H. & Pearson, N.J., 1985. Rare earth partitioning between clinopyroxene and silicate liquid at moderate to high pressure.
Contributions to Mineralogy and Petrology **91**, 24-36.

Green, T.H. & Pearson, N.J., 1987. An experimental study of Nb and Ta partitioning between Ti-rich minerals and silicate liquids at high temperature and pressure.
Geochimica et Cosmochimica Acta **51**, 55-62.

Grove, T.L., Konzler, R.J. & Bartels, K.S., 1989. Effects on pressure on alumina substitution in igneous augite: an empirical barometer.
EOS Transactions, American Geophysical Union **24**, 1401-1402.

Grutzeck, M., Kridelbach, S. & Weill, D., 1974. The distribution of Sr and REE between diopside and silicate liquid.
Geophysical Research Letters **1**, 273-275.

Hauri, E.H., Wagner, T.P. & Groove, T.L., 1994. Experimental and natural partitioning of Th, U, Pb and other trace elements between garnet, clinopyroxene and basaltic melts.
Chemical Geology **117**, 149-166.

Holik, J.S. & Rabinowitz, P.D., 1992. Structural and tectonic evolution of oceanic crust within the Jurassic quiet zone, offshore Marocco. In: Watkins, J.S., Zhiqiang, F. & McMillen, K.J. (eds). Geology and geophysics of continental margins.
American Association of Petroleum Geologists Memoirs **53**, 259-282.

Jensen, B.B., 1973. Patterns of trace element partitioning.
Geochimica et Cosmochimica Acta **37**, 2227-2242.

Johnson, D.M., Hooper, P.R. & Conrey, R.M., 1999. XRF analysis of rocks and minerals for major and trace elements on single low dilution Li-tetraborate fused bead.
Advances in X-ray Analysis **41**, 843-867.

Kesson, S. & Price, R.C., 1972. The major and trace element chemistry of kaersutite and its bearing on the petrogenesis of alkaline rocks.
Contributions to Mineralogy and Petrology **35**, 119-124.

Knaack, C., Cornelius, S. & Hooper, P.R., 1994. Trace element analysis of rocks and minerals by ICP-MS.
Washington State University, Department of Geology, Open File Report.

Le Bas, M.J., Le Maitre, R.W., Streckeisen, A. & Sanettin, B., 1986. A chemical classification of volcanic rocks base don the total alkali-silica diagram.
Journal of Petrology **27**, 745-750.

Leeman, W.P., 1978. Distribution of Mg^{2+} between olivine and silicate melt, and its implications regarding melt structure.
Geochemica et Cosmochimica Acta **42**, 789-800.

Le Maitre, R.W., 1989. A classification of igneous rocks and glossary of terms.
Oxford: Blackwell Scientific Publications, 192 pp.

Mahood, G.A. & Hildreth, E.W., 1983. Large partition coefficients for trace elements in silica-high rhyolites.
Geochemica et Cosmochimica Acta **47**, 11-30.

McDonough, W.F. & Sun, S.-s., 1995. The composition of the Earth.
Chemical Geology **120**, 223-253.

McKenzie, D. & O'Nions, R.K., 1991. Partial melt distributions from inversion of rare Earth element concentrations.
Journal of Petrology **32**, 1021-1091.

Martí, J. & Villa, I.M., 1990. Stratigraphy and K-Ar ages of the Diego Hernández wall and their significance to the las Cañadas caldera formation (Tenerife, Canary Islands).
Terra Nova **2**, 148-153.

Martí, J., Mitjavila, J. & Araña, V., 1994. Stratigraphy, strucure and geochronolgy of the Las Cañadas caldera (Tenerife, Canary Islands).
Geological Magazine **131**, 715-727.

Martí, J., Mitjavila, J. & Araña, V., 1995. The Las Cañadas edifice and caldera. In: Martí, J. & Mitjavila, J. (eds.). A field guide to the Central Complex of Tenerife (Canary Islands).
Serie Casa los Volcanos, **4**, 19-38.

Martí, J., Hürlimann, M., Ablay, G.J. & Gudmundsson, A., 1997. Vertical and laterl collapses on Tenerife (Canary Islands) and other volcanic ocean islands.
Geology **25**, 879-882.

Matsui, W.P., Onuma, N., Nagasawa, H., Higuchi, H. & Banno, S., 1977. Crystal structure control in trace element partitioning between crystal and magma.
Bulletin de ls Société Française de Minéralogie et de Cristallographie **100**, 315-324.

McKay, G., Wagstaff, J. & Yang, S.-R., 1986. Clinopyroxene REE distribution coefficients for shergottites: The REE content of the Shergotty melt
Geochimica et Cosmochimica Acta **50**, 927-937.

Mitjavila, J. & Villa, I.M., 1993. Temporal evolution of the Diego Hernàndez Formation (Las Cañadas, Tenerife) and confirmation of the age of the caldera using the $^{40}Ar/^{39}Ar$ method.
Revista de la Sociedad Geologica de España **6**, 61-65.

Morgan, M.J., 1972. Plate motions and deep mantle convection plumes.
Geological Society of America Memoirs **132**, 7-22.

Nabelek, P.I., 1980. Nickel partitioning between olivine and liquid in natural basalts: Henry's Law behavior.
Earth and Planetary Science Letters **48**, 293-302.

Nagasawa, H., 1973. Rare-Earth distribution in alkali rocks from Oki-Dogo Island, Japan.
Contributions to Mineralogy and Petrology **39**, 301-308.

Nash, W.P. & Crecraft, H.R., 1985. Partition coefficients for trace elements in silicic magmas.
Geochimica et Cosmochimica Acta **49**, 2309-2322.

Nernst, W., 1891. Verteilung eines Stoffes zwischen zwei Lösungsmitteln unt zwischen Lösungsmitteln unt Dampfraum.
Zeitschrift für Physikalische Chemie **8**, 110-139.

Neumann, E.-R., Wulff-Pedersen, E., Simonsen, S.L., Pearson, N.J., Mitjavila, J. & Martí, J., 1999. Evidence for fractional crystallization of periodically refilled magma chambers in Tenerife, Canary Islands.
Journal of Petrology **40**, 1089-1123.

Neumann, E.-R., Wulff-Pedersen, E., Pearson, N.J. & Spencer, E.A., 2002. Mantle xenoliths from Tenerife (Canary Islands): Evidence for reactions between mantle peridotites and silicic arbonatite melts inducing Ca metasomatism.
Journal of Petrology **42**, 825-857.

Neumann, E.-R., Griffin, W.L., Pearson, N.J. & O'Reilly, S.Y., 2004. The evolution of the upper mantle beneath the Canary Islands: Information from trace elements and Sr isotope ratios in minerals in mantle xenoliths.
Journal of Petrology **45**, 2573-2612.

Nicholls, I.A. & Harris, K.L., 1980. Experimental rare earth element partition coefficients for garnet, clinopyroxene and amphibole co-existing with andesitic and basaltic liquids.
Geochimica et Cosmochimica Acta **44**, 287-308.

Norman, M.D., Pearson, N.J., Sharma, A. & Griffin, W.L., 1996. Quantitative analysis of trace elements in geological materials by laser ablation ICPMS: instrumental operating conditions and calibration values of NIST glasses.
Geostandards Newsletter **20**, 247-261.

O'Hara, M.J., 1977. Geochemical evolution during fractional crystallisation of a periodically refilled magma chamber .
Nature **243**, 503-508.

Onuma, N., Higichi, H., Wakita, H. & Nagasawa, H., 1968. Trace element partitioning between two pyroxenes and and the host lava.
Earth and Planetary Science Letters **5**, 47-51.

Onuma, N., Ninomiya, S. & Nagasawa, H., 1981. Mineral/groundmass partition coefficients for nepheline, clinopyroxene and perovskite in melilite-nepheline basalt, Nyragongo, Zaire.
Geochimica et Cosmochimica Acta **15**, 221.228.

Philpotts, A.R., 1990. Principles of igneous and metamorphic petrology.
New Jersey: Prentice Hall, 498 pp.

Pouchou, J.L. & Pichoir, F., 1984. A new model for quantitative X-ray microanalysis. I - Application to the analysis of homogeneous samples
La Recherche Aerospatiale (English Edition) **3**, 13-38.

Putirka, K., 1997. Magma transport at Hawaii: inferences based on igneous thermobarometry.
Geology **25**, 69-72.

Ridley, W.I., 1970. The petrology of the Las Cañadas volcanoes. Tenerife, Canary Islands.
Contributions to Mineralogy and Petrology **26**, 124-160.

Ryerson, F.J. & Hess, P.C., 1978. Implications of liquid-liquid distribution coefficients to mineral-liquid partitioning.
Geochimica et Cosmochimica Acta **42**, 921-932.

Scott, P.W., 1976. Crystallization trends of pyroxenes from the alkaline volcanic rocks of Tenerife, Canary Islands.
Mineralogical Magazine 40, 805-816.

Shimizu, H. (1980). Experimental study on rare-earth element partitioning in minerals formed at 20 and 30kb for basaltic systems.
Geochemical Journal **14**, 185-202.

Sisson, T.W., 1991. Pyroxene-high silica rhyolite trace element partition coefficients measured by ion probe.
Geochimica et Cosmochimica Acta **55**, 1575-1585.

Soesoo, A., 1997. A multivariate statistical analysis of clinopyroxene composition: empirical coordinates for the crystallization PT-estimations.
Geologiska Föreningens i Stockholms Förhandlingar **119**, 55-60.

Sparks, R.S.J., Huppert, H.E. & Turner, J.S., 1984. The fluid dynamics of evolving magma chambers.
Philosophical Transactions of the Royal Society of London **310**, 511-534.

Thirlwall, M.F., Singer, B.S. & Marriner, G.F., 2000. ^{39}Ar-^{40}Ar ages and geochemistry of the basaltic shield stage of Tenerife, Canary Islands, Spain.
Journal of Volcanology and Geothermal Research **103**, 247-297.

Turner, J.S. & Gustavson, L.B., 1981. Fluid motions and compositional gradients produced by crystallisation or melting at verticale boundaries.
Journal of Volcanology and Geothermal Research **11**, 93-125.

Villemant, B., 1988. Trace-Element Evolution in the Phlegrean Fields (Central-Italy) - Fractional Crystallization and Selective Enrichment.
Contributions to Mineralogy and Petrology **98**, 169-183.

Watson, E.B. & Green, T.H., 1981. Apatite/liquid partition coefficients for the rare earth elements and strontium.
Earth and Planetary Science Letters **56**, 405-421.

Watson, E.B. &Harrison, T.M., 1983. Zirkon saturation revisited: temperature and composition effects in a variety of crustal magma types.
Earth and Planetary Science Letters **64**, 295-304.

Wolff, J.A., 1983. Petrology of Quartenary pyroclastic deposits from Tenerife, Canary Islands.
Ph. D. Thesis, Univerity of London, 542 pp.

Wolff, J.A., 1984. Variation in Nb/Ta during differentiation of phonolitic magma, Tenerife, Canary Islands.
Geochemica et Cosmochimica Acta **48**, 1345-1348.

Wolff, J.A. & Storey, M., 1984. Zoning in highly alkaline magma bodies.
Geological Magazine **121**, 563-375.

Wollf, J.A., 1987. Crystallisation of nepheline syenite in a subvolcanic magma system; Tenerife, Canary Islands.
Lithos **20**, 207-223.

Wollf, J.A., 1985. Zonation, mixing and eruption of silica-undersaturated alkaline magma: a case study from Tenerife, Canary Islands.
Geological Magazine **122**, 623-640.

Wolff, J.A., Grandy, J.S. & Larson, P.B., 2000. Interaction of mantle-derived magma with island crust? Trace element and oxygen isotope data from the Diego Hernàndez Formation, Las Cañadas, Tenerife.
Journal of Volcanology and Geothermal Research **103**, 1-4, 343-366.

Wolff, J.A. & Toney, J.B., 1993. Trapped liquid from a nepheline syenite: A re-evaluation of Na-, Zr-, F-rich interstitial glass in a xenolith from Tenerife, Canary Islands.
Lithos **29**, 285-293.

Wulff-Pedersen, E., Neumann, E.-R. & Jensen, J.J., 1996. The upper mantle under La Palma, Canary Islands: Formation of Si-K-Na-rich melt and its importance as a metasomatic agent.
Contributions to Mineralogy and Petrology **125**, 113-139.

Wörner, G., Beusen, J.-M., Duchateau, N., Gijbels, R. & Schmincke, H.-U., 1983. Trace element abundances and mineral/melt distribution coefficients in phonolites from the Laacher See volcano (Germany).
Contributions to Mineralogy and Petrology **84**, 152-173.

Yoder, H.S. & Tilley, C.E., 1962. Origin of basalt magmas: An experimental study of natural and synthetic rock system.
Journal of Petrology **3**, 342-532.